REPORT DOCUMENTATION PAGE

Form Approved
OMB No. 0704-0188

1. AGENCY USE ONLY (Leave blank)	2. REPORT DATE	3. REPORT TYPE AND DATES COVERED
	10/29/96	Final Technical Report; 10/01/95-09/30/96

4. TITLE AND SUBTITLE
SUBGRID SCALE MODELS WITH BACKSCATTER

5. FUNDING NUMBERS
N00014-96-1-0015

6. AUTHOR(S)
Prof. J.A. Domaradzki

7. PERFORMING ORGANIZATION NAME(S) AND ADDRESS(ES)
University of Southern California
Department of Aerospace Engineering
Los Angeles, CA 90089-1191

8. PERFORMING ORGANIZATION REPORT NUMBER

9. SPONSORING/MONITORING AGENCY NAME(S) AND ADDRESS(ES)
Dr. Pat Purtell
Office of Naval Research
Ballston Tower One
800 North Quincy St.
Arlington, VA 22217-5660

10. SPONSORING/MONITORING AGENCY REPORT NUMBER

11. SUPPLEMENTARY NOTES

12a. DISTRIBUTION/AVAILABILITY STATEMENT
Approved for public release; distribution unlimited

12b. DISTRIBUTION CODE

13. ABSTRACT *(Maximum 200 words)*

A new method for large eddy simulations is described and evaluated. In the proposed method the primary modeled quantity is the unfiltered velocity field appearing in the definition of the subgrid-scale stress tensor. An estimate of the unfiltered velocity is obtained by expanding the resolved large scale velocity field to subgrid-scales two times smaller than the grid scale. The estimation procedure consists of two steps. The first step utilizes properties of a filtering operation and the representation of quantities in terms of basis functions such as Fourier polynomials. In the second step, the phases associated with the newly computed smaller scales are adjusted in order to correspond to the small scale phases generated by nonlinear interactions of the large scale field. The estimated velocity field is expressed entirely in terms of the known, resolved velocity field without any adjustable constants. The modeling procedure is evaluated in a priori analyses using direct numerical simulation results of channel flow at low Reynolds number and in actual large eddy simulations of channel flow at two different Reynolds numbers. In all cases, the new model performs better than or comparable to classical eddy viscosity models for the majority of physical quantities. In particular, the subgrid-scale stress tensor is predicted very accurately and the procedure naturally accounts for backscatter without any adverse effects on the numerical stability.

14. SUBJECT TERMS
turbulence modeling

15. NUMBER OF PAGES
68

16. PRICE CODE

17. SECURITY CLASSIFICATION OF REPORT	18. SECURITY CLASSIFICATION OF THIS PAGE	19. SECURITY CLASSIFICATION OF ABSTRACT	20. LIMITATION OF ABSTRACT
Unclassified	Unclassified	Unclassified	UL

1 Summary of the Research Results

The following goals have been accomplished in the course of this research project: A method for large eddy simulations which estimates subgrid scales in terms of the resolved scales was developed. In the procedure the resolved large scale velocity field is expanded to subgrid scales two times smaller than the LES grid scale by utilizing properties of a filtering procedure and the representation of quantities in terms of basis functions such as Fourier or Legendre polynomials. The phases associated with the newly computed smaller scales are then adjusted in order to correspond to the small scale phases generated by nonlinear interactions of the large scale field. The subgrid-scale term in the LES equation can then be evaluated directly using the modified velocity field. This approach to determine the subgrid-scale term naturally accounts for backscatter and does not require any adjustable constants.

The modeling procedure was implemented for isotropic turbulence and turbulent channel flow. In *a priori* tests for isotropic turbulence databases correlation coefficients between modeled and exact stresses exceeded 90% and the modeled mean and rms values were within 5% of the exact values (for nonvanishing components). The level of agreement between the modeled and the exact SGS quantities is significantly better than for typical models currently in use, and is achieved without the presence of any adjustable constants. Forward and backscatter are also predicted in a very good agreement with the exact values. *A priori* analysis of the channel flow databases for $Re_\tau = 180$ gave equally encouraging results.

The model has also been implemented in the actual large eddy simulations of channel flow at two different Reynolds number and was compared with the Smagorinsky model optimized for this case as well as with the exact values computed from the well resolved DNS. For all quantities the prediction of the new model is much better than obtained with the Smagorinsky model. In particular plane averages of the diagonal components of the SGS stress tensor for the Smagorinsky model are essentially equal to zero while the DNS results and the new model give non-zero results in good mutual agreement. The only non-zero component τ_{13} for the Smagorinsky model is significantly underpredicted compared with the DNS data and the new model. Very similar results would be expected if the dynamic model were used in place of the Smagorinsky model because of the basic assumption in both models of the proportionality between stresses and rates-of-strain. In all investigated cases the conclusion is that the estimation model is very robust and provides results in excellent agreement with the exact numerical or experimental data and generally performs much better than typical SGS models currently in use. Among its strengths is lack of adjustable constants, presence of the local backscatter which does not cause any numerical instabilities so that ad hoc averaging procedures can be avoided, and by construction the Galilean invariance and the proper near-wall behavior.

2 Publications/Presentations

Refereed Journals

1. J.A. Domaradzki and E.M. Saiki, "Backscatter Models for Large Eddy Simulations", submitted to *Phys. Fluids.*

2. J.A. Domaradzki and E.M. Saiki, "A Subgrid-Scale Model Based on the Estimation of Unresolved Scales of Turbulence", submitted to *Phys. Fluids.*

Conference Proceedings/Abstracts

1. J.A. Domaradzki, "Subgrid-Scale Modeling Based on Small-Scale Nonlinear Dynamics", *Bull. Am. Phys. Soc.* **40**, 1999 (1995).

2. E.M. Saiki and J.A. Domaradzki, "A Subgrid-Scale Model Based on the Estimation of Unresolved Scales of Turbulence", 49th APS Division of of Fluid Dynamics Meeeting, Syracuse, NY (1996).

Invited Talks

1. 06/1996 Institute for Computer Applications in Science and Engineering, NASA Langley Research Center, Hampton, Virginia.

2. 12/1996 Graduate Aerospace Laboratory, Claifornia Institute of Technology, Pasadena, California.

3 Research Personnel

1. J.A. Domaradzki (Principal Investigator), Associate Professor, Department of Aerospace Engineering, University of Southern California, Los Angeles, CA 90089-1191. Dates supported: 01/10/95-09/30/96.

2. E.M. Saiki (Research Associate), Department of Aerospace Engineering, University of Southern California, Los Angeles, CA 90089-1191. Dates supported: 01/10/95-09/30/96.

Degrees Granted: None

Honors/Awards/Promotions: None

4 Research Results

This section consists of submitted journal papers which provide detailed information about research results summarized in section 1.

A subgrid-scale model based on the estimation of unresolved scales of turbulence

J. Andrzej Domaradzki and Eileen M. Saiki
Department of Aerospace Engineering,
University of Southern California,
Los Angeles, CA 90089-1191, U.S.A.,
tel. 213-740-5357, FAX 213-740-7774
(October 15, 1996)

A new method for large eddy simulations is described and evaluated. In the proposed method the primary modeled quantity is the unfiltered velocity field appearing in the definition of the subgrid-scale stress tensor. An estimate of the unfiltered velocity is obtained by expanding the resolved large scale velocity field to subgrid-scales two times smaller than the grid scale. The estimation procedure consists of two steps. The first step utilizes properties of a filtering operation and the representation of quantities in terms of basis functions such as Fourier polynomials. In the second step, the phases associated with the newly computed smaller scales are adjusted in order to correspond to the small scale phases generated by nonlinear interactions of the large scale field. The estimated velocity field is expressed entirely in terms of the known, resolved velocity field without any adjustable constants. The modeling procedure is evaluated in *a priori* analyses using direct numerical simulation results of channel flow at low Reynolds number and in actual large eddy simulations of channel flow at two different Reynolds numbers. In all cases, the new model performs better than or comparable to classical eddy viscosity models for the majority of physical quantities. In particular, the subgrid-scale stress tensor is predicted very accurately and the procedure naturally accounts for backscatter without any adverse effects on the numerical stability.

47.27.Eq

I. INTRODUCTION

The large eddy simulation equations for an incompressible flow are conventionally written as

$$\frac{\partial}{\partial t}\overline{u}_i + \frac{\partial}{\partial x_j}\overline{u}_i\,\overline{u}_j = -\frac{1}{\rho}\frac{\partial}{\partial x_i}\overline{p} + \nu\frac{\partial^2}{\partial x_j \partial x_j}\overline{u}_i - \frac{\partial}{\partial x_j}\tau_{ij} \tag{1}$$

$$\frac{\partial}{\partial x_i}\overline{u}_i = 0. \tag{2}$$

The overbar denotes spatial filtering which, for a quantity $f(\mathbf{x})$, is defined by the integral

$$\overline{f}(\mathbf{x}) = \int G(\mathbf{x},\mathbf{x}')f(\mathbf{x}'), \tag{3}$$

where G is a given kernel function. Using the filtering operation (3), f is decomposed into a large scale (or resolved) component $\overline{f}$ and a subgrid-scale (or unresolved) component f':

$$f(\mathbf{x}) = \overline{f}(\mathbf{x}) + f'(\mathbf{x}). \tag{4}$$

In Eq. (1), u_i, p, and ν are the velocity, pressure, and the kinematic viscosity, respectively, and the effects of subgrid-scale quantities on the resolved velocity are described by a subgrid-scale stress tensor

$$\tau_{ij} = \overline{u_i u_j} - \overline{u}_i\,\overline{u}_j, \tag{5}$$

which must be modeled in terms of the resolved quantities to close Eq. (1).

Currently, several subgrid-scale (SGS) models are commonly used in large eddy simulations (LES) of turbulence. Recent reviews of SGS modeling are given by Piomelli [1] and Lesieur [2] and many applications are described in the Proceedings edited by Galperin and Orszag [3]. The SGS models fall into three general categories: eddy viscosity models, similarity models, and so-called mixed models which combine eddy viscosity and similarity expressions.

The eddy viscosity models assume that

$$\tau_{ij} = 2\nu_t\overline{S}_{ij} + \frac{1}{3}\tau_{kk}\delta_{ij}, \tag{6}$$

where $\overline{S}_{ij}$ is the resolved rate-of-strain tensor

$$\overline{S}_{ij} = \frac{1}{2}\left(\frac{\partial\overline{u}_i}{\partial x_j} + \frac{\partial\overline{u}_j}{\partial x_i}\right), \tag{7}$$

and ν_t is the eddy viscosity. The trace term in (6) is always combined with the pressure term in Eq. (1). Among the eddy viscosity models, the Smagorinsky model [4] and the models for homogeneous turbulence proposed by Kraichnan [5] and Chollet and Lesieur [6] have a status of classical models. These models are also used as a starting point to construct more recent models: the dynamic model of Germano *et al.* [7] and its variations [8–10], and the structure function model of Métais and Lesieur [11]. The most common and important feature of the SGS eddy viscosity models is that they properly account for global subgrid-scale dissipation, *i.e.* the net energy flux from the resolved to the unresolved subgrid-scales. This feature results in good predictions of important turbulent quantities such as mean velocities and rms velocity fluctuations. On the other hand, the models often fail in predicting other quantities. For example, in *a priori* analyses of direct numerical simulations (DNS), correlation coefficients between the actual and modeled SGS quantities (stresses, dissipation, nonlinear term, etc.) are very low, usually between 0.1 and 0.3 [12–14]. Moreover, the eddy viscosity formulation is inherently ill-suited to model the phenomenon of inverse energy transfer from the subgrid-scales to the resolved scales. This process, frequently referred to as backscatter, may be quite significant. In analyses of direct numerical simulations of various turbulent flows [14–17], backscatter was found to be comparable to or often larger than the net subgrid-scale dissipation. The Smagorinsky and the structure function models are unable to predict backscatter, and attempts to model backscatter in the framework of the dynamic model may lead to numerical instabilities, because the dissipative Smagorinsky expression is used to describe non-dissipative backscatter effects. Additional procedures limiting excessive backscatter are needed to prevent the numerical instabilities in this latter case [10,18]. In order to model backscatter effectively, the common practice is to introduce an additional forcing term, which is either random or deterministic, in the LES equations [19–22]).

Backscatter is naturally present in similarity models. Similarity models [23,24] assume that the unknown subgrid-scale stress tensor can be approximated by a stress tensor calculated from the resolved field employing an additional filtering with the filter width equal to or larger than the one used to obtain the original resolved field. The Bardina model is given by the following expression

$$\tau_{ij} \approx \overline{\overline{u}_i \, \overline{u}_j} - \overline{\overline{u}}_i \, \overline{\overline{u}}_j. \tag{8}$$

The similarity model of Liu *et al.* [24] assumes that the SGS stress tensor is proportional to the resolved stress tensor L_{ij} which is computed from the resolved velocity using a wider filter (denoted by hat)

$$\mathrm{L}_{ij} = \widehat{\overline{u}_i \, \overline{u}_j} - \widehat{\overline{u}}_i \, \widehat{\overline{u}}_j. \tag{9}$$

The stresses calculated in the similarity models are found to correlate very well with the exact stresses in *a priori* analyses. However, because of the additional filtering the modeled SGS interactions affect scales larger than those affected by the exact SGS interactions. This feature appears as a mismatch in the characteristic length scales for the modeled and the exact SGS fields [24]. Also, the model of Bardina [23] significantly under predicts net SGS dissipation and consequently, it cannot be used to reliably predict mean and rms quantities in actual large eddy simulations. In particular, the SGS stress tensor in the Bardina model vanishes if the sharp spectral filter is employed. In *a priori* analyses, the similarity model proposed by Liu *et al.* [24] provides correct amounts of SGS dissipation in addition to good correlations between the modeled and exact stresses. However, when the model is used in actual LES it appears to experience the same difficulties as the Bardina model (C. Meneveau, private communication).

Mixed models [23,25,26] attempt to combine the good dissipative features of the eddy viscosity models with the good predictive capabilities of the similarity models for correlations between the modeled and exact quantities. They are obtained by adding an eddy viscosity expression to a similarity model. Mixed models were found to provide LES results comparable to or better than those obtained with the classical Smagorinsky model with the additional benefit of accounting for the backscatter [27]. However, because the results do not dramatically improve and the dependence of the models on a filter introduces an additional complication, mixed models have found only limited acceptance.

Due to the difficulties encountered by the above procedures in describing the observed properties of turbulence, none of them has been accepted as a fully satisfactory solution to the problem of subgrid-scale modeling. This motivates further efforts to improve the status of SGS modeling. It can be argued that improvements in modeling can only be made if more detailed information about the SGS nonlinear interactions is employed than information available to developers of the older models. During the last several years it has become possible to investigate in great detail the nonlinear interactions in turbulent flows at low Reynolds numbers using direct numerical simulation databases [28–31] and more recently, experimental measurements [24]. In particular, SGS interactions have been investigated extensively for isotropic and wall-bounded turbulence [14,16,32,33]. The results of these investigations were used to demonstrate that many of the observed features of the exact SGS interactions can be inferred from the dynamics of the resolved scales alone [14,34] (the essential goal of SGS modeling) using procedures entirely different from the traditional SGS models. These procedures are mostly of theoretical interest since they have not been implemented in actual, time evolving large eddy simulations. However, they imply a possibility of improved SGS models developed by using the observed properties of the nonlinear subgrid-scale interactions. The purpose of this paper is to describe and evaluate a new approach to SGS modeling which is based largely on concepts derived from such detailed analyses of nonlinear interactions in a variety of turbulent flows.

II. VELOCITY ESTIMATION CONCEPT

The eddy viscosity models and the similarity models illustrate two different approaches to SGS modeling. The eddy viscosity models assume that the functional form of the SGS stress tensor is proportional to the resolved rate-of-strain and attempt to provide expressions for the proportionality coefficient, the eddy viscosity. In the similarity approach, the primary modeled quantity is the full velocity field and no functional form of the SGS stress is assumed. After a model for the full velocity field is introduced, the stress tensor is computed directly from the definition (5) using an appropriate filter. The idea of estimating the unknown velocity field from the resolved one for the purpose of SGS modeling has been used previously, in one form or another, by several authors. For example, the Bardina model is obtained formally by approximating the full velocity by the filtered velocity, $u_i \approx \overline{u}_i$, and computing τ_{ij} according to Eq. (5). Liu *et al.* [24] make the same approximation for the velocity, but use a wider filter to compute the resolved stress tensor (9) which is then assumed to be proportional to the actual SGS stress tensor τ_{ij}. Shah and Ferziger [35] have recently developed a procedure to compute a higher order approximation to the full velocity field than the velocity $\overline{u}_i$ used in traditional similarity models. The approximated velocity and a modified filter definition were used

to compute the SGS stress tensor which provided good results in LES of turbulent channel flow. McDonough proposed a so-called additive turbulent decomposition [36] for simulations of turbulence where separate equations are written for large and small scales in the decomposition. The equations for large (small) scales were then solved with a proposed model of small (large) scales. Jiménez [37] successfully simulated inertial range dynamics using a numerical scheme which enforced for a range of small scales the $k^{-5/3}$ energy spectrum. In the work of Kerr *et al.* [14], the authors modeled unresolved subgrid-scale vorticity by calculating properly normalized vorticity production by the resolved scales in a limited range of wavenumbers outside the resolved range. The modeled subgrid-scale vorticity was used in *a priori* tests to compute the SGS quantities which were found to compare very favorably with the exact quantities. This also implies that the nonlinear interactions among resolved scales provide significant amounts of information about the largest subgrid-scales. This conclusion is quite consistent with the classical picture of turbulence, where the smaller scales are generated by the nonlinear interactions among the larger scales.

Despite the shortcomings of specific methods used to estimate the full velocity field, the above results taken together suggest that this approach to SGS modeling may become viable if better estimation procedures are developed. In this paper, we investigate a procedure which develops a significantly better model for the velocity field than the above approximations. The procedure explicitly uses properties of the filtering operation and properties of SGS interactions established in previous investigations.

An obvious application of the properties of a filtering operation is a requirement that the estimated velocity after filtering with a given filter G used in a LES is equal (or close) to the resolved field $\overline{u}_i$ on the resolved mesh. This requirement will be used explicitly in the next section.

The properties of SGS interactions described below lead to additional conditions imposed on the estimated velocity. Subgrid-scale energy transfer in isotropic turbulence at large Reynolds numbers has been investigated extensively in the framework of analytical theories of turbulence [5], for LES databases [31,32], and at small Reynolds numbers using well resolved DNS fields [16,32]. If a sharp spectral filter with a cutoff wavenumber, k_c, is used, the spectral eddy viscosities in all cases exhibit a strong cusp in the vicinity of the cutoff wave number. The cusp behavior reflects significant SGS energy transfer associated with modes in the vicinity of the cutoff. Kraichnan's analysis [5] for an infinite inertial range shows that close to 75% of the SGS energy transfer is from the range of the resolved scales $0.5k_c < k < k_c$. In DNS data for low Reynolds number flows, this range is responsible for almost the entire SGS energy transfer [16,32]. Additional analysis of the DNS data also revealed that the observed SGS energy transfer is caused almost exclusively by interactions of the resolved scales with a limited range of subgrid-scales with wavenumbers $k_c < k < 2k_c$, and the nonlocal, eddy-viscosity type energy transfer between resolved modes and modes $k > 2k_c$ was not observed [16]. At high Reynolds numbers, Kraichnan's analysis implies that the nonlocal transfer is not negligible and may contribute about 25% to the net SGS transfer. These results strongly suggest that the SGS energy transfer is dominated by energy exchanges among resolved and unresolved scales from the vicinity of the cutoff. Similar analyses have been performed for turbulent wall-bounded flows (channel flow and Rayleigh-Bénard convection) and the same conclusions have been reached [33]. Also, the analysis of the experimental data by Liu *et al.* [24] identified interactions between neighboring scales as dominant in the SGS dynamics. A major conclusion from these investigations is that the nonlinear dynamics of the resolved modes with wave numbers $k < k_c$ are governed almost exclusively by their interactions with a limited range of modes with wave numbers not exceeding $2k_c$ and that much smaller scales have a negligible effect on the resolved ones. This conclusion is entirely consistent with the classical picture of the turbulent cascade [38], where the large scales of a turbulent flow determine the energy flux down the spectrum and the very small scales play an entirely passive role by adjusting themselves in such a way as to accommodate this energy flux prescribed by the large scales. In the context of SGS modeling, this result implies that in the definition of the SGS stress tensor (5) the full velocity field u_i may be replaced by a field truncated to wavenumbers $k < 2k_c$, *i.e.* to scales not smaller than about half of the smallest resolved scale. More generally, consider a filtering operation (3) with two filter widths Δ and $\Delta/2$ denoted by an overbar and a tilde, respectively. The above properties of the SGS dynamics imply the following approximation

$$\tau_{ij} = \overline{u_i u_j} - \overline{u}_i\,\overline{u}_j \approx \overline{\tilde{u}_i \tilde{u}_j} - \overline{\tilde{u}}_i\,\overline{\tilde{u}}_j. \tag{10}$$

Of course, the approximation in its present form does not provide an expression for τ_{ij} in terms of the resolved quantities, because $\tilde{u}_i$ still depends on the unresolved subgrid-scales in the range between $\Delta/2$ and Δ. However, the approximation (10) simplifies the task of modeling the velocity field, because for the purpose of SGS modeling its dependence on scales smaller than $\Delta/2$ can be neglected.

Another previously mentioned property of the SGS interactions is the observation that, because of the turbulent cascade, the subgrid-scales in the range between $\Delta/2$ and Δ must be strongly influenced by the resolved scales larger than Δ. In particular, during the initial stages of the evolution of a turbulent flow the smaller scales are generated by the larger eddies and the phases of the subgrid-scales are determined by the nonlinear interactions among the large scales.

Using the qualitative properties of filtering and SGS interactions described above, we develop in the subsequent sections a specific method for estimating the velocity $\tilde{u}_i$. The expectation is that it should be possible to develop a good model for the velocity $\tilde{u}_i$ by accounting for the physics of the nonlinear interactions and that the procedure will result in a better model for the full SGS stress tensor than could be obtained with traditional approaches to SGS modeling. There are two important theoretical advantages of such an approach. First, the definition (10) guarantees that the model based on the estimated velocity is Galilean invariant [39]. Second, all of the SGS stress components will have correct near-wall behavior, because the estimated velocity $\tilde{u}_i$ is approximated to the lowest order by the filtered velocity $\overline{u}_i$ for which the correct wall behavior is enforced by the LES equations.

III. A VELOCITY ESTIMATION PROCEDURE

Consider a velocity field $u_i(\mathbf{x},t)$ which is fully resolved in a particular direction, say x, on M equally spaced grid points

$$x_m = m\delta, \ (m = 0, 1, \ldots, M-1) \tag{11}$$

where $\delta = L_x/M$ is a mesh size. Such a field could be obtained in adequately resolved direct numerical simulations. A collocation pseudo-spectral method with Fourier expansions is used later in the numerical implementation of the model, therefore the velocity u_i for all x will be represented by a trigonometric polynomial of order M (Canuto *et al.* [40])

$$u_i^{(M)}(x) = \sum_{m=-M/2}^{M/2} c_m \exp(ik_m x), \tag{12}$$

where the discrete wavenumbers are $k_m = 2\pi m/L_x = m\Delta k$ and the dependence of u_i on other variables is neglected in the notation. The superscript M signifies the M mode Fourier representation of the field and i in the argument of the exponent is $\sqrt{-1}$. The Fourier coefficients c_m in (12) are expressed in terms of the nodal values of the velocity u_i

$$c_m = \frac{1}{Md} \sum_{p=0}^{M-1} u_i(x_p) \exp(-ik_m x_p), \tag{13}$$

where $d = 1$ for all values of m except $m = \pm M$ when $d = 2$. The velocity field $u_i^{(M)}(x)$ is a real function of x, thus the complex Fourier coefficients must satisfy the relation $c_m^* = c_{-m}$. Equation (13) also reveals that c_m is real for $m = 0$ and $m = \pm N$. All of the coefficients c_m are determined by M real numbers, *i.e.* the same number of nodal values in physical space.

In Fourier representation, the top hat filter is particularly easy to implement. The filter function G for a top hat filter with a width Δ is

$$G(x,x') = \begin{cases} \frac{1}{\Delta} & \text{if } |x-x'| < \Delta/2 \\ 0 & \text{otherwise.} \end{cases} \tag{14}$$

Integrating (12) with the filter (14) we obtain

$$\overline{u}_i^{(M)}(x) = \sum_{m=-M/2}^{M/2} \left[c_m \frac{\sin(k_m\Delta/2)}{k_m\Delta/2} \right] \exp(ik_m x). \tag{15}$$

The filtered field is smooth over the length scale Δ and for the purpose of LES it can be accurately represented by sampling it on a courser mesh with the mesh size Δ. It is convenient to assume that Δ is a multiple of the smaller mesh size δ, $\Delta = r\delta$, such that the field (15) is sampled on the subset of $2N = M/r$ grid points from the fine mesh. If only the sampled values of (15) on the mesh points $x_j = j\Delta$, $(j = 0, 1, \ldots, 2N-1)$ are used, the $2N$ mode Fourier representation of $\overline{u}_i$ is

$$\overline{u}_i^{(2N)}(x) = \sum_{l=-N}^{N} a_l \exp(ik_l x), \tag{16}$$

where $k_l = 2\pi l/L_x$ and

$$a_l = \frac{1}{2Nd} \sum_{j=0}^{2N-1} \overline{u}_i^{(2N)}(x_j) \exp(-ik_l x_j). \tag{17}$$

Since (16) is the same quantity as the velocity $\overline{u}_i$ in actual large eddy simulations, the superscript $2N$ in (16) will often be omitted.

The maximum wavenumber in the representation (16) is $N\Delta k$. According to the discussion in the previous section, we will seek a model velocity $\tilde{u}_i$ which contains scales by at most a factor of two smaller than the smallest resolved scale. In Fourier representation, it is equivalent to doubling the maximum wavenumber which requires an increase to $4N$ modes in the expansion

$$\tilde{u}_i^{(4N)}(x) = \sum_{n=-2N}^{2N} b_n \exp(ik_n x). \tag{18}$$

The modeling procedure attempts to express $4N$ unknown coefficients b_n in (18) in terms of $2N$ known coefficients a_l in the expansion (16). Such a procedure will not be unique, but if the observed physics of the nonlinear interactions are accounted for, good models for a SGS stress tensor may be expected.

We propose a procedure which consists of two steps, one which is purely kinematical and the other which accounts for the dynamics of SGS nonlinear interactions. In the kinematic step, we first require that $\tilde{u}_i^{(4N)}$ filtered with a top hat filter with the width Δ is equal to the known values of $\overline{u}_i^{(2N)}$ on the resolved mesh

$$\overline{\tilde{u}}_i^{(4N)}(x_j) = \overline{u}_i^{(2N)}(x_j),\ x_j = j\Delta,\ (j = 0, 1, \ldots, 2N-1). \tag{19}$$

This equation reflects the compatibility condition between the resolved velocity and the filtered estimated velocity and it constitutes $2N$ equations relating coefficients b_n and a_l. The additional $2N$ equations are obtained by requiring that $\overline{u}_i^{(2N)}$ and $\tilde{u}_i^{(4N)}$ filtered with a wider filter (denoted by a hat) $\hat{\Delta} = 2\Delta$ are equal on the resolved mesh

$$\hat{\tilde{u}}_i^{(4N)}(x_j) = \hat{\overline{u}}_i^{(2N)}(x_j),\ x_j = j\Delta,\ (j = 0, 1, \ldots, 2N-1). \tag{20}$$

The use of the wider filter in the above condition is reminiscent of the test filtering in the dynamic model [7]. While reasonable, the condition (20) is less justified than the condition (19) since it does not reflect the straightforward properties of filtering as does Eq. (19). Other ways of obtaining the remaining $2N$ equations may be considered. For example, the relation (19) may be enforced on points interpolated between resolved grid points or the coefficients b_k may be chosen to provide the optimal approximation to $\overline{u}_i^{(2N)}(x)$ by $\overline{\tilde{u}}_i^{(4N)}(x)$ (both depending on the continuous variable x). We are planning to explore such methods in future work.

Introducing the notation

$$\alpha(k) = \frac{\sin(k\Delta/2)}{k\Delta/2}, \tag{21}$$

$$\gamma(k) = \frac{\sin(k\hat{\Delta}/2)}{k\hat{\Delta}/2}, \tag{22}$$

equations (19) and (20) are rewritten as follows

$$\sum_{n=-2N}^{2N} \alpha(k_n) b_n \exp(i\frac{njn}{N}) = \sum_{l=-N}^{N} a_l \exp(i\frac{ljn}{N}),\ j = 0, 1, \ldots, 2N-1, \tag{23}$$

$$\sum_{n=-2N}^{2N} \gamma(k_n) b_n \exp(i\frac{njn}{N}) = \sum_{l=-N}^{N} a_l \gamma(k_l) \exp(i\frac{ljn}{N}),\ j = 0, 1, \ldots, 2N-1. \tag{24}$$

Using the summation formula (see Canuto *et al.* [40])

$$\frac{1}{2N}\sum_{j=0}^{2N-1}\exp(i\frac{pj\pi}{N}) = \begin{cases} 1 \text{ if } p = 2Nm,\ m = 0, \pm 1, \pm 2, ... \\ 0 \text{ otherwise.} \end{cases} \tag{25}$$

we derive a set of equations for the coefficients b_n. From equation (23)

$$\alpha(k_l)b_l + \alpha(k_{l+2N})b_{l+2N} = a_l,\ -N < l < 0 \tag{26}$$

$$\alpha(k_l)b_l + \alpha(k_{l-2N})b_{l-2N} = a_l,\ 0 < l < N, \tag{27}$$

and from equation (24)

$$\gamma(k_l)b_l + \gamma(k_{l+2N})b_{l+2N} = \gamma(k_l)a_l,\ -N < l < 0, \tag{28}$$

$$\gamma(k_l)b_l + \gamma(k_{l-2N})b_{l-2N} = \gamma(k_l)a_l,\ 0 < l < N. \tag{29}$$

Solving the above equations, we get explicit expressions for the coefficients

$$b_l = b_{-l} = \frac{\gamma(k_{l-2N})/\gamma(k_l) - \alpha(k_{l-2N})}{\alpha(k_l)\gamma(k_{l-2N})/\gamma(k_l) - \alpha(k_{l-2N})}a_l,\ 0 < l < N, \tag{30}$$

$$b_{l-2N} = b_{-l+2N} = \frac{\alpha(k_l) - 1}{\alpha(k_l)\gamma(k_{l-2N})/\gamma(k_l) - \alpha(k_{l-2N})}a_l,\ 0 < l < N. \tag{31}$$

In special cases $l = \pm N$ and $l = 0$, we obtain the following equations

$$\alpha(k_N)b_N + \alpha(k_{-N})b_{-N} = a_N, \tag{32}$$

$$\gamma(k_N)b_N + \gamma(k_{-N})b_{-N} = \gamma(k_N)a_N, \tag{33}$$

$$\alpha(k_{2N})b_{2N} + \alpha(k_{-2N})b_{-2N} + \alpha(k_0)b_0 = a_0, \tag{34}$$

$$\gamma(k_{2N})b_{2N} + \gamma(k_{-2N})b_{-2N} + \gamma(k_0)b_0 = \gamma(k_0)a_0. \tag{35}$$

Using the facts that $\alpha(k_0) = \gamma(k_0) = 1$, $\gamma(k_{\pm 2N}) = \alpha(k_{\pm 2N}) = 0$, and $\gamma(k_{\pm N}) = 0$,

$$b_{\pm N} = \frac{a_N}{2\alpha(k_N)},\ b_0 = a_0, \tag{36}$$

and the coefficients b_{2N} and b_{-2N} can be set to zero. It can be shown that the same values of the coefficients b_l are obtained for any $\hat{\Delta}$ which is an even multiple of Δ. Such a partial independence of the modeled field $\tilde{u}_i$ on the secondary filtering operation is an attractive feature of the modeling procedure.

The above method provides the velocity field (18) using only properties of the filtering operation by enforcing the condition that the filtered modeled field is equal to the known LES field (16) on a selected number of mesh points. The procedure does not contain any information about the fact that the small scales in such a field are dynamically coupled to large scales through nonlinear interactions. In order to account for such couplings, the coefficients b_l must be modified. According to the discussion in section II, it may be expected that the smaller scales are generated by the nonlinear interactions between large eddies. In spectral methods, the large scales with wavenumbers $k < k_c$ will generate modes with wavenumbers $k_c < k < 2k_c$ through the nonlinear term in the Navier-Stokes equations, even if initially the domain $k_c < k < 2k_c$ is empty. We use the velocity field (18) truncated spectrally to $k_{-N} < k < k_N$, *i.e.*

$$\tilde{u}_i^{(2N)}(x) = \sum_{n=-N}^{N} b_n \exp(ik_n x), \tag{37}$$

and compute for this field the nonlinear term for wavenumbers $|k| > k_N$. The complex coefficients b_n for $|n| > N$ in the original expansion (18) are modified by setting their phases equal to the phases of the computed nonlinear term,

while keeping their amplitudes unchanged. This way, the highest wavenumber modes in the Fourier expansion will carry limited information about the process of generation of small scales through nonlinear interactions. The actual phases and amplitudes of high wavenumber modes are generated by a much larger number of interactions acting over at least one large eddy turnover time. In the above procedure, this process is simplified by assuming that only a single act of large scale interactions determines the phases of subgrid-scales and their amplitudes can be determined by the filtering compatibility conditions rather than by time evolution. The validity of these assumptions can only be tested by using this procedure in practice.

In summary, the procedure described above allows us to estimate the velocity field with subgrid-scales (18) using only information about the filtered, LES field (16). The only free parameter is the additional filter width $\hat{\Delta}$, but the estimated velocity is the same if $\hat{\Delta}$ is any even multiple of the primary filter width Δ. A closed form expression for the estimated velocity cannot be easily given, because of the modification of the subgrid-scale phases by the nonlinear term. The generalization of the estimation procedure to more dimensions is straightforward if Fourier decomposition in other directions can be used. For two and three dimensional fields, the kinematic part of the procedure is applied sequentially in each direction, followed by a phase correction on such an expanded field. Only cases allowing Fourier expansions will be considered in this paper.

As already noted, the procedure is not unique and it is possible that it could be improved by imposing additional conditions on the the estimated field (18). For instance, because of the phase correction the representation (18) no longer satisfies the kinematic conditions (19) and (20) exactly. However, these conditions are satisfied approximately because the large scale modes and the amplitudes of the small scale modes are unchanged. The current procedure also does not enforce incompressibility for the estimated field (18). On the other hand it must be remembered that estimating velocity is not a goal in itself, but an intermediate step in calculating the SGS stress tensor. If the estimation procedure properly captures the kinematic and dynamic relations between the resolved and subgrid-scales, it should produce a good approximation for the SGS stress tensor.

IV. NUMERICAL IMPLEMENTATION

We will consider turbulent channel flow as a test case, because of the availability of experimental and DNS data for comparisons. The fluid is contained between two parallel rigid walls separated by a distance L_z in the vertical direction z. The horizontal dimensions of the computational domain are L_x in the streamwise direction x and L_y in the spanwise direction y. In the simulations, no-slip boundary conditions are imposed on the rigid walls and periodic boundary conditions in x and y. We employ a numerical Navier-Stokes code developed by Chan [41] which uses a pseudo-spectral numerical method for spatial discretization [40] with Fourier expansions in the streamwise and spanwise directions, and Legendre polynomials in the wall normal direction. The equations are integrated in time using a second order, predictor-corrector method introduced by Kim and Moin [42]. The LES equations (1) and (2) are nondimensionalized by the channel half width $h = L_z/2$ and the friction velocity $u_\tau = (\tau_0/\rho)^{1/2}$ where τ_0 is the wall shear stress. The pressure term is decomposed into the fluctuating component and the mean pressure gradient driving the flow which, for the nondimensionalization applied, is equal to -1 for the streamwise direction. The nondimensionalized equations are

$$\frac{\partial}{\partial t}\overline{u}_i + \frac{\partial}{\partial x_j}\overline{u}_i\,\overline{u}_j = -\left(\frac{\partial}{\partial x_i}\overline{p} - \delta_{1i}\right) + \frac{1}{Re_\tau}\frac{\partial^2}{\partial x_j \partial x_j}\overline{u}_i - \frac{\partial}{\partial x_j}\tau_{ij}, \tag{38}$$

$$\frac{\partial}{\partial x_i}\overline{u}_i = 0, \tag{39}$$

where $Re_\tau = u_\tau h/\nu$ is the Reynolds number. The filtering in (38) and (39) is applied only in the horizontal directions with the top hat filter with widths Δ_1 and Δ_2 in x and y, respectively. The widths are chosen to be equal to the respective mesh sizes in LES for those directions. Since Fourier expansions are implemented in x and y, a two-dimensional version of the estimation method described in the previous section is used to model the SGS stress tensor, τ_{ij}. For comparison, we also use the Smagorinsky model which provides the following expression for the eddy viscosity in Eq. (6)

$$\nu_t = 2(C_S\Delta)^2|\overline{S}| \tag{40}$$

where $|\overline{S}| = (2\overline{S}_{ij}\,\overline{S}_{ij})^{1/2}$, and the length scale Δ is taken as the geometric average of mesh spacings in the Cartesian directions $\Delta = (\Delta x \Delta y \Delta z)^{1/3}$. The value of the Smagorinsky constant was estimated theoretically by Lilly [43] as

$C_S = 0.18$, but we use $C_S = 0.1$ which is the preferred value for wall-bounded shear flows [25,44]. In order to control excessive dissipation by the model in the vicinity of walls, the length scale Δ is decreased using Van Driest damping [45] as proposed by Moin and Kim [46].

A. *A priori* analysis of DNS data

In order to assess the validity of the assumptions made in developing the velocity estimation model, the modeled SGS quantities are compared in this section with the exact SGS quantities computed for well resolved DNS databases obtained in pseudo-spectral, Fourier-Chebyshev simulations of turbulent channel flow described by Gilbert [47] and Gilbert and Kleiser [48]. The flow was simulated with a resolution of 160^2(horizontal)$\times$129(vertical) modes in a box with dimensions $L_z = 2$ (the unit of length is the channel half width, $h = L_z/2$), $L_x = 3.6\pi$, and $L_y = 1.9\pi$. Simulations were performed enforcing constant mean mass flux at Reynolds number $Re = 5000$ based on the maximum velocity of a laminar flow and the channel half width h. The corresponding Reynolds number based on friction velocity and h is approximately $Re_\tau = 210$. In the spanwise direction a symmetry condition at $y = L_y/2$ was imposed, motivated by the symmetry properties of the transitional flow preceding the fully turbulent stage of the simulation. A comparison with the DNS results of Kim *et al.* [49] and experimental results of Nishino and Kasagi [50] revealed that the influence of the symmetry assumption on horizontally averaged statistical properties of turbulence was negligible. The simulations were run until turbulence reached a statistically steady state, and after that they were continued for long enough times to collect turbulence statistics. For *a priori* analyses only instantaneous fields were used with averaging over planes. Averaging procedures will be denoted by brackets $< ... >$ to distinguish them from the filtering operation which is denoted by the overbar.

The artificial LES velocity field was obtained from the DNS velocity as follows. First, in the wall normal direction the velocity was interpolated from 129 Chebyshev grid points to 65 Legendre-Gauss-Lobatto points on the interval $-1 < z < +1$. Second, the top hat filtering in the form of (15) was applied with $\Delta_1 = L_x/32$ and $\Delta_2 = L_y/32$ in the horizontal directions x and y, respectively. The continuous x and y representation (15) was subsequently sampled on 32×32 grid points uniformly spaced in each direction. The resulting LES field is thus represented on a mesh with $32 \times 32 \times 65$ points. The LES velocity was used to compute SGS quantities using both the Smagorinsky model and the velocity modeled by the estimation procedure described in section III. The exact SGS quantities were calculated from definitions using the full DNS velocity and top hat filtering in x and y with the respective filter widths $\Delta_1 = L_x/32$ and $\Delta_2 = L_y/32$.

In addition to the SGS stress tensor τ_{ij}, several other SGS quantities were computed: the subgrid-scale nonlinear term (or SGS force)

$$N_i^{SGS}(\mathbf{x}) = \frac{\partial}{\partial x_j}\tau_{ij}(\mathbf{x}), \tag{41}$$

the SGS energy transfer

$$T^{SGS}(\mathbf{x}) = -\overline{u}_i(\mathbf{x})N_i^{SGS}(\mathbf{x}), \tag{42}$$

and the SGS dissipation

$$\epsilon_{SGS}(\mathbf{x}) = \tau_{ij}(\mathbf{x})\overline{S}_{ij}(\mathbf{x}). \tag{43}$$

The primary quantity that must be properly predicted by a SGS model is the SGS stress tensor. All of the SGS stress tensor components were calculated exactly from the definition Eq. (5), and using the Smagorinsky and the velocity estimation models. In figure 1, we plot results for four nonvanishing components of the tensor averaged over the horizontal planes. The diagonal components are modified by subtracting one third of the trace of the tensor, because this is the quantity modeled by the Smagorinsky expression (6). The Smagorinsky model predicts essentially a zero value for the plane averaged diagonal components of the stress. The modeled SGS shear stress component τ_{13} is non-zero, but it is significantly under predicted throughout the channel. Note, however, that the shear stress slope is predicted very well at the walls. For the diagonal components, the estimation model properly predicts trends with z and locations of peaks, though the peak values are underestimated by up to 50%. The estimation model also provides qualitatively better results for τ_{13} across the channel, but the slopes at the walls are slightly under predicted.

The plane averages of the SGS force components (41) are plotted in figure 2. Again, for comparison with the Smagorinsky model the expression (41) is computed with the diagonal stress components modified as above. The Smagorinsky model predicts nonzero values only for the streamwise force component N_1^{SGS}. Due to the previously noted favorable prediction for the wall slope of τ_{13}, the SGS force is in very good agreement with the exact quantity in

the immediate vicinity of the wall, but the negative peak in Fig. 2(a) is too narrow. The estimation model captures correctly the locations and widths of the peaks in the exact SGS forces, but underestimates their extrema. A relatively good prediction of the estimation procedure for the wall normal force N_3^{SGS} implies that the wall normal pressure gradient may be equally well predicted since the pressure term does not have to compensate for the errors in the wall normal SGS force. If the Smagorinsky model is used the pressure in Eq. (1) is replaced by the sum, $\overline{p} + 1/3\tau_{kk}\delta_{ij}$, and the pressure itself cannot be computed, because the model does not provide an expression for τ_{kk}.

The plane averaged SGS dissipation is plotted in figure 3(a). Both models give correct qualitative trends and the Smagorinsky model prediction is very accurate in the wall region where the estimation model under predicts the exact quantity. The favorable performance of the Smagorinsky model is not surprising since it is designed to account for the dissipative features of turbulence and, moreover, we use the value of the Smagorinsky constant optimized for the modeled case. In figure 3(b), we plot the SGS dissipation decomposed in each plane into forward transfer (negative values, $< \epsilon_{SGS}^{-} >$) and inverse transfer or backscatter (positive values, $< \epsilon_{SGS}^{+} >$). The actual backscatter is a function of the filter and is fairly small for the top hat filter used here. Nevertheless, the estimation model predicts backscatter in excellent agreement with the exact result while the Smagorinsky model is purely dissipative.

We have also calculated correlation coefficients between the modeled and exact fields for a number of subgrid-scale quantities. The correlation coefficient between two scalar fields $T_1(\mathbf{x})$ and $T_2(\mathbf{x})$ is

$$C(T_1, T_2) = \frac{< T_1(\mathbf{x}) T_2(\mathbf{x}) > - < T_1(\mathbf{x}) >< T_2(\mathbf{x}) >}{\sqrt{\langle (T_1(\mathbf{x}))^2 \rangle - \langle T_1(\mathbf{x}) \rangle^2}\sqrt{\langle (T_2(\mathbf{x}))^2 \rangle - \langle T_2(\mathbf{x}) \rangle^2}}. \tag{44}$$

Here, $< ... >$ denotes averages taken over all mesh points (a global correlation coefficient) or over points in the horizontal planes (a plane correlation coefficient). In the latter case the correlation coefficient is a function of the vertical coordinate z. The global correlation coefficients are summarized in Table I.

The correlations for individual components of the SGS stress tensor are around 0.5 for the estimation model, with the exception of the τ_{23} component, and are much larger than the correlations for the Smagorinsky model. Both models give similar correlation coefficients for the streamwise component of the SGS force as well as for the transfer and dissipation. However, the wall normal SGS force in the estimation model shows a much higher correlation than the force in the Smagorinsky model. The plane correlation coefficients for the important τ_{13} component is shown in figure 4. In the midsection of the channel the estimation model gives very high values of the correlation coefficient, about 0.6, comparable to values observed in consistent *a priori* tests for similarity models [24]. In the same region, the Smagorinsky model gives much lower correlations, about 0.2. The correlations decrease in the vicinity of the walls and even become negative for the Smagorinsky model. The low correlations in the vicinity of the walls may suggest that the model predictions are deficient in this important region where the mean stresses reach maximum values. On the other hand, it is interesting to note in figure 5 that the estimation model predicts the cross-correlation between τ_{13} and the rate of strain component $\overline{S}_{13}$ in very good agreement with the correlations for the exact quantities even in the wall region. One may speculate that in a time evolving LES any inaccuracies in the prediction of the SGS stress in the wall region will be compensated by the fact that the modeled stress is correlated with other physical quantities in a manner similar to the actual stress. This hypothesis can only be confirmed by performing actual large eddy simulations.

In order to assess the dependence of the results on the LES resolution, additional *a priori* tests were also performed using DNS fields filtered to $48 \times 64 \times 65$ grid points. Improved comparisons with the exact results and increased values of the correlation coefficients were observed for all SGS quantities. These results are not reported here in detail, because the actual LES results presented in the next section were obtained from simulations implementing the lower resolution, $32 \times 32 \times 65$ points.

The main conclusions from *a priori* tests are that the SGS modeling procedure based on the velocity estimation predicts most of the SGS quantities in good agreement with the exact SGS quantities and performs much better overall than the classical Smagorinsky model optimized for the evaluated flow. In order to fully assess its utility, it must be implemented and tested in time evolving large eddy simulations. The results from such simulations are presented in the next subsection.

B. Large eddy simulations

The Smagorinsky and the velocity estimation model were implemented in a computer code to solve Eqs. (38) and (39). The parameters used in these simulations are presented in Table II. The computations A, S1, and E1 for $Re_\tau = 180$ are standard test cases for LES, because of the availability of several independent numerical and experimental databases for turbulent channel flow [47,49,50]. Case A is an under-resolved direct numerical simulation

and is used only for comparison with cases S1 and E1 to provide a qualitative estimate of the influence of a SGS model on the flow evolution. Cases S2 and E2 correspond to one of the simulations of Piomelli [51] performed with the dynamic model which compared well with the experimental results of Wei and Willmarth [52]. In all cases the dimensions of the computational domain were equal to the dimensions used in the DNS of channel flow by Kim *et al.* [49] ($L_x = 4\pi$, $L_y = 2\pi$, and $L_z = 2$), and comparable to those used by Gilbert [47]. For the higher Reynolds number cases S2 and E2, the horizontal dimensions are larger than those used by Piomelli [51] ($L_x = 2.5\pi$, $L_y = 0.5\pi$). The number of grid points is typical of other large eddy simulations at these Reynolds numbers. In cases S2 and E2, the number of grid points is the same as in Case 3 of Piomelli [51], but the grid resolution is lower, because of the larger size of the computational domain.

All of the cases were started from the same initial condition which was generated in the following manner. The code with the Smagorinsky model was initialized with one of the DNS fields of Gilbert [47] and run until a statistically steady state was reached. The restart file from the end of this run was used as the initial condition for all cases which were run for the times (nondimensionalized by u_τ/h) indicated in Table II. A constant time step $\Delta t = 0.001$ was used in all cases. Cases with the estimation model required about 40% more time per time step than cases with the Smagorinsky model. An important quantity monitored for each case was the shear velocity, u_τ, which was computed from the mean velocity in the simulations. For the nondimensionalization used, u_τ must be equal to unity at steady state and in each case u_τ was always within 5% of the steady state value. This is the typical accuracy observed in other large eddy simulations of a channel flow [53]. We found that restarting the higher Reynolds number case E2 from the lower Reynolds number case led to a very slow evolution of the mean flow, and the computation required more than 22 time units for the shear velocity to approach the steady state value within 5%. The run time was shortened in case S2 by setting the mean velocity in the initial condition to the value estimated for the final steady state. The turbulence statistics were collected over last two time units and they typically involved ten independent realizations. For consistent comparison with previous results, the raw data from the current simulations were renormalized with u_τ computed from the mean velocity.

All of the SGS quantities computed and analyzed *a priori* in the previous section were also calculated in the LES cases S1 and E1. The general behavior observed in the LES is very similar to that observed in *a priori* analysis. In figure 6, we plot the non-vanishing components of the SGS stress tensor with one third of the trace of the tensor subtracted for the diagonal components. As in the *a priori* analysis, the diagonal components are zero for the Smagorinsky model. All of the stress components for the estimation model have peak values larger than in *a priori* analysis and are in much better agreement with the exact quantities than could be expected from *a priori* results. Similar behavior is also observed for the SGS force components plotted in figure (7). The results obtained in case S1 are consistent with *a priori* analysis while the SGS force from case E1 is in much closer agreement with the exact quantity for both force components plotted. These results suggest that the velocity estimation procedure is more robust than *a priori* analyses indicate. We speculate that the modeled velocity must adjust itself to more appropriate values through repeated application of the estimation procedure over many time steps.

The plane averaged SGS dissipation for cases S1 and E1 is plotted in figure 8(a). The dissipation peaks are higher in case S1 than in case E1, but the difference is much less than what was observed in *a priori* analysis and the SGS dissipation in both cases agrees quite well with the exact quantity. This feature of the model is quite important, because it distinguishes it from other non-eddy viscosity models which are known to seriously under predict SGS dissipation. In figure 8(b), we plot the SGS dissipation decomposed in each plane into forward transfer (negative values, $< \epsilon^-_{SGS} >$) and backscatter (positive values, $< \epsilon^+_{SGS} >$). The forward transfer in case E1 is very close to the exact forward transfer and to the total SGS dissipation of the Smagorinsky model. However, contrary to the results of *a priori* analysis the modeled backscatter is now larger than the actual backscatter. The values of the forward transfer and the backscatter integrated across the channel for all of the LES cases and the exact results for the DNS data are shown in Table III. The SGS dissipation results for case E1 are important, because they demonstrate that LES with the estimation model can be run for thousands of time steps in a numerically stable manner with significant local backscatter. This distinguishes the estimation model from the dynamic model where the backscatter inherent in the model must be limited by additional procedures in order to prevent numerical instabilities.

The plane correlations between τ_{13} and the rate of strain component $\overline{S}_{13}$ in LES are shown in figure 9. A slight improvement in the prediction of the correlation peaks for the estimation model is observed. The good quality of the comparison with the correlation coefficients for the exact quantities implies that the correct correlations between τ_{13} and $\overline{S}_{13}$ are maintained in time evolving large eddy simulations using the estimation procedure.

The SGS stresses are intermediate quantities modeled to predict mean and fluctuating turbulent velocities which are the primary quantities of interest in actual LES. To obtain these quantities from the computational data of cases S1, E1, and A, averages were taken over ten realizations and over each horizontal plane. The exact DNS results were also horizontally averaged, but only four statistically independent realizations were available. In figure 10, we plot mean velocity in wall coordinates for the well resolved DNS data and for the three cases A, S1, and E1. The standard linear law of the wall and the logarithmic law with the additive constant 5.5 are also included in the plot.

In the low resolution DNS case A, the mean velocity is under predicted in the log region. The mean velocity in case S1 slightly underestimates the exact DNS result up to $z^+ = 30$, but then overestimates it in the log region $z^+ > 30$. In case E1, the mean velocity follows the exact DNS result very closely up to $z^+ = 10-20$, and then slightly underestimates it throughout the rest of the channel $z^+ > 20$. Overall, in all of the cases the mean velocity profiles are in reasonable agreement with the exact DNS result throughout the wall region, but then vary in the log region. In particular, case E1 reveals improvement over the under resolved DNS case A and lies closer to the exact DNS
S1 results than the Smagorinsky case S2. The plane averaged root-mean-square (rms) turbulent velocities are plotted in figure 11. The turbulent velocity in LES is defined as $u_i'' = \overline{u}_i - U_i$, where U_i is the plane and time averaged mean velocity $U_i =< \overline{u}_i >$. This quantity differs from the standard fluctuating velocity $u_i' = u_i - < u_i >$, which includes contributions from the unknown subgrid-scales. Frequently, in comparing LES results with the experimental data, this distinction is not made, because experiments only provide the fluctuating velocity u_i'. However, consistent comparisons can be made if well resolved DNS data are used. In Fig. 11, we compare rms velocities predicted by the models with the exact DNS results calculated for u_i' and u_i''. First we concentrate on the consistent comparison with the filtered DNS results u_i''. In case A, we observe that without a SGS model v_{rms} and w_{rms} are significantly over predicted compared with the filtered DNS results and the predictions of the models. This points to an appreciable effect of the models on the simulations. However, for u_{rms} case A gives results intermediate between cases S1 and E1. In cases S1 and E1, the peak values in u_{rms} are over predicted by about 25% and the Smagorinsky model also over predicts u_{rms} inside channel. The estimation model gives a good prediction for $z^+ > 30$. For the other two velocity components, both models over predict the exact rms values with the Smagorinsky model giving slightly better results. As expected, the rms values for the unfiltered velocities u_i' are greater than those of the filtered velocities u_i''. These results also illustrate that different conclusions about the performance of the models may be reached if only rms values of the unfiltered velocities u_i' are available. Indeed, in such a case the Smagorinsky model gives the best results for u_{rms} and the new model is better for the other two velocity components. The differences between filtered and unfiltered rms velocities will be even larger for higher Reynolds numbers, because the subgrid-scales contain a larger fraction of the total turbulent kinetic energy. Therefore, comparisons between rms velocities in LES and experiments must be interpreted with caution.

The main conclusion from the results for the mean and fluctuating turbulent velocities is that the estimation model, without any adjustable constants, gives results of comparable quality to the results obtained with the Smagorinsky model optimized for channel flow by a proper choice of the Smagorinsky constant and the wall damping function.

The effects of grid resolution were investigated by changing the resolution to 48×64 and 16×16 mesh points in the horizontal directions. For both models, the increased resolution improved predictions of the rms velocities, but the mean velocity was slightly over predicted. Nevertheless, the conclusions previously drawn about the models remain unchanged. For the lower resolution of 16×16 points, the predictions deteriorated markedly, especially for the streamwise rms velocity. Inspection of the horizontal energy spectra in the fully resolved DNS revealed that this resolution corresponded to a truncation of spectra just before the energy peaks and that the resolution of 32×32 points was adequate to capture the peaks. These observations suggest that the minimum resolution requirements for reasonable LES results is that the energy containing range is resolved in the simulations.

Cases S2 and E2 were done to assess the performance of the estimation procedure for high Reynolds numbers flows. The results of the large eddy simulations of Piomelli [51] performed with the dynamic model at the same Reynolds number serve as a useful benchmark dataset. However, there are several differences between his simulations and cases S2 and E2 which need to be pointed out. Piomelli used the spectral cutoff filter while we used the tophat filter, and his simulations were better resolved with the same number of grid points, because his computational domain was smaller. Also, the Chebyshev mesh used by Piomelli for the normal direction had better resolution in the wall region than the Legendre mesh employed in our simulations.

In figure 12 we present mean velocity profiles in wall units for cases S2 and E2 and for Piomelli's [51] case 3. In case S2 with the Smagorinsky model, the mean velocity approaches the logarithmic curve away from the walls, but it is significantly underestimated for $10 < z^+ < 100$. It appears that this problem is related to the particular value $C_S = 0.1$ of the Smagorinsky constant chosen here. Piomelli estimates the effective Smagorinsky constant for his simulations as 0.06. Shah and Ferziger [35] used $C_S = 0.065$ which resulted in the mean flow overshooting the logarithmic curve and Piomelli's data for $z^+ > 10$. The mean velocity in case E2 departs from the Piomelli's result around $z^+ \approx 20$ and lies above the logarithmic curve throughout most of the channel width.

The rms turbulent velocities are plotted in figure 13. The curves for the Smagorinsky model do not exhibit gradients at the wall as steep as the other two curves and they generally lie below Piomelli's data. The exception is in u_{rms} where the peak in the vicinity of the wall is broader for case S2 than for the other two cases, and the Smagorinsky curve lies above Piomelli's results for $-0.96 < z < -0.7$. For a lower value of the Smagorinsky constant, $C_S = 0.065$, Shah and Ferziger [35] obtained the location of the peak in better agreement with Piomelli's results, but the peak value was over predicted ($u_{rms}/u_\tau \approx 3.5$), and for $|z| < 0.9$, the u_{rms} results were consistently below Piomelli's curve. In case E2, the rms velocities outside of the wall boundary layers are consistently below the values predicted by the

Smagorinsky and the dynamic model. As noted previously, the performance of the models is difficult to judge based on the rms velocities because of differences between the respective LES and actual turbulent velocities u_i'' and u_i'. In fact, the rms velocity results for the low Reynolds number cases suggest that good SGS models should predict lower rms velocities in LES than measured experimentally. This is the case for run E2, because Piomelli's [51] data match or lie below the experimental results of Wei and Willmarth [52]. However, without more detailed information about the scale decomposition of the energy in experiments it is not possible to decide which model gives the best results. In the immediate vicinity of the wall, the curves from case E2 exhibit the same steep gradients observed in Piomelli's data and similar locations of the peak values, but the peak values themselves are not the same. In particular, the peak values of u_{rms} in case E2 are larger than in the other two cases. This behavior seems to suggest that the estimation procedure provides less dissipation in the wall region and more dissipation in the mid-channel than the Smagorinsky and the dynamic models. This conclusion is only partially supported by the SGS dissipation results plotted in figure 14. It is seen that in the wall region $-1.0 < z < -0.9$ the Smagorinsky model indeed predicts substantially higher dissipation than the estimation model. Outside of the wall region the forward transfer predicted by the estimation model is the same as that predicted by the Smagorinsky model, but the total dissipation is lower, because of the non-vanishing backscatter in the former case. The lower SGS dissipation in case E2 may thus explain higher u_{rms} peaks than observed in case S2, but lower values of all rms velocities in the mid-channel are not consistent with such a simple energetic argument.

The decomposition of the SGS dissipation into positive and negative components in Fig. 14 reveals substantial values of backscatter in case E2. According to Table III, the backscatter equals 60% of the net SGS dissipation. The local physical space backscatter appears naturally in the procedure and did not lead to any numerical instabilities in simulations extending for thousands of time steps. The net SGS dissipation in case S2 is much larger than in case E2. Decreasing the Smagorinsky constant from 0.1 to 0.06 in the definition of the SGS dissipation would reduce the dissipation in case S2 to -8.2, bringing it much closer to the value obtained in case E2.

The resolved and SGS shear stresses are plotted in figure 15. The SGS shear stresses for the Smagorinsky model and the dynamic model are concentrated in the wall regions and are close to zero outside of the wall boundary layers. The estimation procedure gives SGS stress distributed with a fairly constant slope across the entire channel width and a required decay to zero at the walls. The behavior of all models in this case is consistent with the behavior observed in the low Reynolds number cases (see Figs. 1(d) and 6(d)), which favored predictions of the estimation procedure. The large values of the SGS stress concentrated in the wall region for the Smagorinsky model and the dynamic model are the result of the dependence of the eddy viscosity formulation on the resolved rate-of-stress tensor which is dominated by large vertical gradients of the streamwise velocity in the boundary layers. Adjusting the Smagorinsky constant from 0.1 to 0.06 would lower the peak values in case S2 from 0.6 to 0.22 which is much closer to the dynamic model value. The differences in model predictions for the SGS shear stress lead to substantial differences in predicted profiles of the resolved shear stress shown in Fig. 15(b). This is because in a steady state the total shear stress (sum of viscous, resolved, and SGS components) depends linearly on the wall normal coordinate z. Since the mean velocities are similar in all cases, the viscous stresses are also similar and differences in the modeled SGS stresses must be compensated by differences in the resolved stresses.

The results from the high Reynolds number LES cases confirm conclusions about the estimation procedure drawn previously from *a priori* analysis and LES for low Reynolds number turbulence. The procedure predicts mean and fluctuating velocities in general agreement with standard eddy viscosity models, gives better representation of SGS stresses, and accounts naturally for backscatter without any numerical instabilities.

V. CONCLUSIONS

In this paper, we have proposed a new approach to the problem of subgrid-scale modeling where one attempts to find an estimation of a velocity field which contains a limited range of subgrid-scales unknown in LES and which is consistent with the resolved velocity. The estimated velocity is then used to compute the SGS stress from the definition. Thus, in the proposed method focus is not on devising an expression for the SGS stress tensor, but on modeling unknown subgrid-scales. Using results from previous *a priori* analyses of DNS databases, it was concluded that only subgrid-scales which are at most a factor of two smaller than the smallest resolved scales need to be modeled. This distinguishes the proposed method from the traditional eddy viscosity concepts which rely implicitly on the assumption of wide separation between interacting scales. The subgrid-scales are determined using kinematic compatibility conditions between the unknown and the resolved field and a dynamic condition reflecting the influence of nonlinear interactions between resolved scales on subgrid-scales. Through the kinematic condition the estimated velocity and in turn the SGS stress tensor depend explicitly on the filtering procedure used. This is an attractive feature of the method, because the SGS stress computed from a given fully resolved velocity field must depend on the

filter and many SGS models fail to exhibit such a dependence. For example, the classical Smagorinsky expression is used in exactly the same form for the LES equations obtained with different filters. The velocity estimation procedure has been implemented in the current study only for the tophat filter and for fields which can be represented in terms of Fourier expansions. Since the explicit properties of the tophat filter and of the discrete Fourier transforms were used, the method in its current form cannot be applied directly for other combinations of the filter and the numerical representation of the velocity field. The expression for the SGS stress does not depend on any adjustable constants, because beyond the need for an additional filter width, no adjustable constants are introduced in the velocity estimation procedure. By construction, the SGS stress is Galilean invariant and has the correct near wall behavior.

The proposed SGS model was implemented in a channel flow code and evaluated in both *a priori* analysis and actual large eddy simulations at two different Reynolds numbers. The results were compared with results provided by LES performed with the Smagorinsky model and, at higher Reynolds number, with the dynamic model results of Piomelli [51]. The estimation procedure was found to predict mean and rms velocities with accuracy comparable to the eddy viscosity models. However, the predictions for the SGS stresses themselves were in much better qualitative and quantitative agreement with the exact results than those obtained with the Smagorinsky model. The non-eddy viscosity models usually encounter problems with inadequate SGS dissipation, forcing the addition of dissipative eddy viscosity expressions in actual LES. The estimation procedure in low Reynolds number LES was found to produce SGS dissipation comparable to the Smagorinsky model. From the results for the high Reynolds number case, we can infer that the estimation procedure gives SGS dissipation comparable to the dissipation for the dynamic model and the Smagorinsky model with a constant $C_S \approx 0.06$. In all cases the net SGS dissipation is sufficient to guarantee the correct evolution of the flow. The new model also predicts significant local backscatter without any adverse effects on the numerical stability of the simulations. The above results strongly suggest that the estimation procedure proposed and investigated in this paper is a physically and numerically viable approach to the problem of SGS modeling.

The proposed modeling procedure should be investigated further to answer several important questions. The procedure is not unique, because there are many possible estimated fields which will be consistent with a resolved field. What is the optimal procedure for choosing from such possible fields? The simulations with the estimation model at higher Reynolds number were started with the initial condition taken from the lower Reynolds number case, and then run until steady state was reached. However, the transient evolution was not studied. How will the model behave in non-stationary and nonequilbrium flows? The estimated velocity is represented on a mesh with twice as many grid points as the resolved velocity in each Cartesian direction in which filtering is applied. Such a representation could be numerically expensive in three dimensional simulations if filtering is applied in all three directions. Is it possible to obtain good results with fewer points? Can the procedure be sequentially applied in each direction rather than simultaneously in all directions as done in this work? For very high Reynolds numbers nonlocal interactions between the resolved scales and subgrid-scales in the range $k > 2k_c$ no longer will be negligible. Can their effect be properly represented by a simple eddy viscosity because of the separation of scales? Currently, LES with the estimation model require about 40% more time to run than LES with the standard Smagorinsky model. Can this timing be improved? Finally, an important question is how to implement the modeling principles in general finite difference codes. We plan to address the above questions in future work.

VI. ACKNOWLEDGEMENTS

This work was supported by contract No. N00014-96-1-0015 from the Office of Naval Research (contract monitor, Dr. L. P. Purtell) and partially by the Rocketdyne Division of Rockwell International Corporation. The supercomputer time was provided by the San Diego Supercomputer Center. Additional computer resources were provided by a NSF Research Equipment Grant, No. ECS-9424385. The authors thank L. Kleiser and U. Piomelli for providing data from their numerical studies.

---

[1] U. Piomelli, "Large -eddy simulations of turbulent flows", TAM Report No. 767, University of Illinois, Urbana-Champaign, 1994.

[2] M. Lesieur, "New trends in large-eddy simulations of turbulence", Annu. Rev. Fluid Mech. **28**.

[3] "Large eddy simulation of complex engineering and geophysical flows", B. Galperin and S.A. Orszag, eds., (Cambridge University Press, Cambridge, 1993).

[4] J. Smagorinsky, "General circulation experiments with the primitive equations", Mon. Weath. Rev. **93**, 99 (1963).
[5] R.H. Kraichnan, "Eddy viscosity in two and three dimensions", J. Atmos. Sci. **33**, 1521 (1976).
[6] J. Chollet and M. Lesieur, "Parameterization of small scales of three-dimensional isotropic turbulence utilizing spectral closures", J. Atmos. Sci. **38**, 2767 (1981).
[7] M. Germano, U. Piomelli, P. Moin, and W.H. Cabot, "A dynamic subgrid-scale eddy viscosity model", Phys. Fluids A**3**, 1760 (1991).
[8] D.K. Lilly, "A proposed modification of the Germano subgrid-scale closure method", Phys. Fluids A**4**, 633 (1992).
[9] V.C. Wong and D.K. Lilly, "A comparison of two dynamic closure methods for turbulent thermal convection", Phys. Fluids A**6**, 1016 (1994).
[10] S. Ghosal, T.S. Lund, P. Moin, K. Akselvoll "A dynamic localization model for large-eddy simulation of turbulent flows", J. Fluid Mech. **286**, 229 (1995).
[11] O. Metais and M. Lesieur, "Spectral large-eddy simulations of isotropic and stably-stratified turbulence", J. Fluid Mech. **239**, 157 (1992).
[12] R.A. Clark, J.H. Ferziger, and W.C. Reynolds, "Evaluation of subgrid-scale models using an accurately simulated turbulent flow", J. Fluid Mech. **91**, 1 (1979).
[13] T.S. Lund , "On dynamic models for large eddy simulations" in *Annual Research Briefs*, Center for Turbulence Research, NASA Ames - Stanford University, 177 (1991).
[14] R.M. Kerr, J.A. Domaradzki, G. Barbier "Small-scale properties of nonlinear interactions and subgrid-scale energy transfer in isotropic turbulence",Phys. Fluids **8**, 197 (1996).
[15] U. Piomelli, W.H. Cabot, P. Moin, and S. Lee, "Subgrid-scale backscatter in turbulent and transitional flows", Phys. Fluids A**3**, 1766 (1991).
[16] J.A. Domaradzki, W. Liu, and M.E. Brachet, "An analysis of subgrid-scale interactions in numerically simulated isotropic turbulence", Phys. Fluids A**5**, 1747 (1993).
[17] J.A. Domaradzki, W. Liu, C. Härtel, and L. Kleiser, "Energy Transfer in Numerically Simulated Wall-Bounded Turbulent Flows", Phys. Fluids A **6**, 1583 (1994).
[18] D. Carati, S. Ghosal, and P. Moin, "On the representation of backscatter in dynamic localization models", Phys. Fluids **7** 606 (1995).
[19] C.E. Leith, "Stochastic backscatter in a subgrid-scale model: plane shear mixing layer", Phys. Fluids A **2**, 297 (1990).
[20] J.R. Chasnov, "Simulation of the Kolmogorov inertial subrange using an improved subgrid model", Phys. Fluids A**3**, 188 (1991).
[21] U. Schumann, "Stochastic backscatter of turbulence energy and scalar variance from random subgrid-scale fluxes", Proc. R. Soc. Lond. A**451**, 293 (1995).
[22] J.A. Domaradzki, E.M. Saiki, "Backscatter models for large eddy simulations", submitted to Phys. Fluids (1996)
[23] J. Bardina, J.H. Ferziger, and W.C. Reynolds, "Improved turbulence models based on large eddy simulation of homogeneous incompressible turbulence", Stanford University, Report TF-19, 1983.
[24] S. Liu, C. Meneveau, and J. Katz, "On the properties of similarity subgrid-scale models as deduced from measurements in a turbulent jet", J. Fluid Mech. **275**, 83 (1994).
[25] U. Piomelli, P. Moin, and J.H. Ferziger, "Model consistency in large eddy simulation of turbulent channel flow", Phys. Fluids **31**, 1884 (1988).
[26] Y. Zang, R.L. Street, and J.R. Koseff, "A dynamic mixed subgrid-scale model and its applications to turbulent recirculating flows", Phys. Fluids A**5**, 318 (1993).
[27] K. Horiuti, "The role of the Bardina model in large eddy simulation of turbulent channel flow", Phys. Fluids A **1**, 426 (1989).
[28] J.A. Domaradzki and R.S. Rogallo, "Local energy transfer and nonlocal interactions in homogeneous, isotropic turbulence", Phys. Fluids A **2**, 413 (1990).
[29] P.K. Yeung and J.G. Brasseur, "The response of isotropic turbulence to isotropic and anisotropic forcing at the large scales", Phys. Fluids A**3**, 413 (1991).
[30] K. Ohkitani and S. Kida, "Triad interactions in a forced turbulence", Phys. Fluids A **4**, 794 (1992).
[31] Y. Zhou, "Degrees of locality of energy transfer in the inertial range", Phys. Fluids A**5**, 1092 (1993).
[32] Y. Zhou, G. Vahala, "Reformulation of recursive-renormalization-group-based subgrid modeling of turbulence", Phys. Rev. E **47**, 2503 (1993).
[33] J.A. Domaradzki, W. Liu, C. Härtel, and L. Kleiser, "Energy Transfer in Numerically Simulated Wall-Bounded Turbulent Flows",
[34] J.A. Domaradzki and W. Liu, "Approximation of Subgrid-Scale Energy Transfer Based on the Dynamics of Resolved Scales of Turbulence", *Phys. Fluids* A **7**, 2025-2035 (1995).
[35] K.B. Shah and J.H. Ferziger, "A new non-eddy viscosity subgrid-scale model and its application to channel flow", in *Annual Research Briefs*, Center for Turbulence Research, NASA Ames - Stanford University, 73 (1995).
[36] J.M. McDonough and R.J. Bywater, "Turbulent solutions from an unaveraged, additive decomposition of Burgers' equation", in *Forum on Turbulent Flows-1989*, eds. W.W. Bower and M.J. Morris, ASME, FED **76**, 7 (1989).
[37] J. Jiménez, "Energy transfer and constrained simulations in isotropic turbulence",in *Annual Research Briefs*, Center for

Turbulence Research, NASA Ames - Stanford University, 171 (1993).
[38] G.K. Batchelor, "The theory of homogeneous turbulence", (Cambridge University Press, Cambridge, 1953), p. 113.
[39] M. Germano, "A proposal for a redefinition of the turbulent stresses in the filtered Navier-Stokes equations", Phys. Fluids **29**, 2323 (1986).
[40] C. Canuto, M.Y. Hussaini, A. Quarteroni, and T.A. Zang, "Spectral Methods in Fluid Dynamics", (Springer-Verlag, New York, 1988).
[41] D.C. Chan, "Effects of rotation on turbulent convection: direct numerical simulation using parallel computers", Ph.D. Thesis, University of Southern California, 1996.
[42] J. Kim and P. Moin, "Application of a fractional-step method to incompressible Navier-Stokes equations", J. Comput. Phys. **59**, 308 (1985).
[43] D.K. Lilly, "On the application of the eddy viscosity concept in the inertial sub-range of turbulence", NCAR manuscript 123, NCAR, Boulder, CO, 1966.
[44] J.W. Deardorff, "A numerical study of three-dimensional turbulent channel flow at large Reynolds numbers", J. Fluid Mech. **41**, 453 (1970).
[45] E.R. Van Driest, "On the turbulent flow near a wall", J. Aerospace Sci. **23**, 1007 (1956).
[46] P. Moin and J. Kim, "Numerical investigation of turbulent channel flow", J. Fluid Mech. **118**, 341 (1982).
[47] N. Gilbert, "Numerische Simulation der Transition von der laminaren in die turbulente Kanalströmung", DFVLR-Forschungsbericht 88-55, (DLR Göttingen, Germany, 1988).
[48] N. Gilbert and L. Kleiser, "Turbulence model testing with the aid of direct numerical simulation results", in *Proceedings of 8th Symposium on Turbulent Shear Flows*, (Munich, 1991).
[49] J. Kim, P. Moin, R.D. Moser, "Turbulence statistics in fully developed channel flow at low Reynolds number", J. Fluid Mech. **177**, 133 (1987).
[50] K. Nishino and N. Kasagi, "Turbulence statistics measurements in a two-dimensional channel flow using a three-dimensional particle tracing velocimeter", in *Proc. 7th Symposium on Turbulent Shear Flows*, (Stanford University, U.S.A., 1989).
[51] U. Piomelli, "High Reynolds number calculations using the dynamic subgrid-scale model", Phys. Fluids A**5**, 1484 (1993).
[52] T. Wei and W.W. Willmarth, "Reynolds-number effects on the structure of a turbulent channel flow", J. Fluid Mech. **204**, 57 (1989).
[53] F.M. Najjar and D.K. Tafti, "Study of discrete test filters and finite difference approximations for the dynamic subgrid-scale models", Phys. Fluids **8**, 1076 (1996).

FIG. 1. The plane averaged components of the SGS stress tensor modified by subtracting $\frac{1}{3}\delta_{ij}\tau_{kk}$. Solid line: DNS; dashed line: the Smagorinsky model; dashed-dotted line: the velocity estimation model. (a) $< \tau_{11} - \frac{1}{3}\tau_{kk} >$; (b) $< \tau_{22} - \frac{1}{3}\tau_{kk} >$; (c) $< \tau_{33} - \frac{1}{3}\tau_{kk} >$; (d) $< \tau_{13} >$.

FIG. 2. The plane averaged components of the SGS force (41). Solid line: DNS; dashed line: the Smagorinsky model; dashed-dotted line: the velocity estimation model. (a) $< \frac{\partial}{\partial x_j}(\tau_{1j} - \frac{1}{3}\delta_{1j}\tau_{kk}) >$; (b) $< \frac{\partial}{\partial x_j}(\tau_{3j} - \frac{1}{3}\delta_{3j}\tau_{kk}) >$.

FIG. 3. SGS dissipation. Solid line: DNS; dashed line: the Smagorinsky model; dashed-dotted line: the velocity estimation model. (a) The local SGS dissipation averaged over horizontal planes. (b) Negative values of the local SGS dissipation (forward transfer) and positive values (backscatter) averaged over horizontal planes.

FIG. 4. The plane correlation coefficients between the DNS and modeled components of τ_{13}. Solid line: the Smagorinsky model; dashed-dotted line: the velocity estimation model.

FIG. 5. The plane correlation coefficients between the SGS stress component τ_{13} and the resolved rate-of-strain tensor component $\overline{S}_{13}$. Solid line: DNS; dashed line: quantities modeled using the Smagorinsky model; dashed-dotted line: quantities modeled using the velocity estimation model.

FIG. 6. The SGS stress tensor modified by subtracting $\frac{1}{3}\delta_{ij}\tau_{kk}$. Solid line: DNS; dashed line: case S1; dashed-dotted-dotted line: case E1. (a) $< \tau_{11} - \frac{1}{3}\tau_{kk} >$; (b) $< \tau_{22} - \frac{1}{3}\tau_{kk} >$; (c) $< \tau_{33} - \frac{1}{3}\tau_{kk} >$; (d) $< \tau_{13} >$.

FIG. 7. The plane averaged components of the SGS force. Solid line: DNS; dashed line: case S1; dashed-dotted-dotted line: case E1. (a) $< \frac{\partial}{\partial x_j}(\tau_{1j} - \frac{1}{3}\delta_{1j}\tau_{kk}) >$; (b) $< \frac{\partial}{\partial x_j}(\tau_{3j} - \frac{1}{3}\delta_{3j}\tau_{kk}) >$.

FIG. 8. SGS dissipation. Solid line: DNS; dashed line: case S1; dashed-dotted-dotted line: case E1. (a) The local SGS dissipation averaged over horizontal planes. (b) Negative values of the local SGS dissipation (forward transfer) and positive values (backscatter) averaged over horizontal planes.

FIG. 9. The plane correlation coefficients between the SGS stress component τ_{13} and the resolved rate-of-strain tensor component $\overline{S}_{13}$. Solid line: DNS; dashed line: case S1; dashed-dotted-dotted line: case E1.

FIG. 10. Mean velocity profiles. Solid line: DNS; dashed line: case S1; dashed-dotted-dotted line: case E1; dotted line: case A; dashed-dotted line: $u^+ = 2.5\ln(z^+) + 5.5$; long dashed line: $u^+ = z^+$.

FIG. 11. Rms turbulent velocity. Solid line: DNS (filtered); dashed-dotted line: DNS (unfiltered); dashed line: case S1; dashed-dotted-dotted line: case E1; dotted line: case A. (a) Streamwise component u_{rms}. (b) Spanwise component v_{rms}. (c) Wall-normal component w_{rms}.

FIG. 12. Mean velocity profiles. Solid line: Piomelli (1993); dashed line: S2; dashed-dotted-dotted line: E2; dashed-dotted line: $u^+ = 2.5\ln(z^+) + 5.5$; long dashed line: $u^+ = z^+$.

FIG. 13. Rms turbulent velocity. Solid line: Piomelli (1993); dashed line: S2; dashed-dotted-dotted line: E2. (a) Streamwise component u_{rms}. (b) Spanwise component v_{rms}. (c) Wall-normal component w_{rms}.

FIG. 14. The decomposition of SGS dissipation averaged over horizontal planes into forward transfer (negative values) and backscatter (positive values). Dashed line: case S2; dashed-dotted-dotted line: case E2. The peak in the forward transfer for case S2 is ≈ -256.

FIG. 15. Shear stress profiles. Solid line: Piomelli (1993); dashed line: case S2; dashed-dotted-dotted line: case E2. (a) SGS stress component $< \tau_{13} >$. (b) Resolved stress component $< \overline{u}\,\overline{w} >$.

TABLE I. The global correlation coefficients between exact and modeled SGS quantities. EM-estimation model; EM1-estimation model with modified stresses $\tau_{ij} - \frac{1}{3}\delta_{ij}\tau_{kk}$; SM-Smagorinsky model.

Quantity	EM	EM1	SM
τ_{11}	0.53	0.52	0.12
τ_{12}	0.44	0.44	0.07
τ_{13}	0.51	0.51	0.31
τ_{22}	0.54	0.46	-0.003
τ_{23}	0.32	0.32	0.06
τ_{33}	0.52	0.55	0.16
N_1^{SGS}	0.15	0.14	0.13
N_2^{SGS}	0.12	-0.02	-0.02
N_3^{SGS}	0.25	0.43	0.12
T^{SGS}	0.15	0.14	0.1
ϵ_{SGS}	0.4	0.4	0.38

TABLE II. The parameters implemented in the numerical simulations

Case	Grid	Re_τ	time	Model
A	$32 \times 32 \times 65$	180	4.2	No model
S1	$32 \times 32 \times 65$	180	4.2	Smagorinsky
E1	$32 \times 32 \times 65$	180	4.2	Estimation
S2	$48 \times 64 \times 65$	1050	6.2	Smagorinsky
E2	$48 \times 64 \times 65$	1050	22.2	Estimation

TABLE III. The integrated values of SGS dissipation.

Case	Re_τ	$< \epsilon_{SGS}^- >$	$< \epsilon_{SGS}^+ >$	net
DNS	210	-8.3	0.7	-7.6
S1	180	-7.1	0.0	-7.1
E1	180	-6.8	1.8	-5.0
S2	1050	-22.7	0.0	-22.7
E2	1050	-16.9	6.3	-10.6

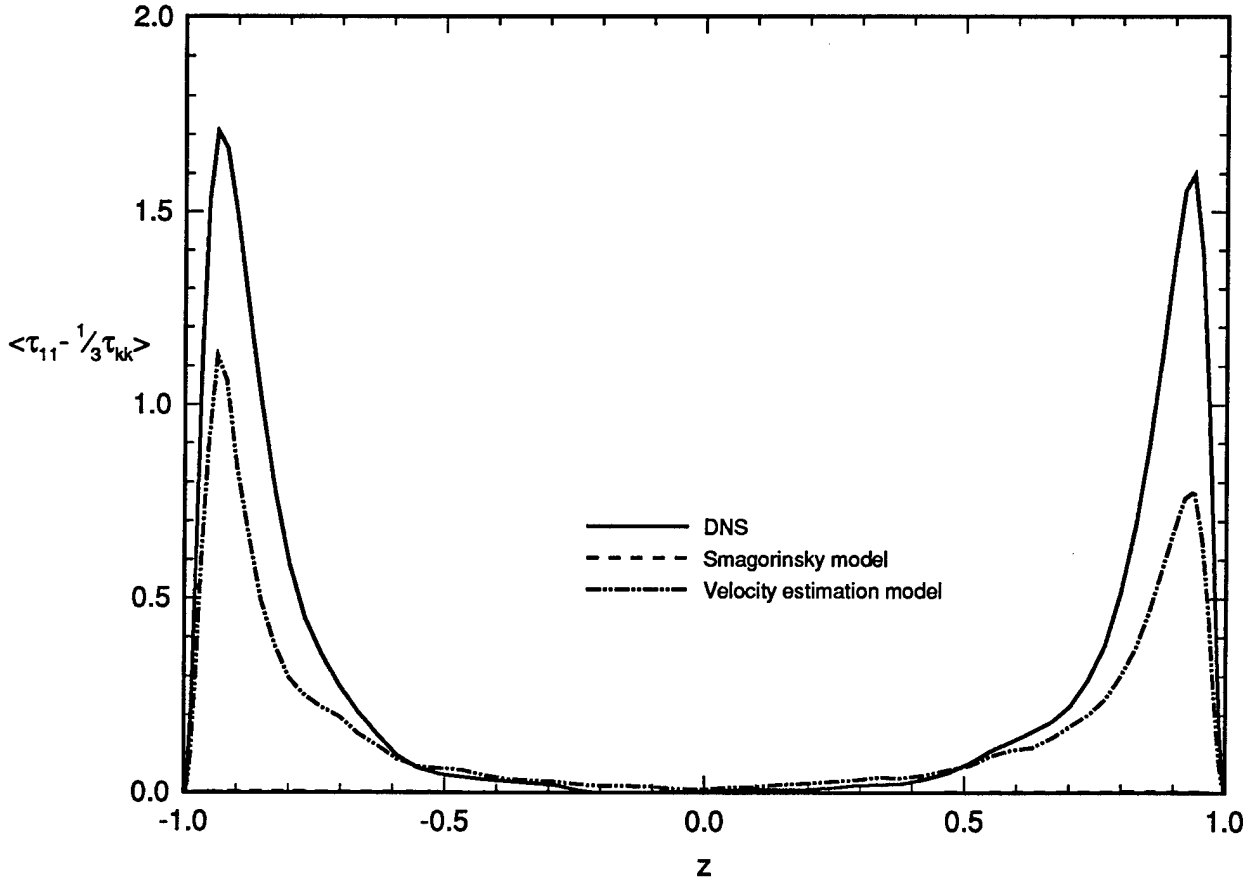

FIG. 1. The plane averaged components of the SGS stress tensor modified by subtracting $\frac{1}{3}\delta_{ij}\tau_{kk}$. Solid line: DNS; dashed line: the Smagorinsky model; dashed-dotted line: the velocity estimation model. (a) $< \tau_{11} - \frac{1}{3}\tau_{kk} >$; (b) $< \tau_{22} - \frac{1}{3}\tau_{kk} >$; (c) $< \tau_{33} - \frac{1}{3}\tau_{kk} >$; (d) $< \tau_{13} >$.

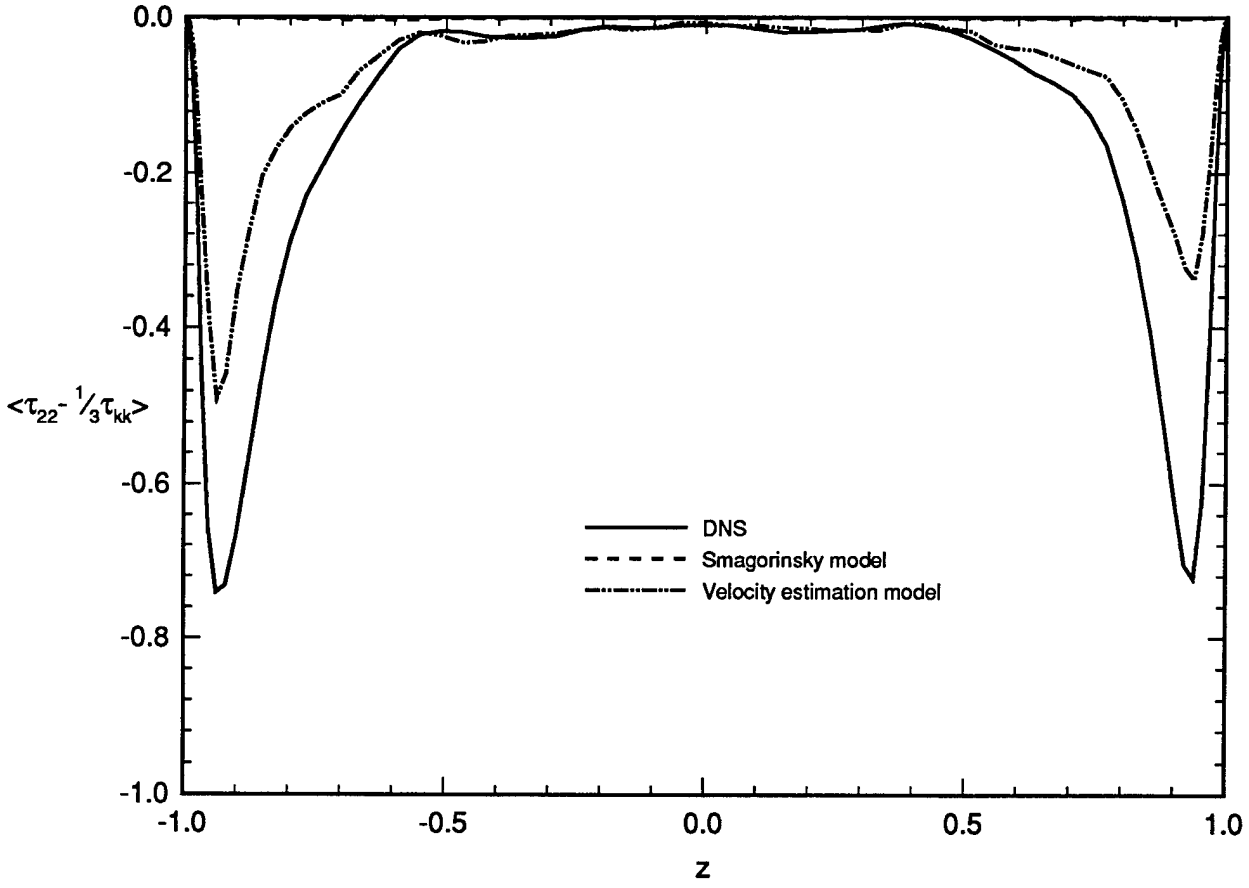
0.0
-0.2
-0.4
-0.6
-0.8
-1.0
-1.0
-0.5
0.0
0.5
1.0
z
<τ22- 1/3τkk>
DNS
Smagorinsky model
Velocity estimation model

FIG. 1(b)

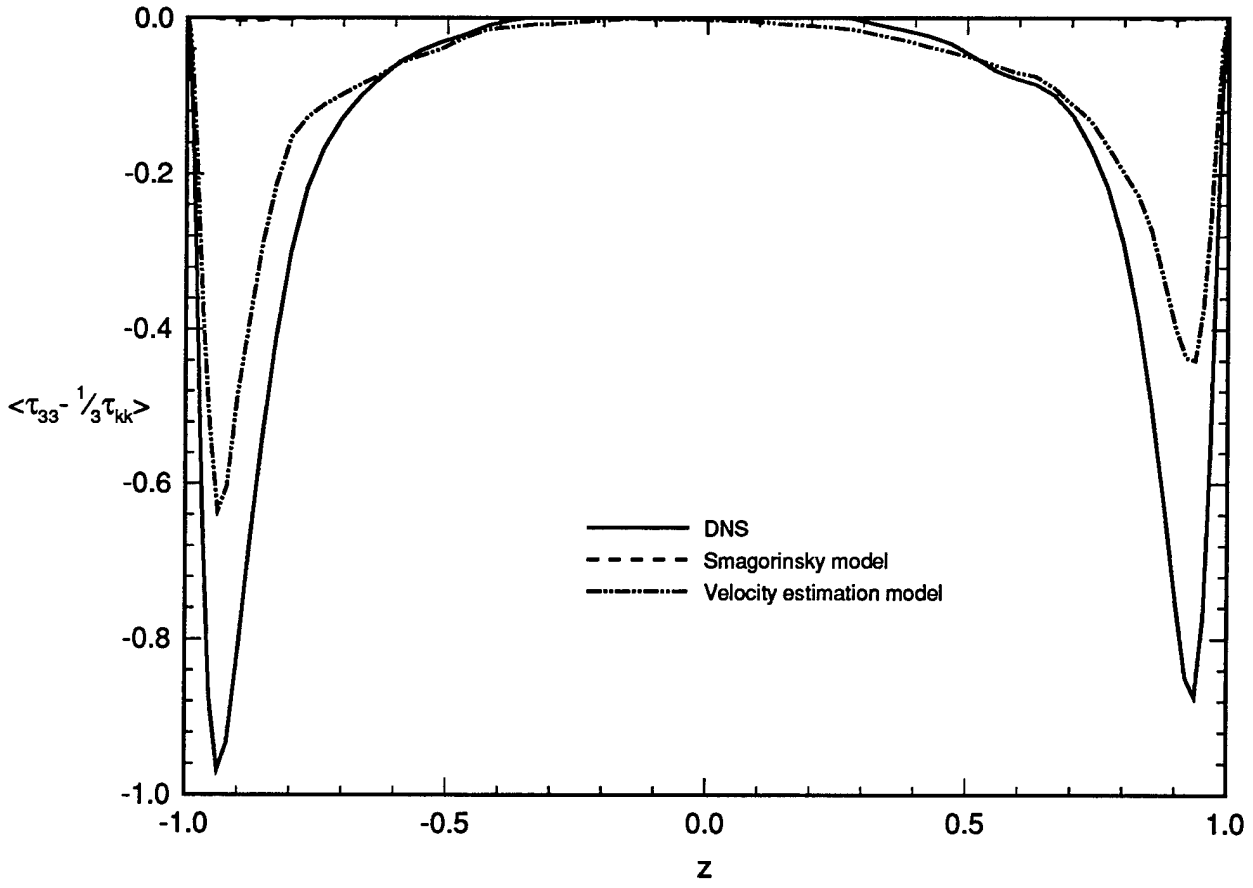
0.0
-0.2
-0.4
-0.6
-0.8
-1.0
-1.0
-0.5
0.0
0.5
1.0
z
<τ33- 1/3τkk>
DNS
Smagorinsky model
Velocity estimation model

FIG. 1(c)

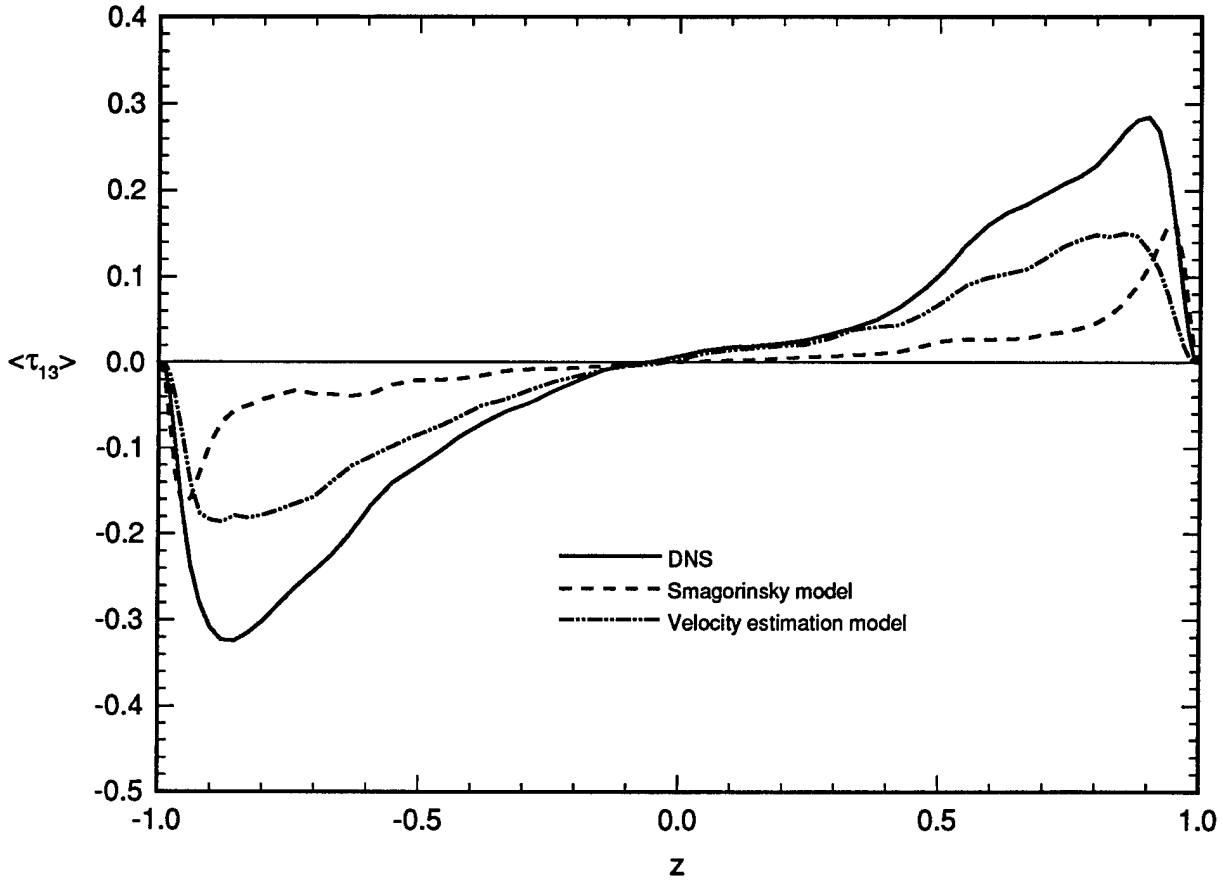
0.4
0.3
0.2
0.1
0.0
-0.1
-0.2
-0.3
-0.4
-0.5
<τ13>
-1.0
-0.5
0.0
0.5
1.0
z
DNS
Smagorinsky model
Velocity estimation model

FIG. 1(d)

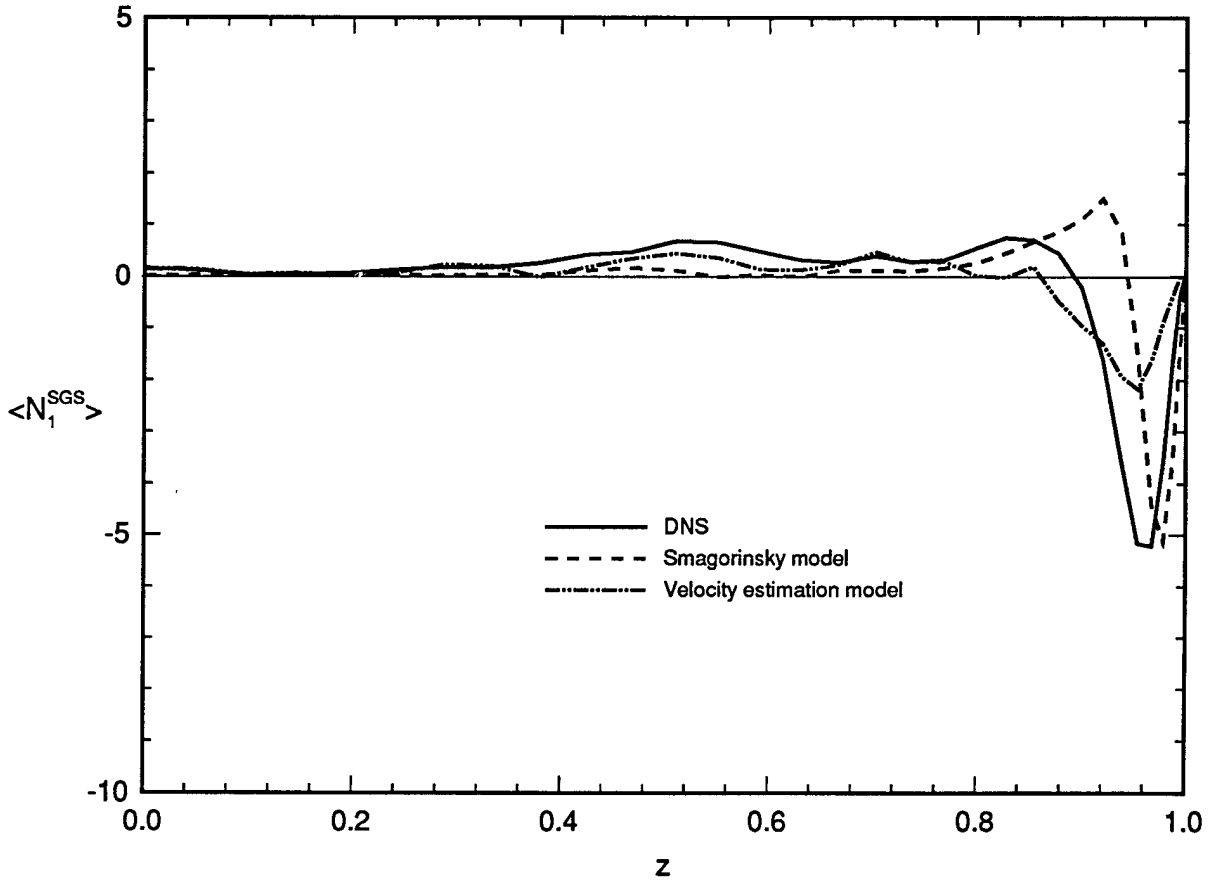

FIG. 2. The plane averaged components of the SGS force (41). Solid line: DNS; dashed line: the Smagorinsky model; dashed-dotted line: the velocity estimation model. (a) $< \frac{\partial}{\partial x_j}(\tau_{1j} - \frac{1}{3}\delta_{1j}\tau_{kk}) >$; (b) $< \frac{\partial}{\partial x_j}(\tau_{3j} - \frac{1}{3}\delta_{3j}\tau_{kk}) >$.

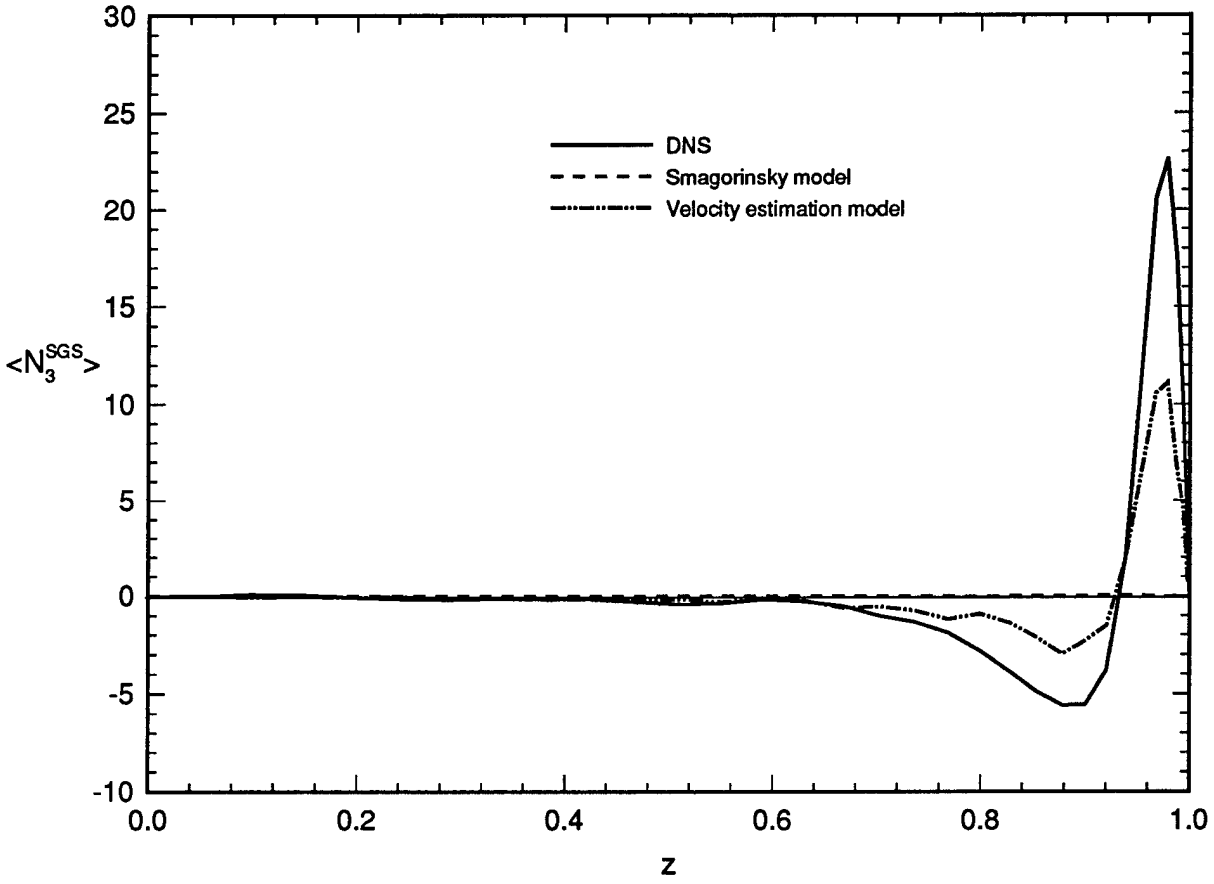
30
25
20
15
10
5
0
-5
-10
0.0
0.2
0.4
0.6
0.8
1.0
z
<N3SGS>
DNS
Smagorinsky model
Velocity estimation model

FIG. 2(b)

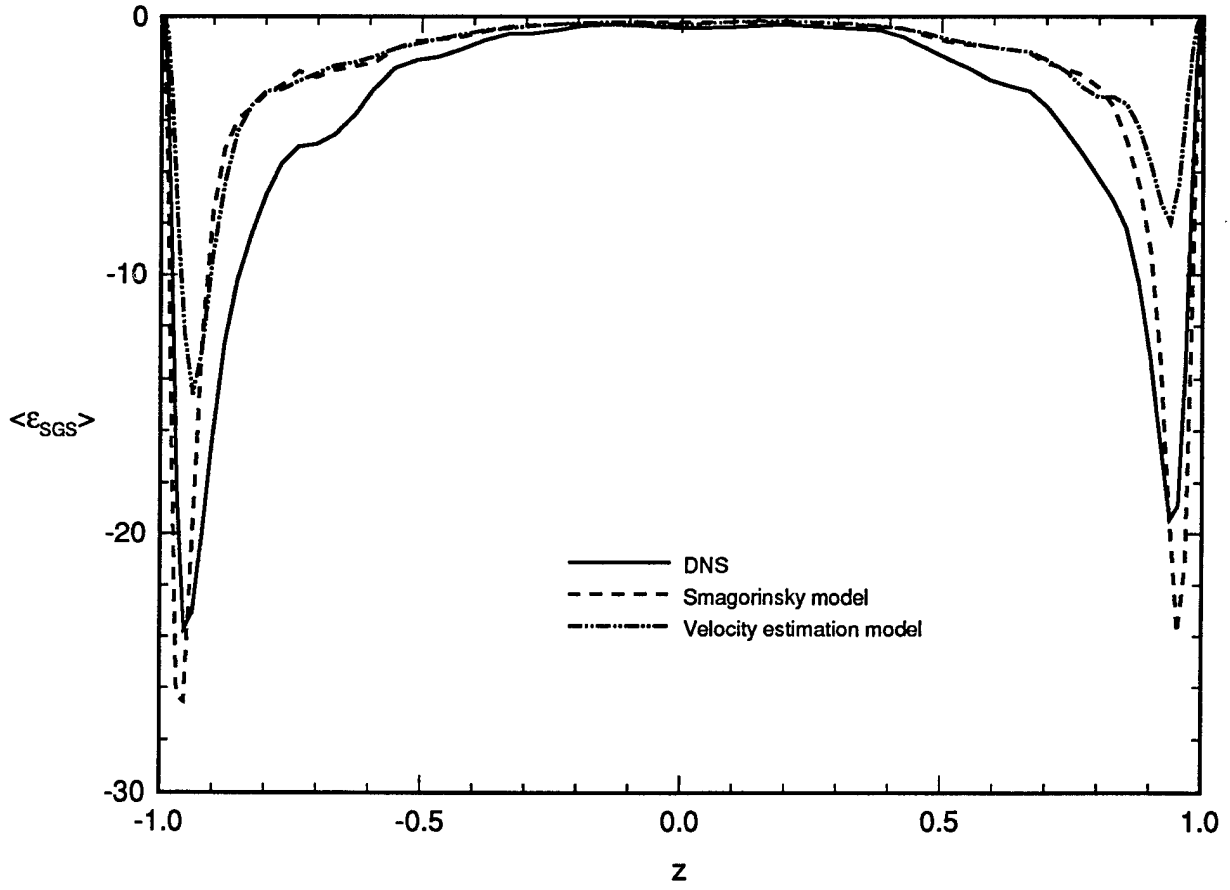

FIG. 3. SGS dissipation. Solid line: DNS; dashed line: the Smagorinsky model; dashed-dotted line: the velocity estimation model. (a) The local SGS dissipation averaged over horizontal planes. (b) Negative values of the local SGS dissipation (forward transfer) and positive values (backscatter) averaged over horizontal planes.

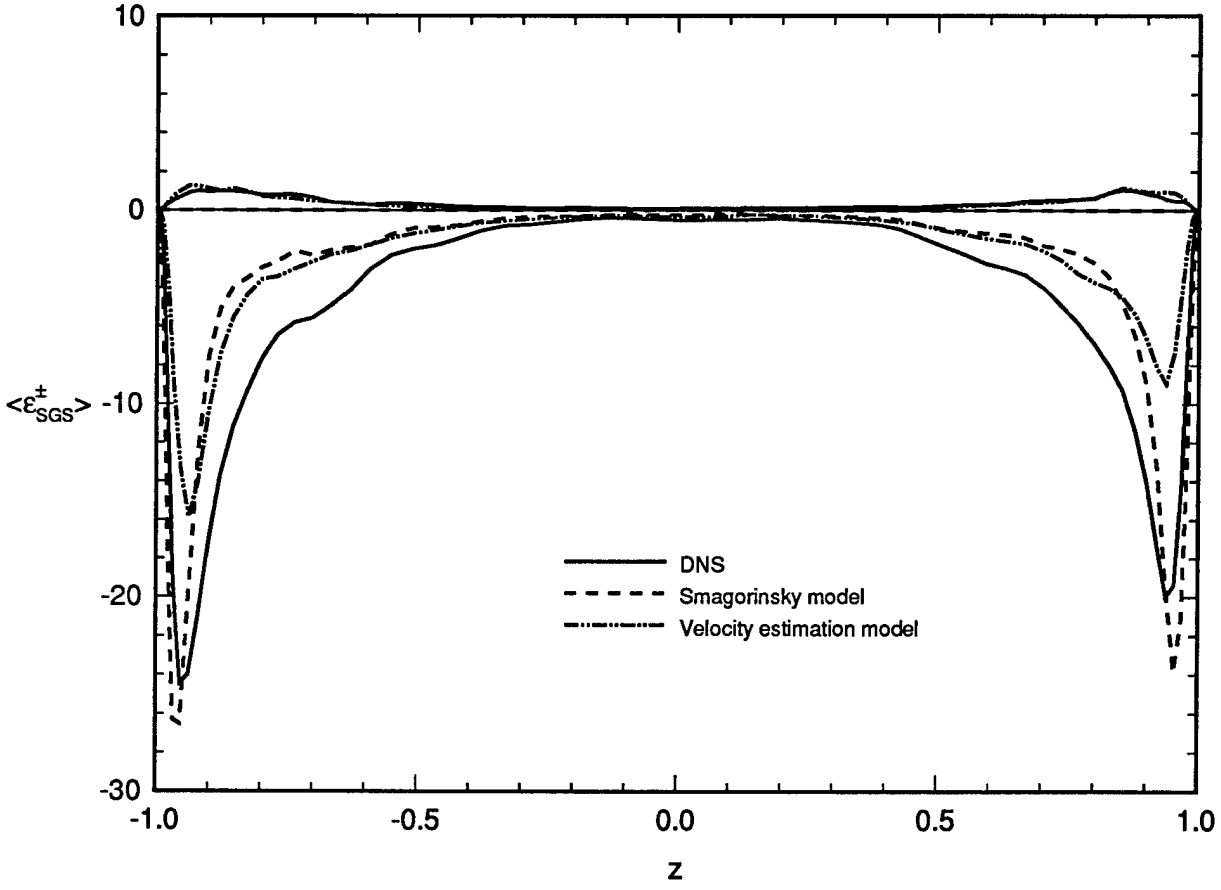
10
0
-10
-20
-30
-1.0
-0.5
0.0
0.5
1.0
z
$<\varepsilon^{\pm}_{SGS}>$
DNS
Smagorinsky model
Velocity estimation model

FIG. 3(b)

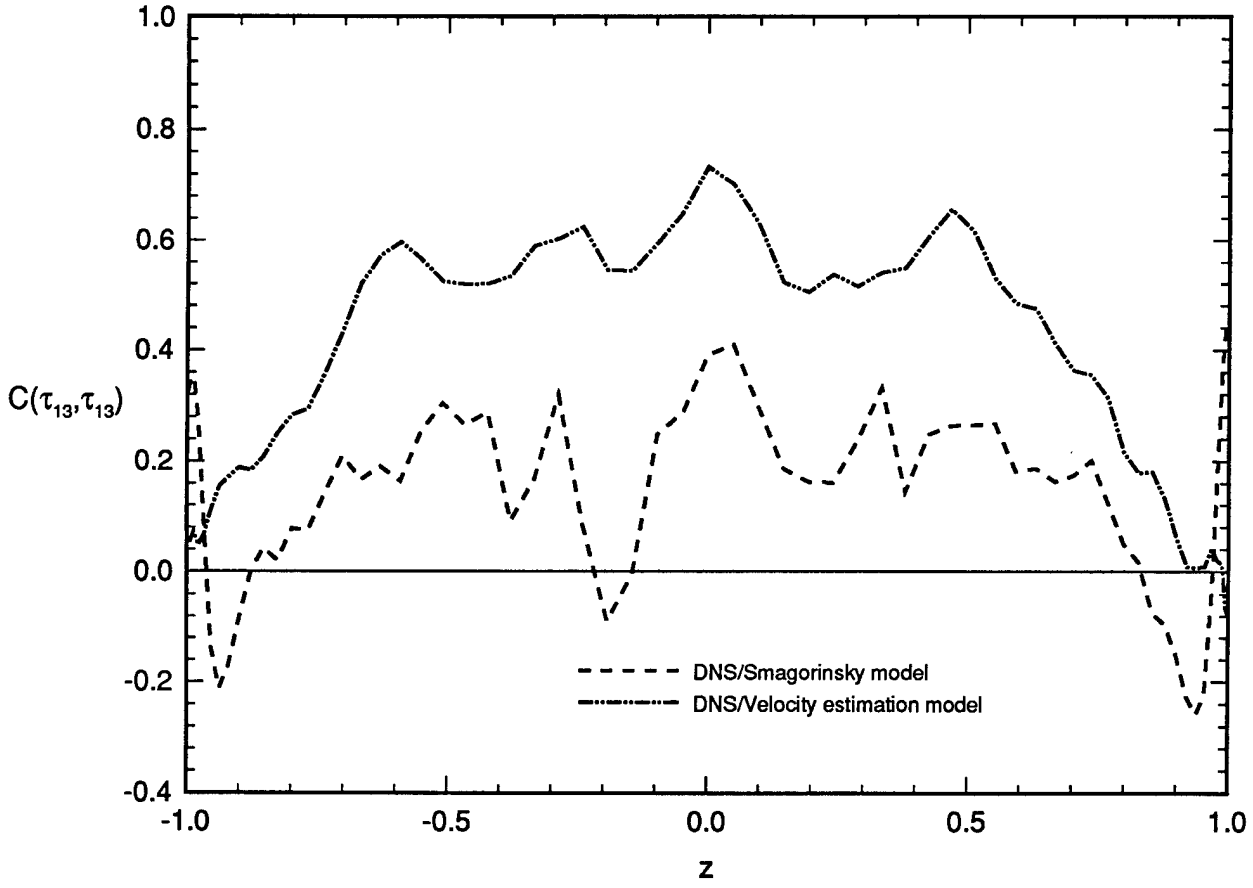

FIG. 4. The plane correlation coefficients between the DNS and modeled components of τ_{13}. Solid line: the Smagorinsky model; dashed-dotted line: the velocity estimation model.

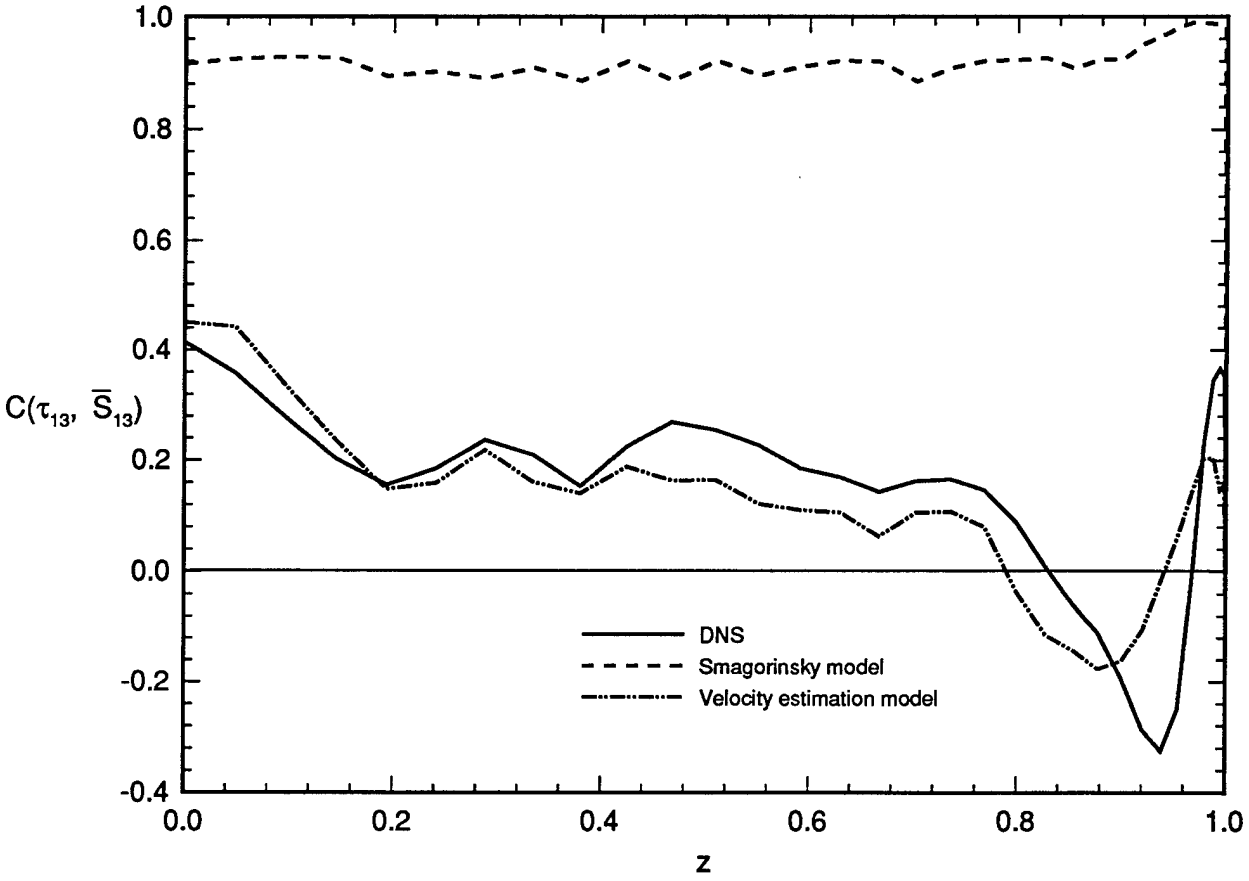

FIG. 5. The plane correlation coefficients between the SGS stress component τ_{13} and the resolved rate-of-strain tensor component $\overline{S}_{13}$. Solid line: DNS; dashed line: quantities modeled using the Smagorinsky model; dashed-dotted line: quantities modeled using the velocity estimation model.

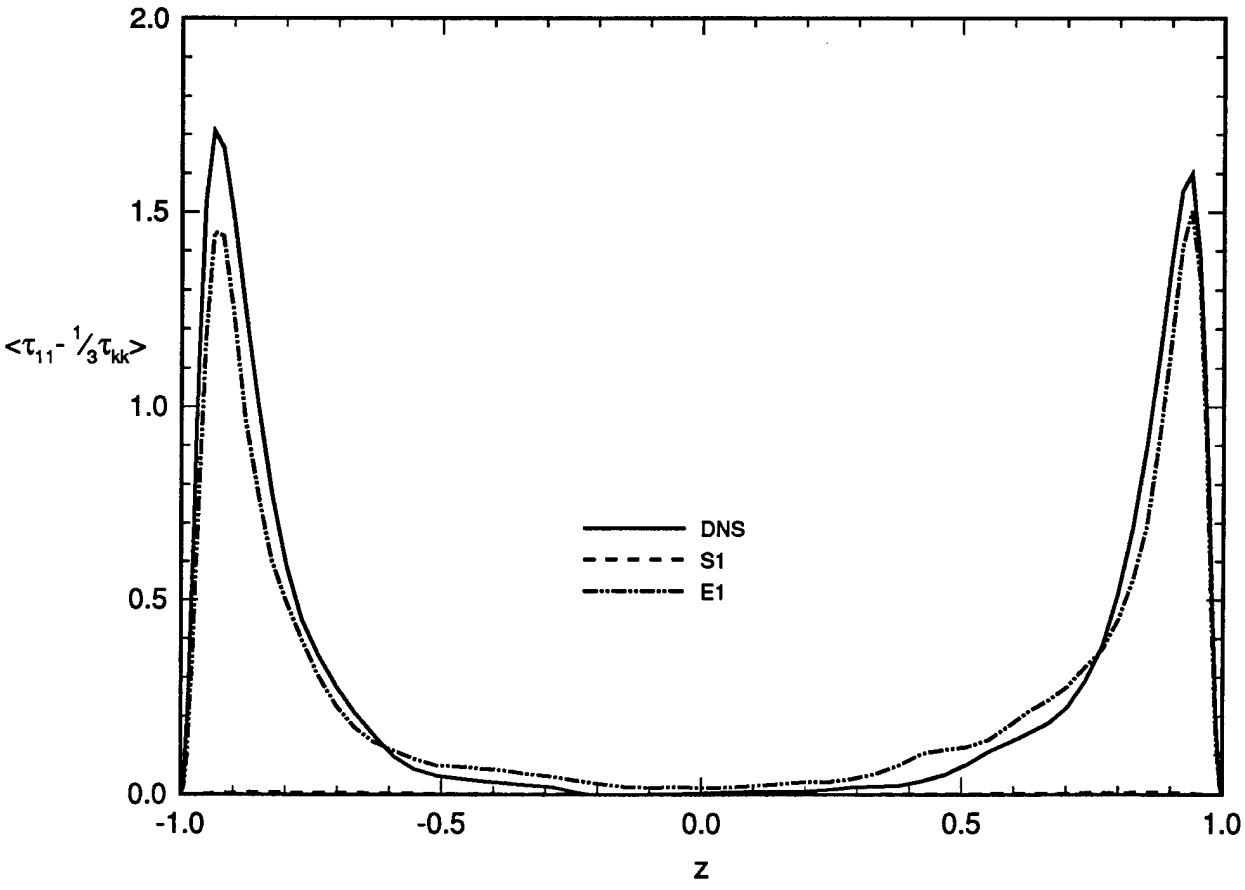

FIG. 6. The SGS stress tensor modified by subtracting $\frac{1}{3}\delta_{ij}\tau_{kk}$. Solid line: DNS; dashed line: case S1; dashed-dotted-dotted line: case E1. (a) $< \tau_{11} - \frac{1}{3}\tau_{kk} >$; (b) $< \tau_{22} - \frac{1}{3}\tau_{kk} >$; (c) $< \tau_{33} - \frac{1}{3}\tau_{kk} >$; (d) $< \tau_{13} >$.

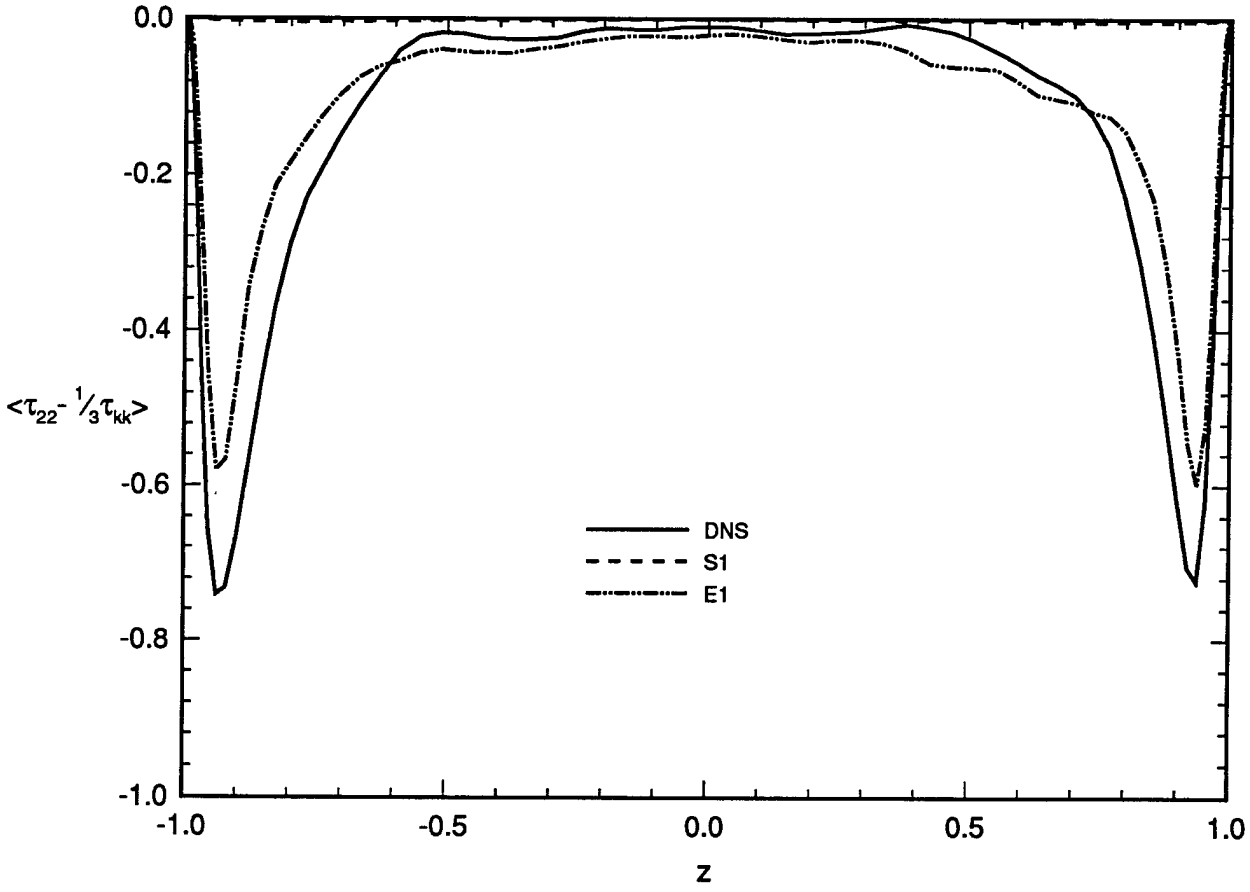

FIG. 6(b)

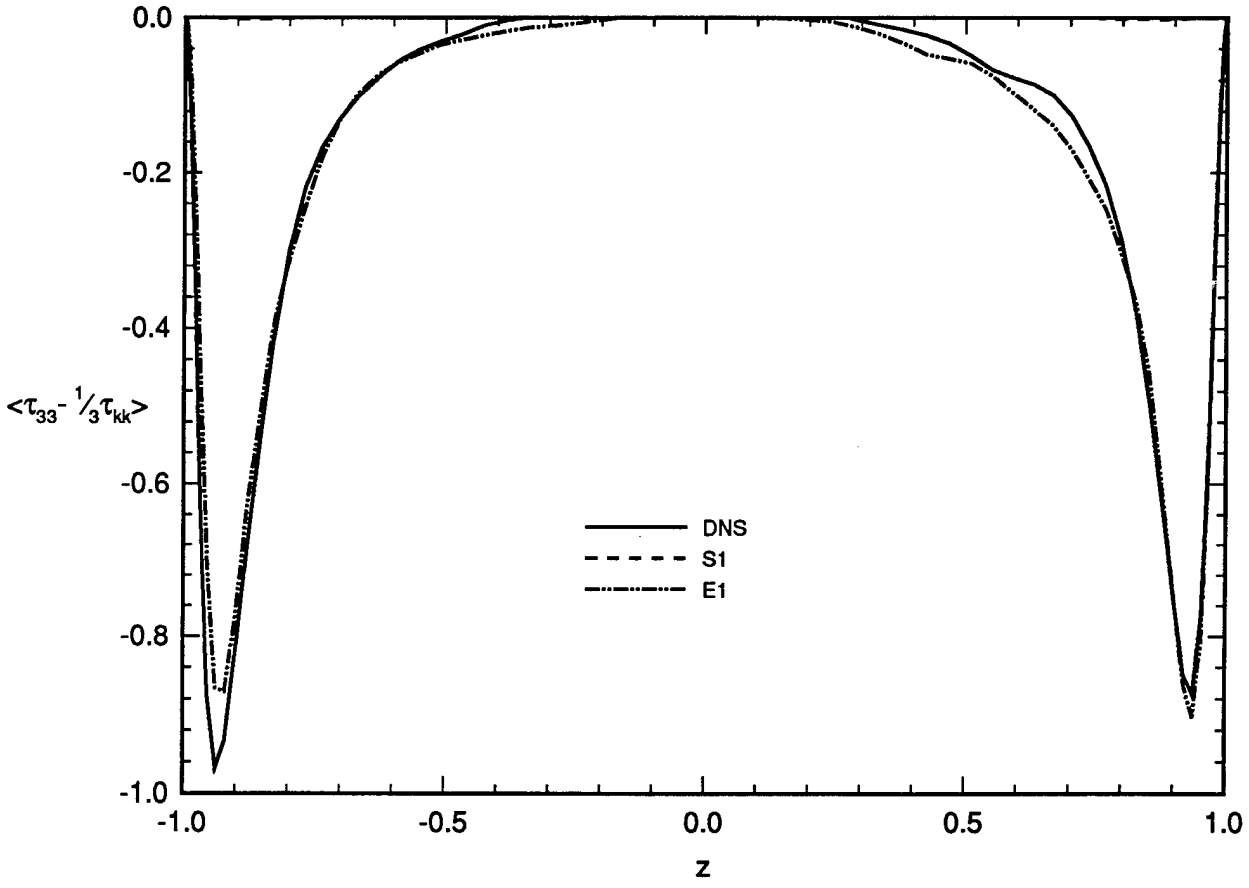

FIG. 6(c)

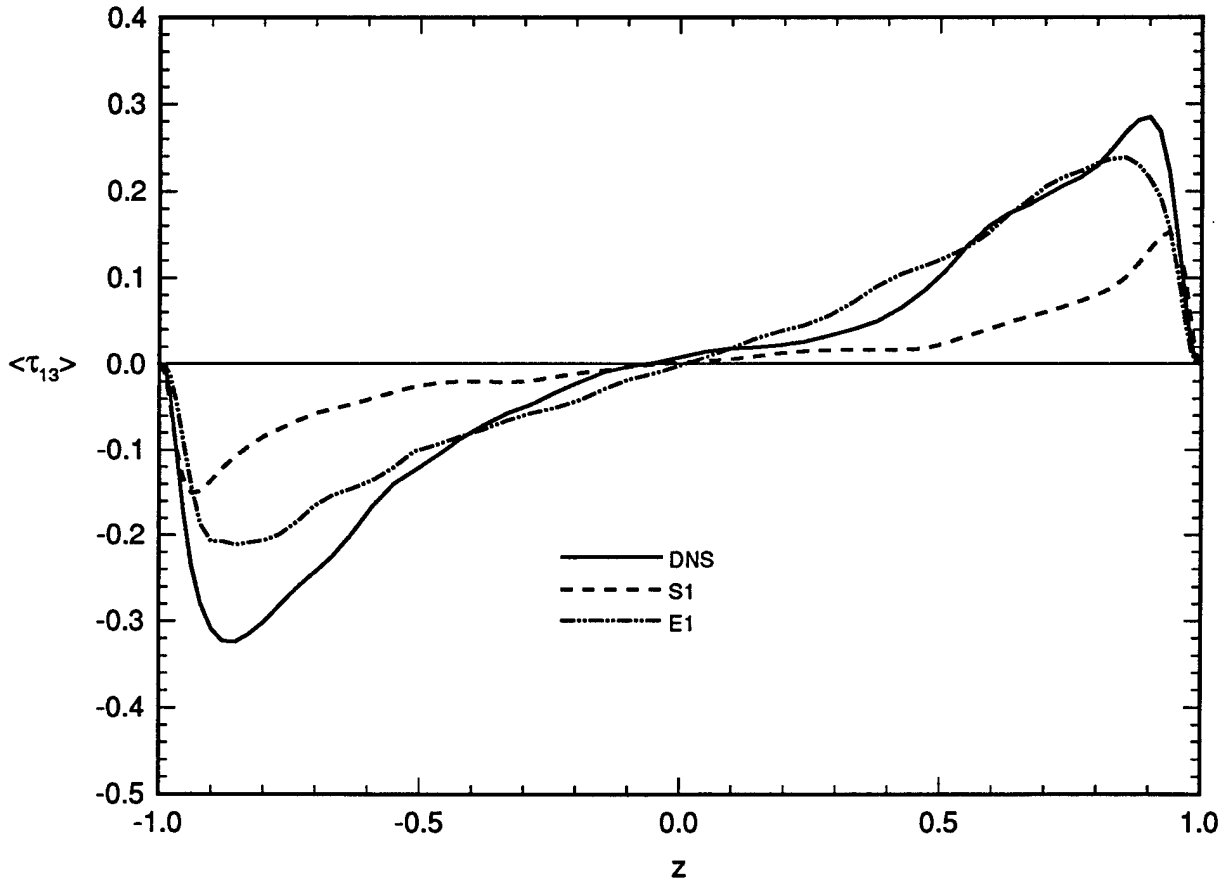

FIG. 6(d)

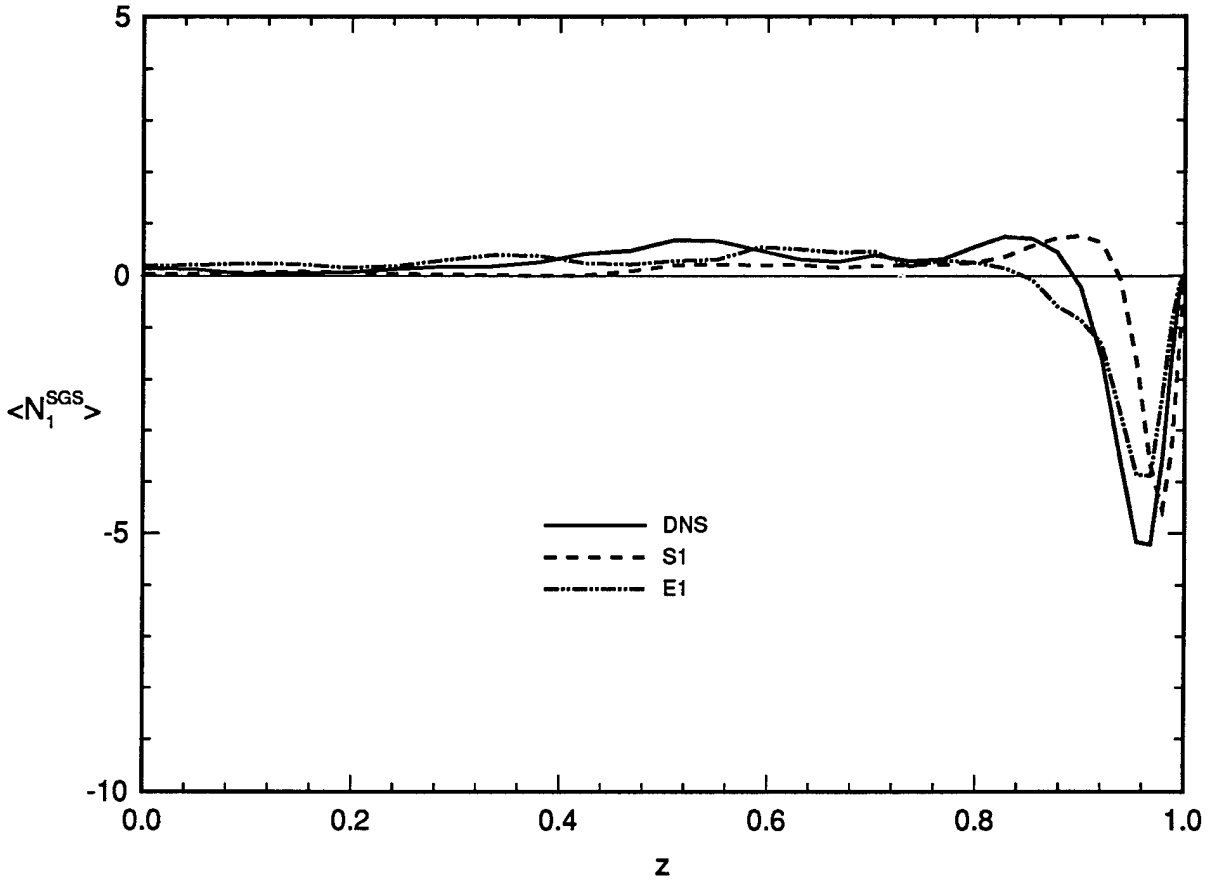

FIG. 7. The plane averaged components of the SGS force. Solid line: DNS; dashed line: case S1; dashed-dotted-dotted line: case E1. (a) $< \frac{\partial}{\partial x_j}(\tau_{1j} - \frac{1}{3}\delta_{1j}\tau_{kk}) >$; (b) $< \frac{\partial}{\partial x_j}(\tau_{3j} - \frac{1}{3}\delta_{3j}\tau_{kk}) >$.

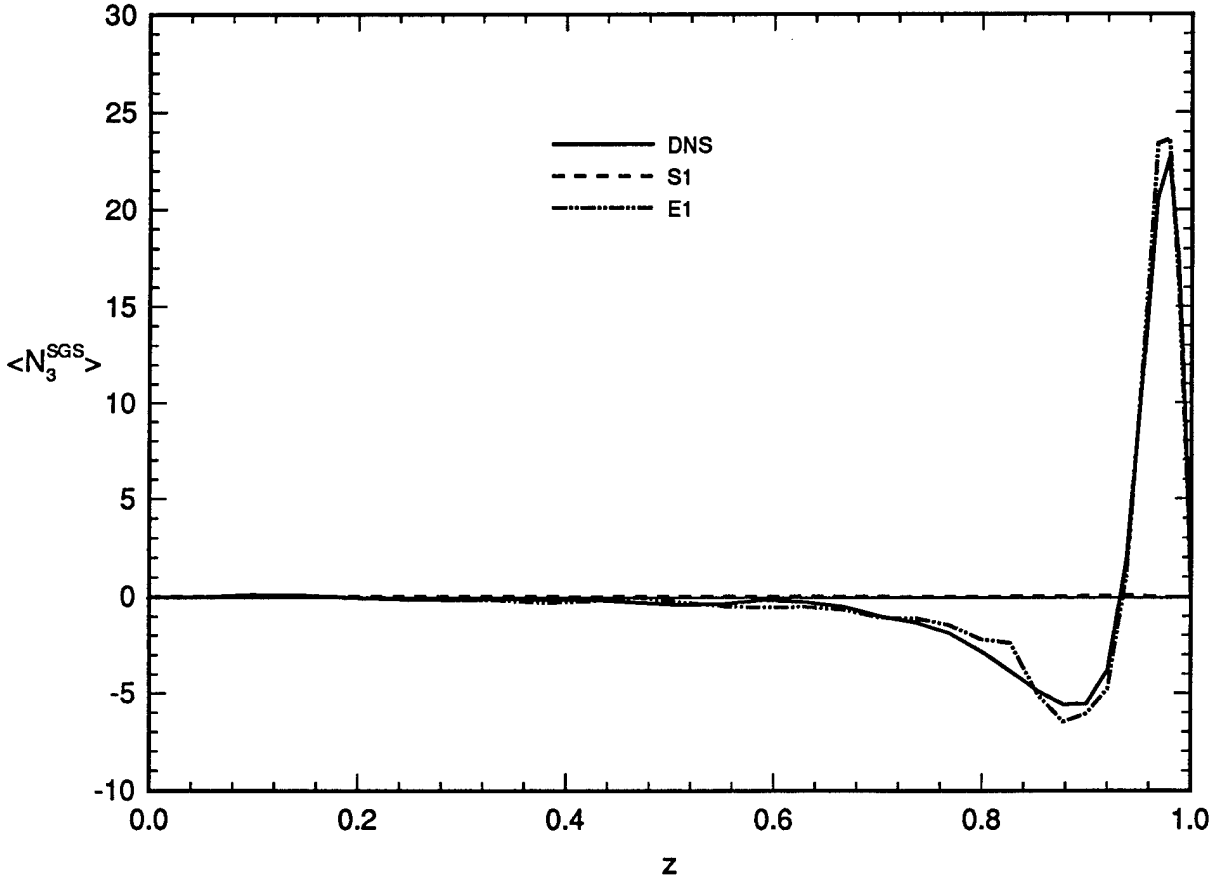

FIG. 7(b)

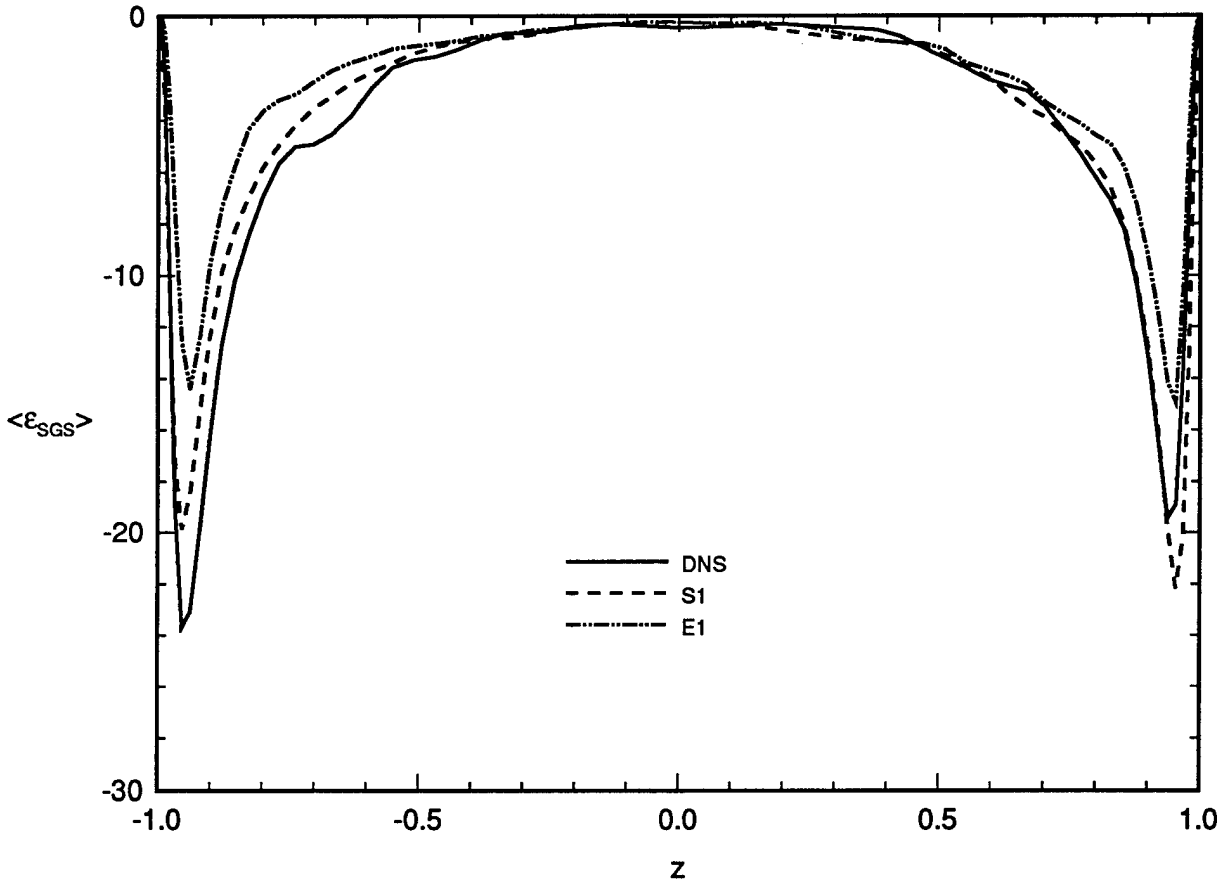

FIG. 8. SGS dissipation. Solid line: DNS; dashed line: case S1; dashed-dotted-dotted line: case E1. (a) The local SGS dissipation averaged over horizontal planes. (b) Negative values of the local SGS dissipation (forward transfer) and positive values (backscatter) averaged over horizontal planes.

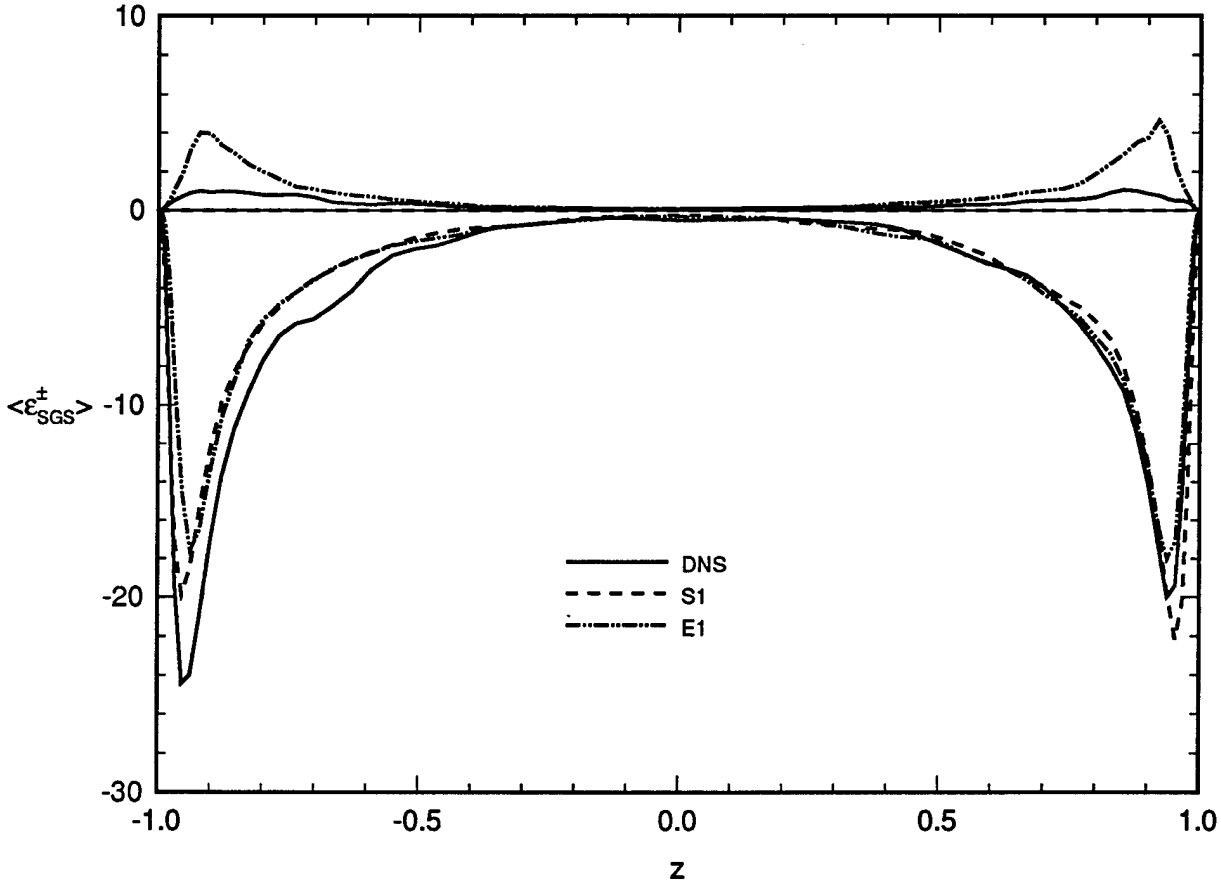
10
0
-10
-20
-30
$\langle \varepsilon^{\pm}_{SGS} \rangle$
-1.0
-0.5
0.0
0.5
1.0
z
DNS
S1
E1

FIG. 8(b)

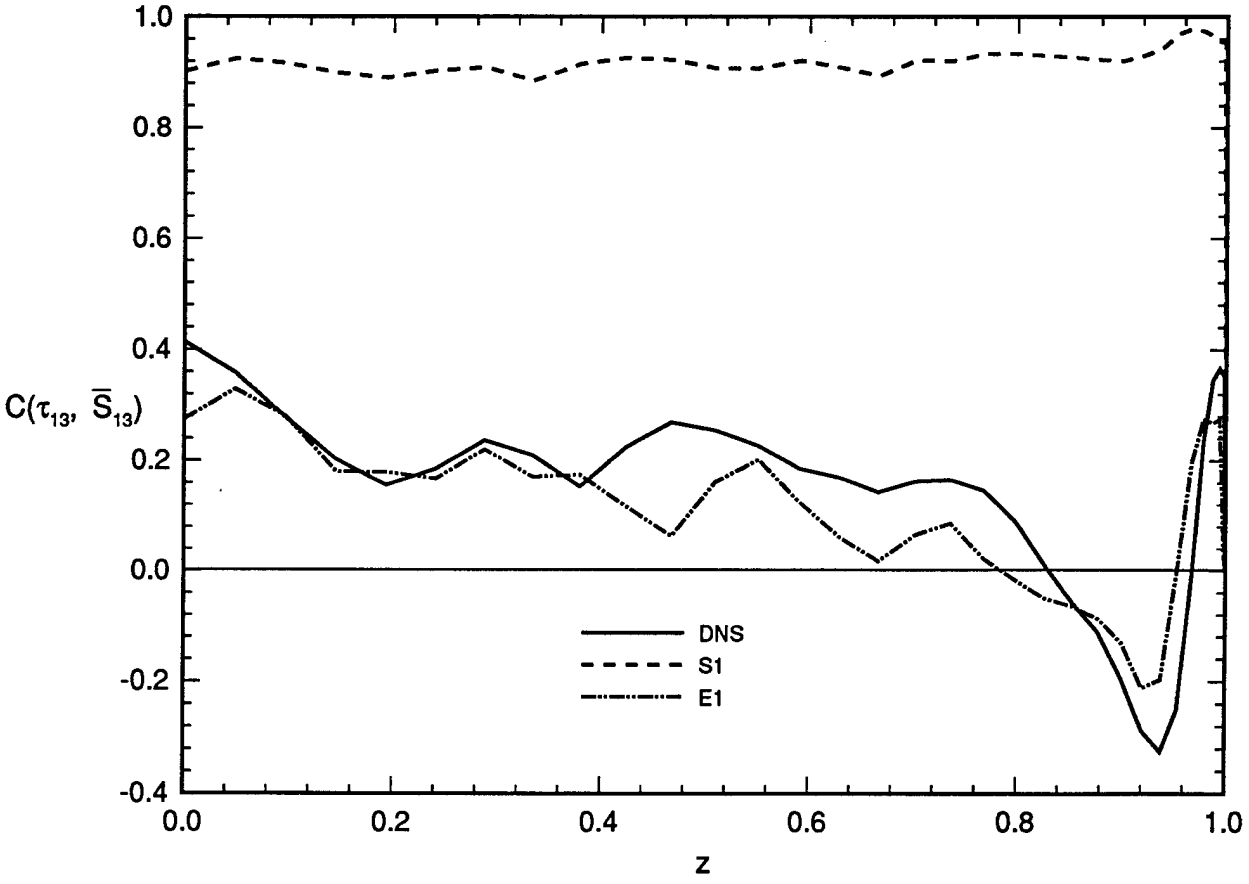

FIG. 9. The plane correlation coefficients between the SGS stress component τ_{13} and the resolved rate-of-strain tensor component $\overline{S}_{13}$. Solid line: DNS; dashed line: case S1; dashed-dotted-dotted line: case E1.

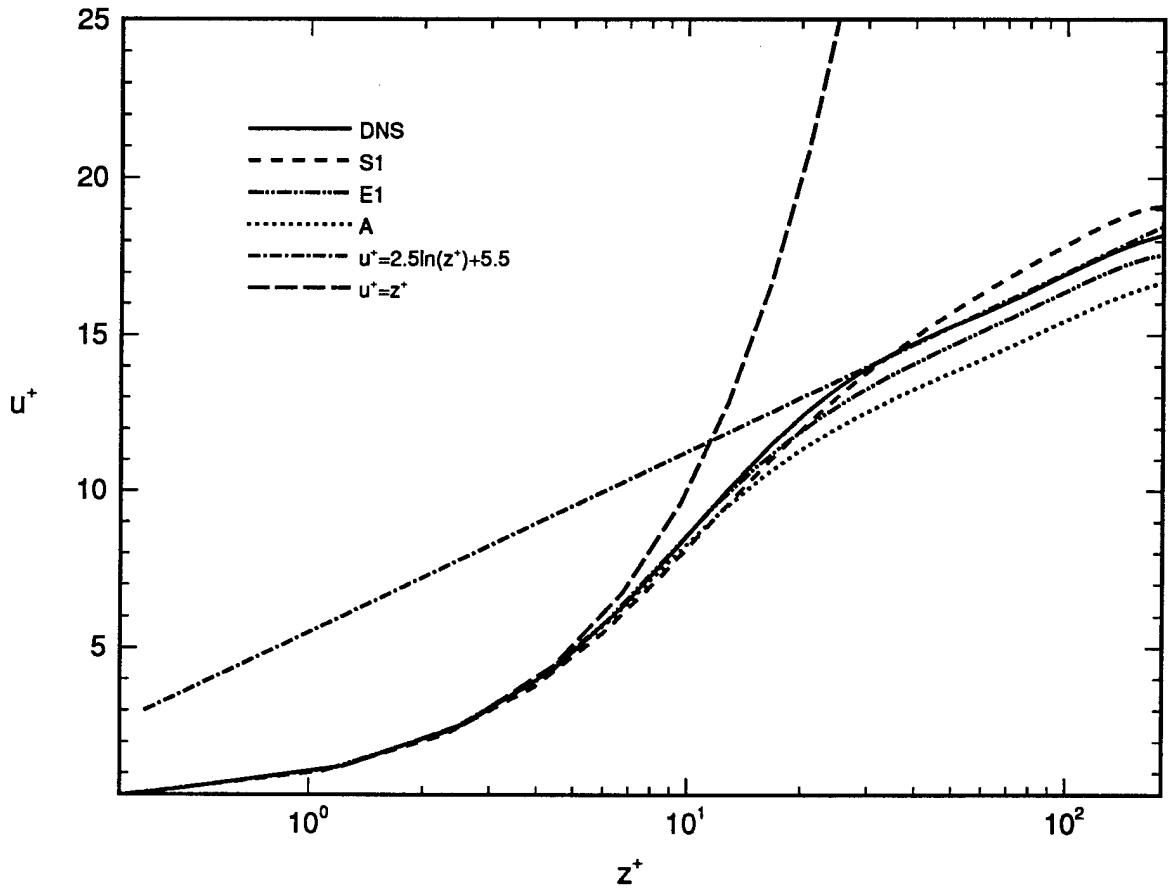

FIG. 10. Mean velocity profiles. Solid line: DNS; dashed line: case S1; dashed-dotted-dotted line: case E1; dotted line: case A; dashed-dotted line: $u^+ = 2.5\ln(z^+) + 5.5$; long dashed line: $u^+ = z^+$.

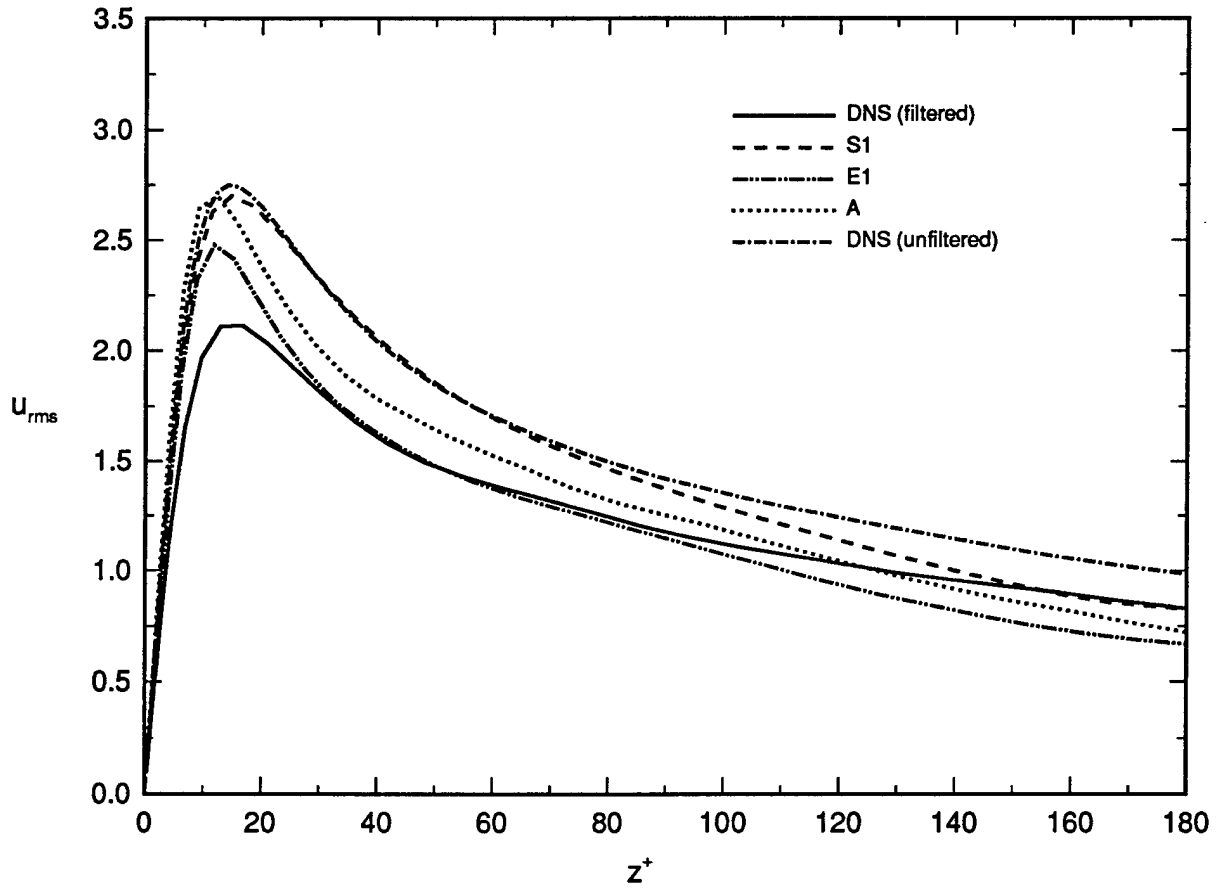

FIG. 11. Rms turbulent velocity. Solid line: DNS (filtered); dashed-dotted line: DNS (unfiltered); dashed line: case S1; dashed-dotted-dotted line: case E1; dotted line: case A. (a) Streamwise component u_{rms}. (b) Spanwise component v_{rms}. (c) Wall-normal component w_{rms}.

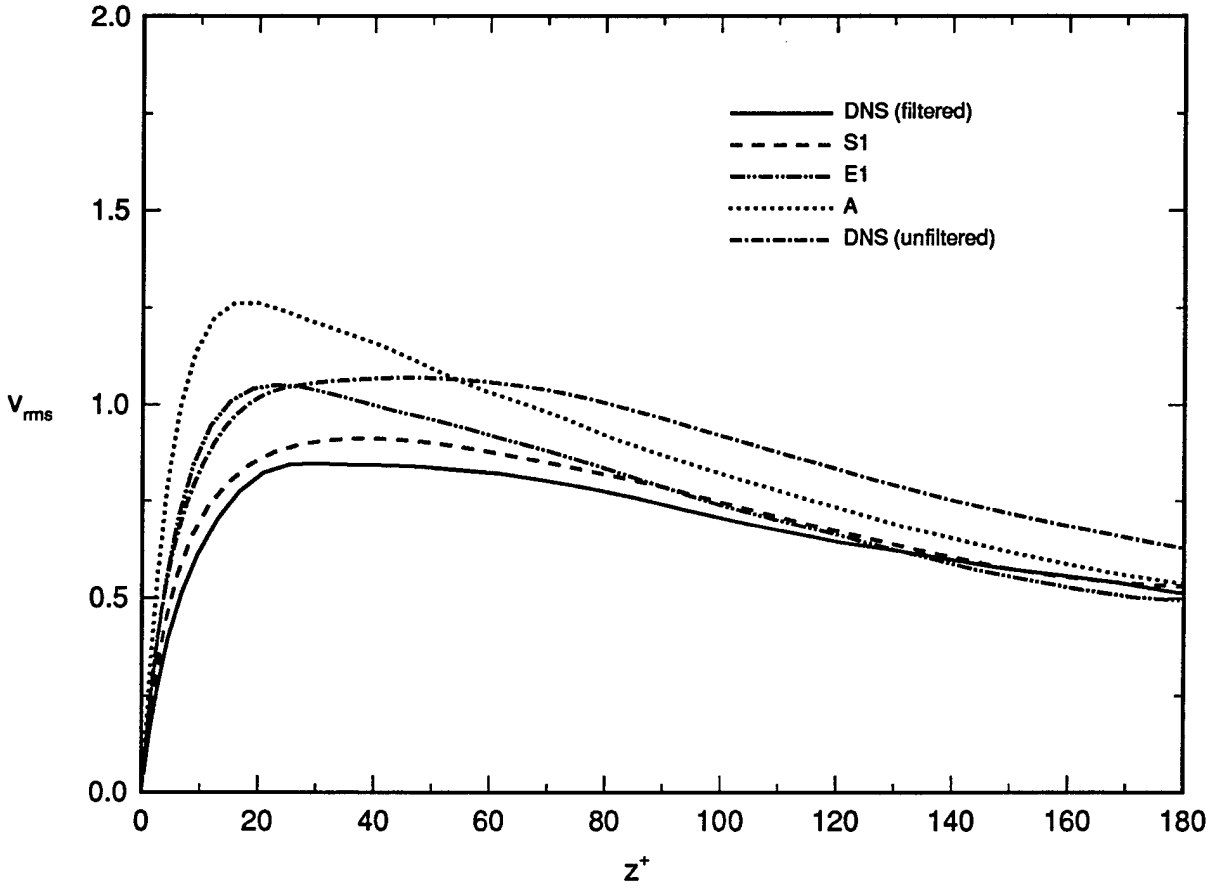
2.0
1.5
1.0
0.5
0.0
v_{rms}
0
20
40
60
80
100
120
140
160
180
z^+
DNS (filtered)
S1
E1
A
DNS (unfiltered)

FIG. 11(b)

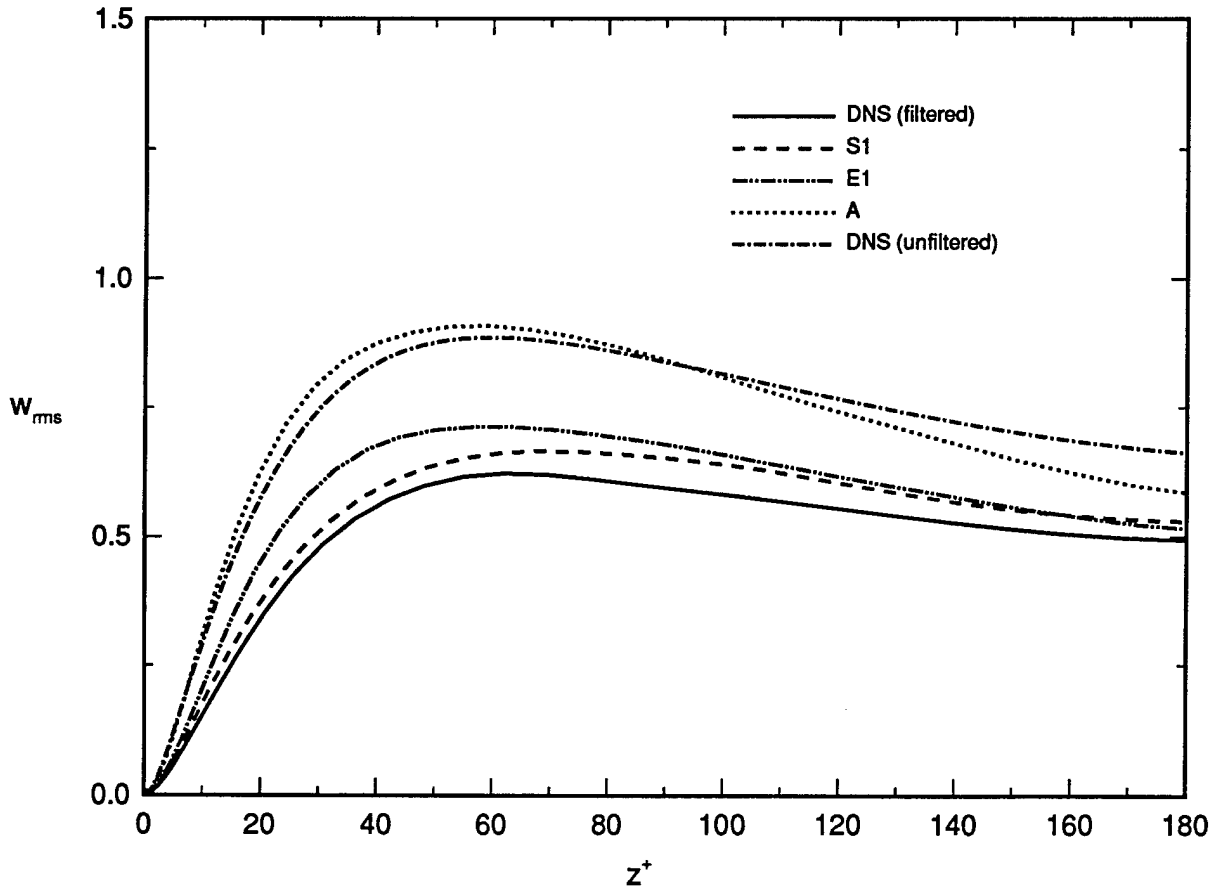
1.5
1.0
0.5
0.0
W_{rms}
0
20
40
60
80
100
120
140
160
180
z^+
DNS (filtered)
S1
E1
A
DNS (unfiltered)

FIG. 11(c)

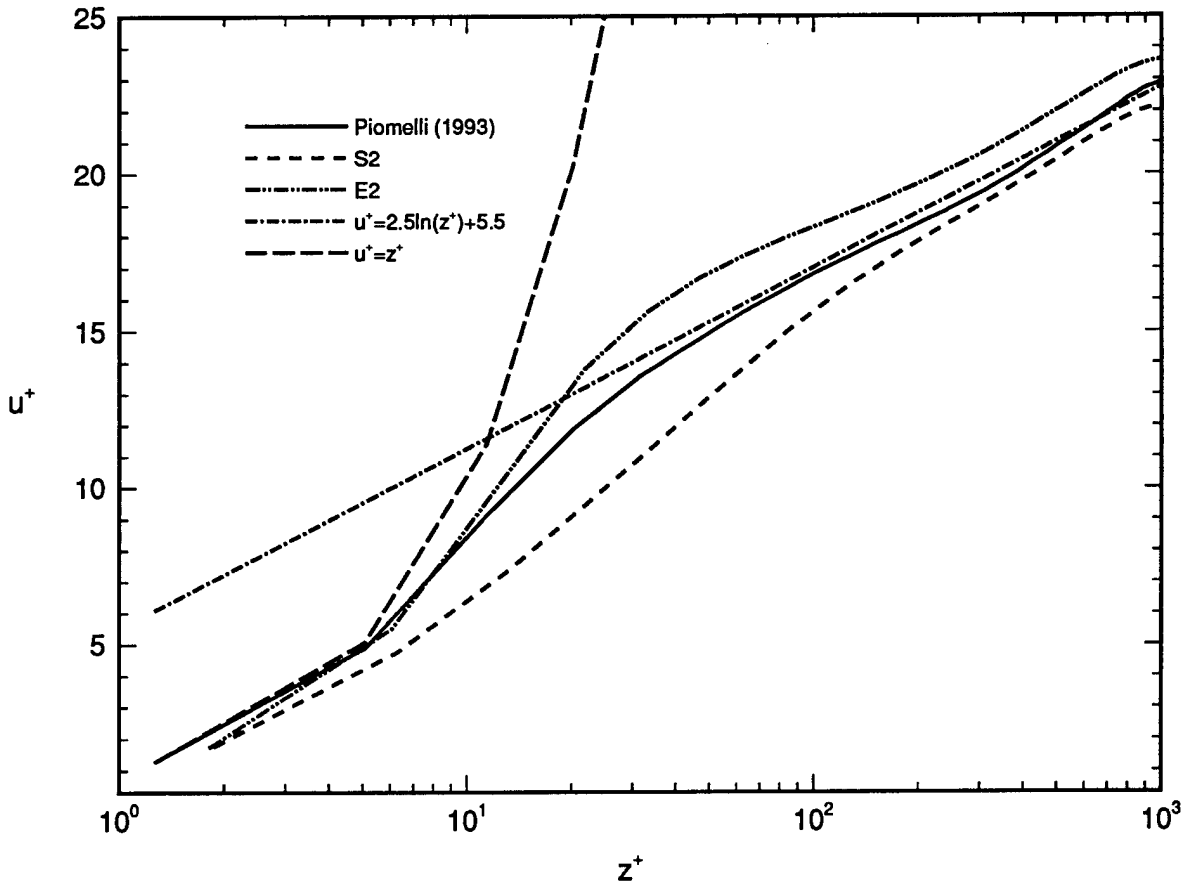

FIG. 12. Mean velocity profiles. Solid line: Piomelli (1993); dashed line: S2; dashed-dotted-dotted line: E2; dashed-dotted line: $u^+ = 2.5\ln(z^+) + 5.5$; long dashed line: $u^+ = z^+$.

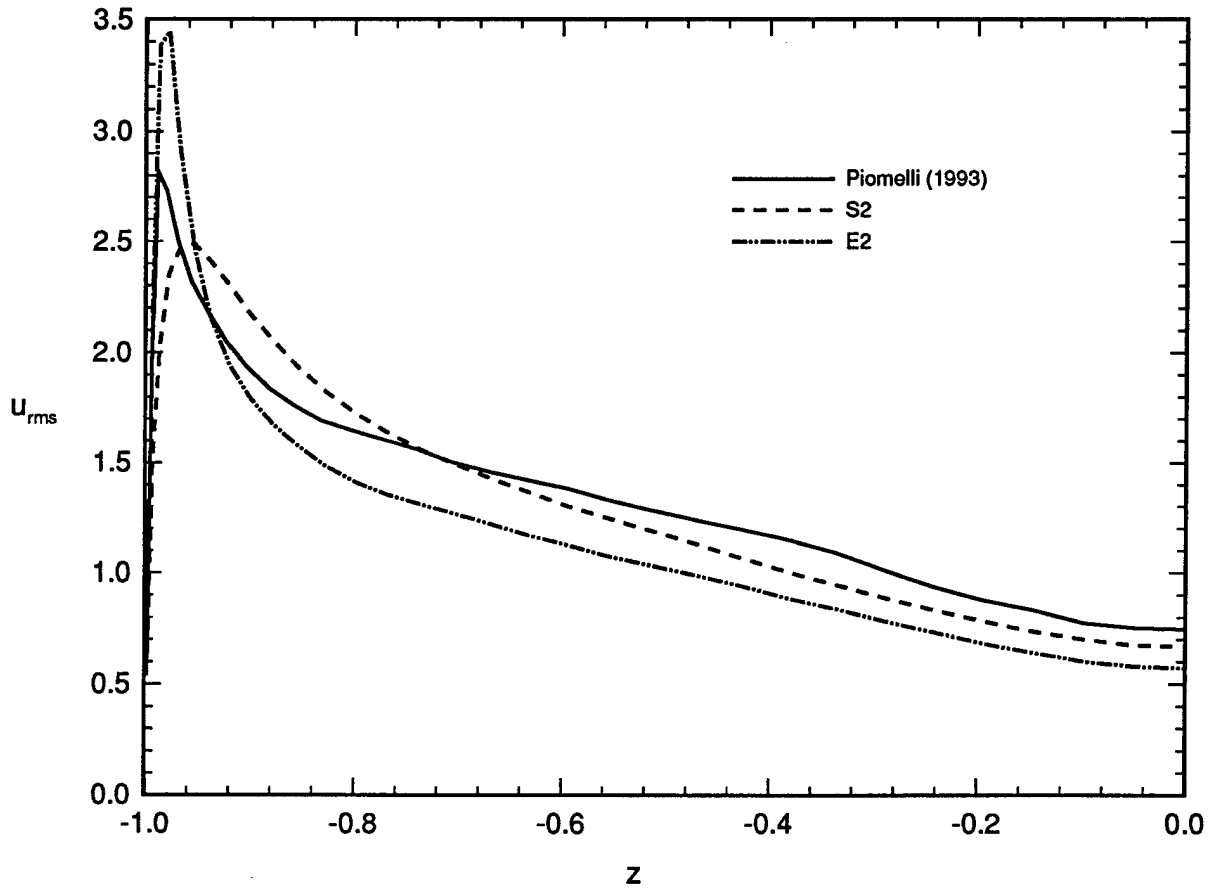

FIG. 13. Rms turbulent velocity. Solid line: Piomelli (1993); dashed line: S2; dashed-dotted-dotted line: E2. (a) Streamwise component u_{rms}. (b) Spanwise component v_{rms}. (c) Wall-normal component w_{rms}.

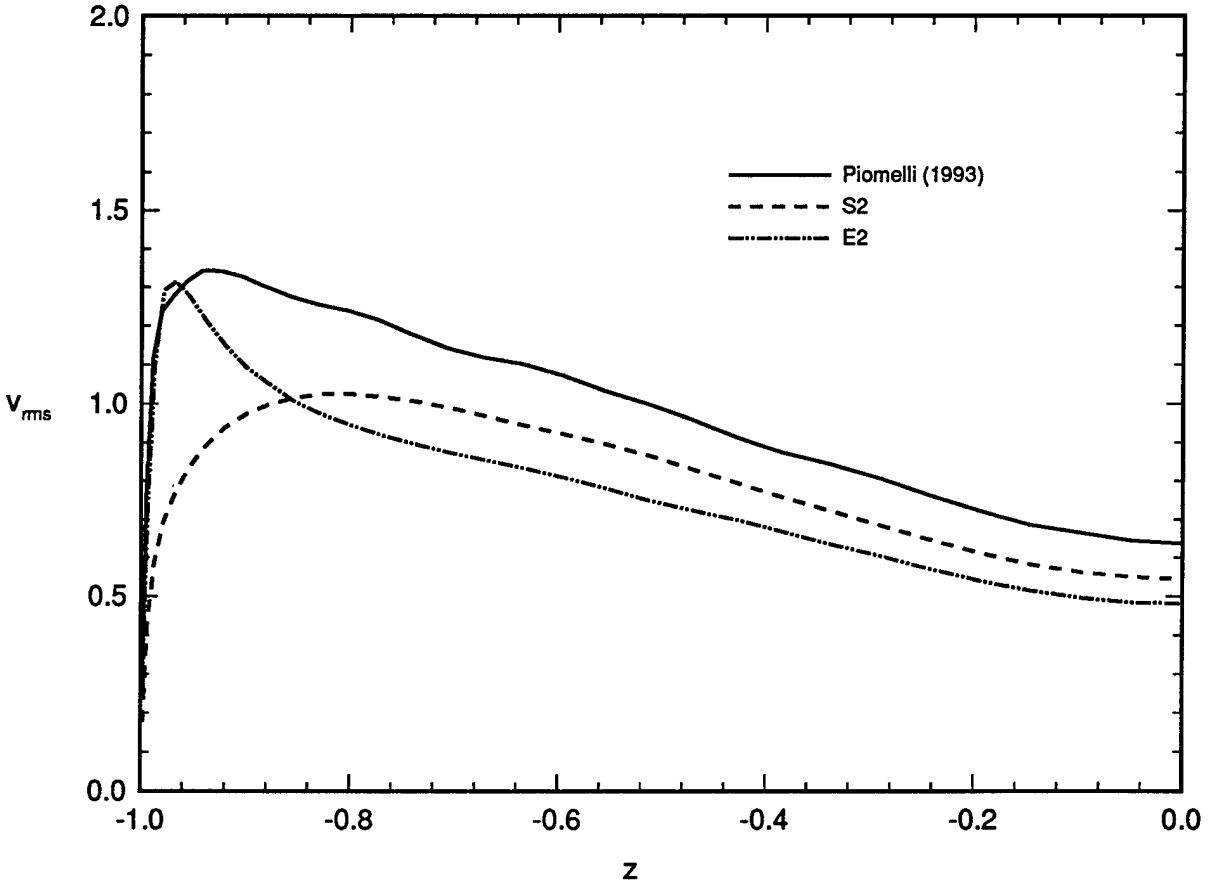

FIG. 13(b)

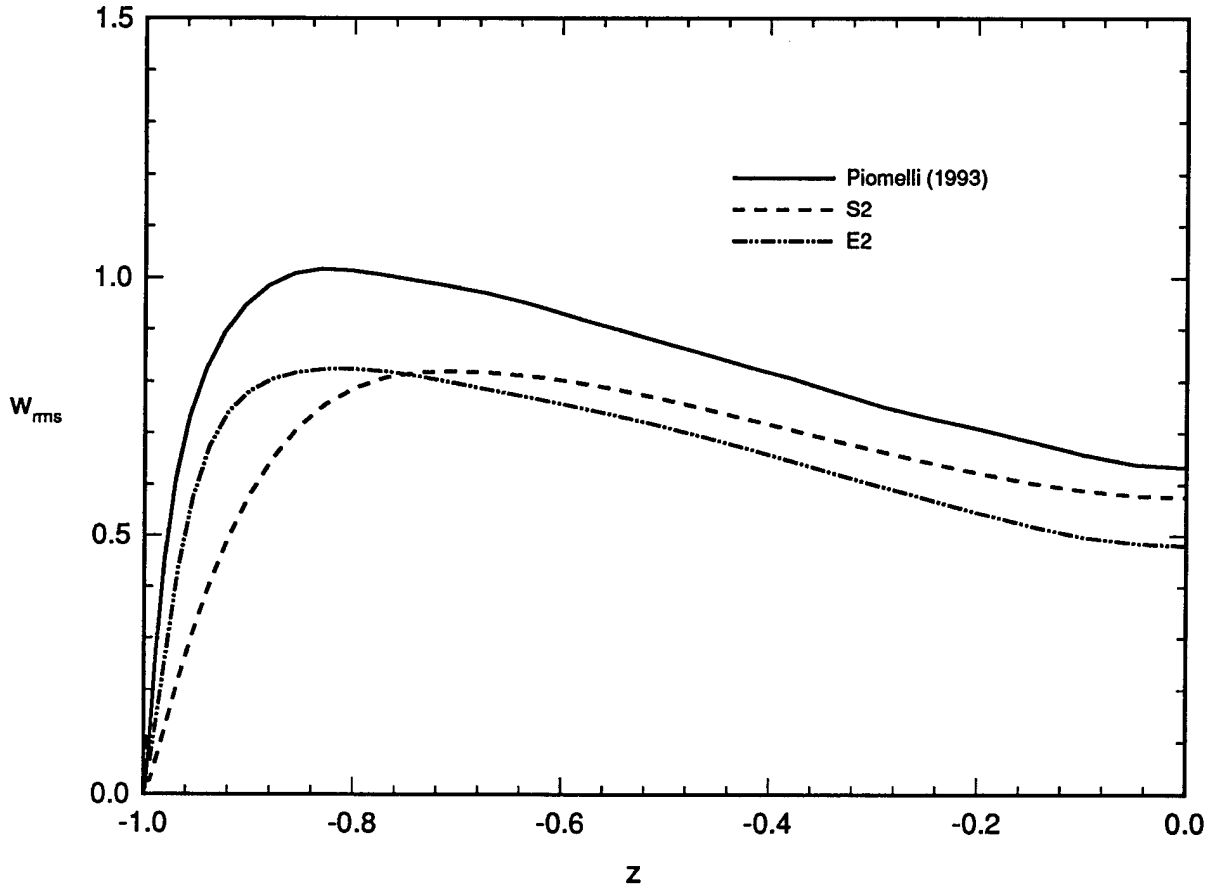

FIG. 13(c)

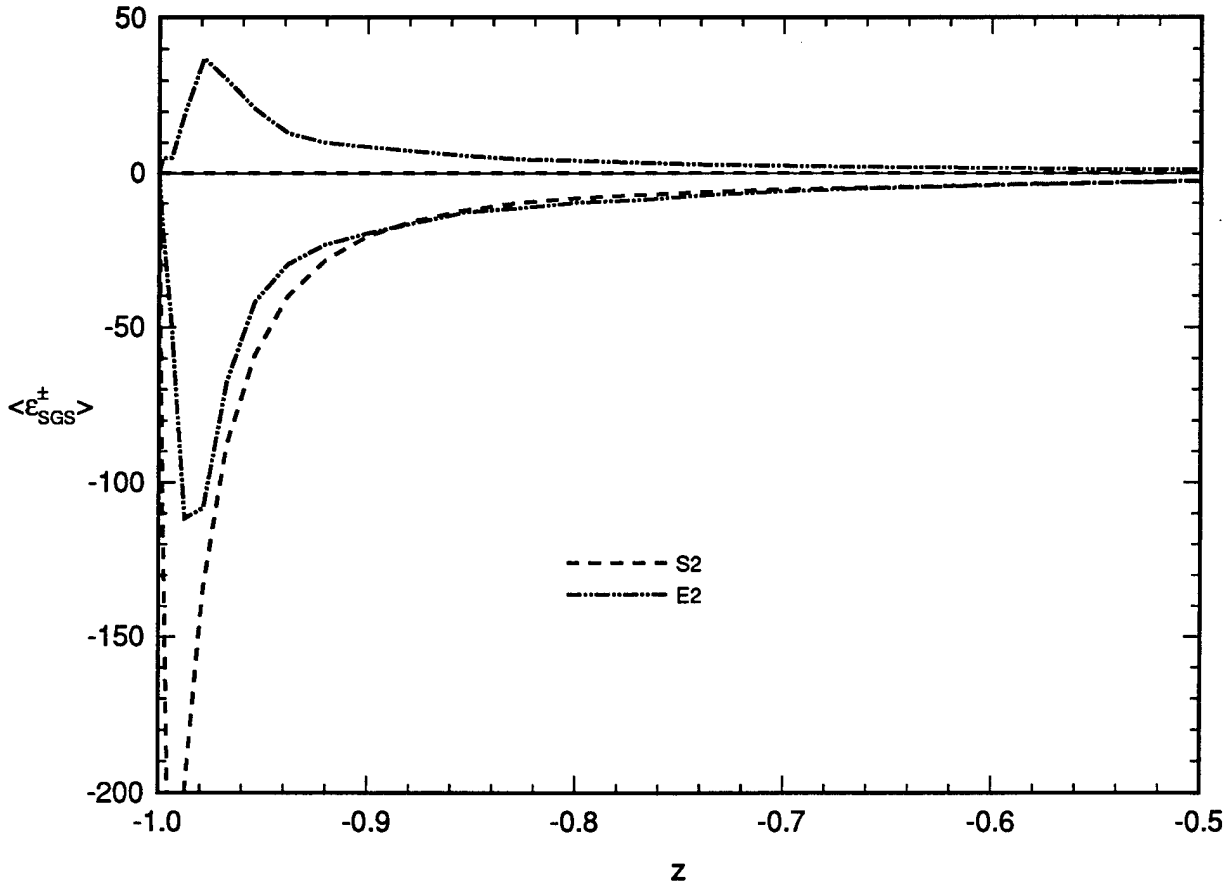

FIG. 14. The decomposition of SGS dissipation averaged over horizontal planes into forward transfer (negative values) and backscatter (positive values). Dashed line: case S2; dashed-dotted-dotted line: case E2. The peak in the forward transfer for case S2 is ≈ -256.

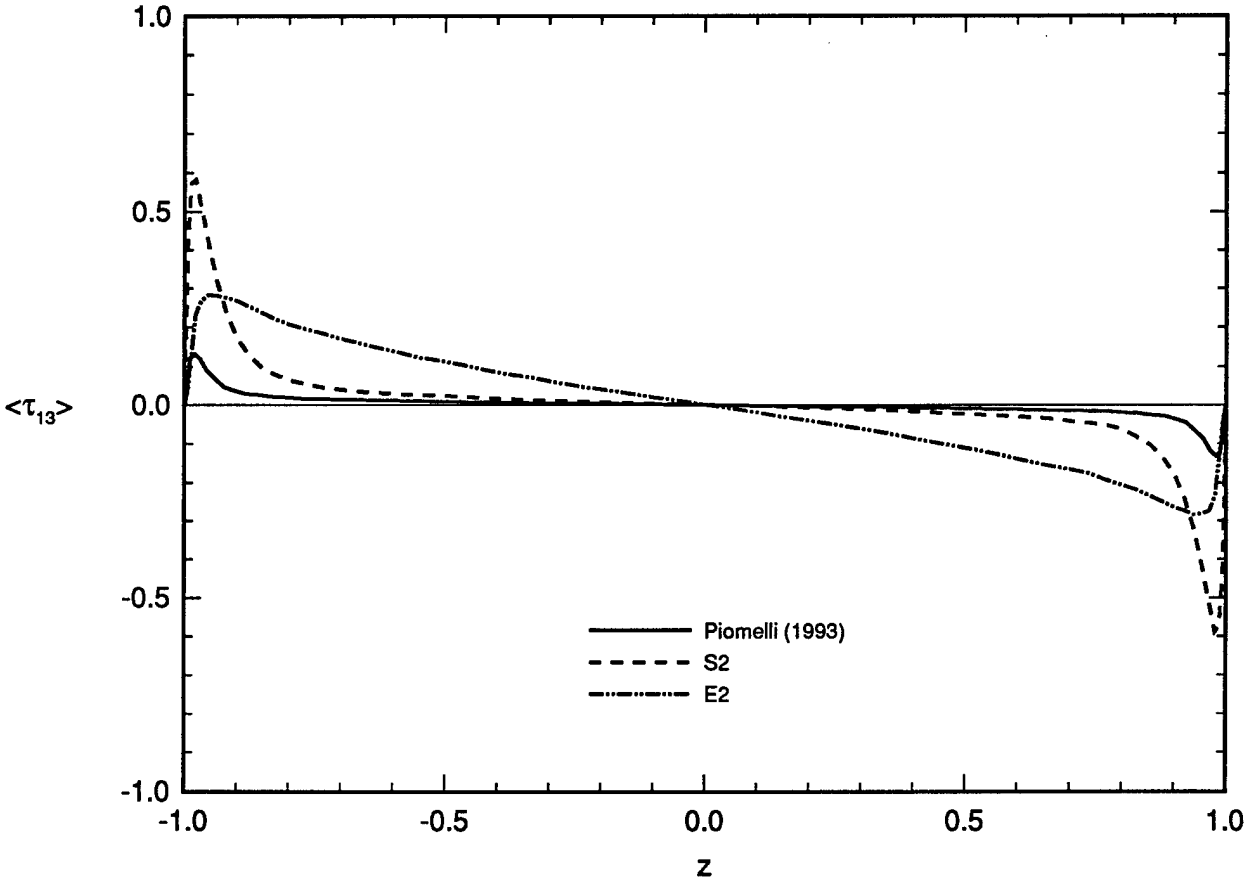

FIG. 15. Shear stress profiles. Solid line: Piomelli (1993); dashed line: case S2; dashed-dotted-dotted line: case E2. (a) SGS stress component $< \tau_{13} >$. (b) Resolved stress component $< \overline{u}\,\overline{w} >$.

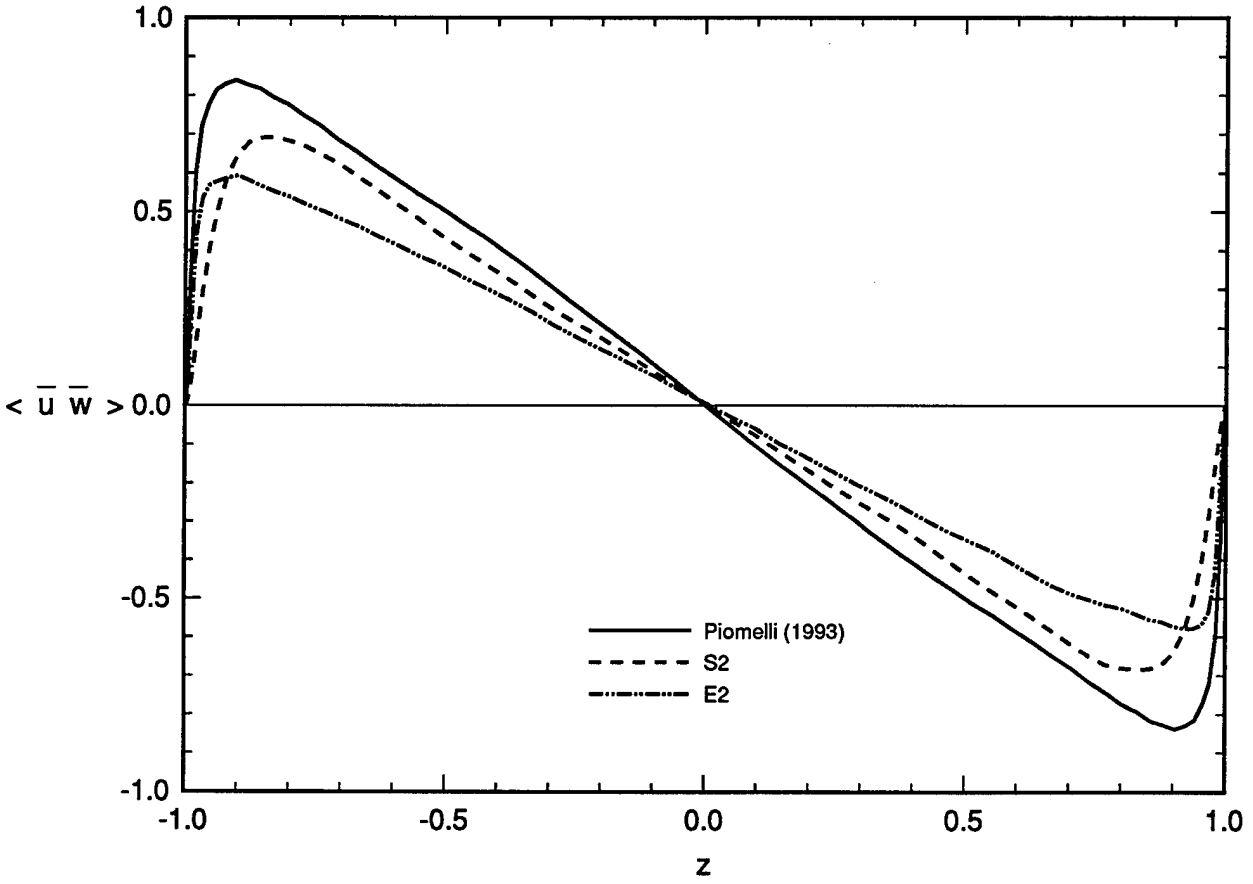

FIG. 15(b)

Backscatter models for large eddy simulations

by J. Andrzej Domaradzki and Eileen M. Saiki
Department of Aerospace Engineering,
University of Southern California,
Los Angeles, CA 90089-1191, U.S.A.,
tel. 213-740-5357, FAX 213-740-7774

July 11, 1996

Submitted to *The Physics of Fluids*

Abstract

Using previously established properties of nonlinear subgrid-scale interactions we derive deterministic models of backscatter for large eddy simulations. The models affect only weakly the total kinetic energy of turbulence providing approximately equal amounts of forward and back-scatter. The modeling procedures are tested on a simple case of forced isotropic turbulence with the inertial range and in turbulent channel flow.

PACS 47.25.Cg

1 Introduction

Currently several subgrid-scale (SGS) models are commonly used in large eddy simulations (LES) of turbulence. The Smagorinsky model [1] and the models for homogeneous turbulence proposed by Kraichnan [2] and Chollet and Lesieur [3] have a status of classical models. These models are also used as a starting point to construct newer models: the dynamic model of Germano *et al.* [4] and its variations [5,6,7] and the structure function model of Métais and Lesieur [8]. A recent review of these as well as several other SGS models is given by Lesieur [9]. The common and important feature of these successful SGS models is that they properly account for the global subgrid-scale dissipation, i.e. the net energy flux from the resolved to the subgrid scales.

The models are less successful in accounting for, or often do not attempt to account directly for the phenomenon of the inverse energy transfer from the subgrid scales to the resolved scales. This process, often called backscatter, is implicitly interpreted in two different ways. In the context of the analytical theories of turbulence Leslie and Quarini [10] noted that the resolved scale energy equation contains two distinct terms, one describing energy drain from the resolved scales to the subgrid scales and the other, the backscatter term, describing energy transfer from the subgrid scales to the resolved scales. The total energy transfer is the sum of these two terms and when it is represented in a form of the eddy viscosity the resulting net eddy viscosity contains contributions from both forward and inverse energy transfers. Therefore such a net eddy viscosity takes indirectly into account the presence of the backscatter by decreasing the value of the eddy viscosity associated with the forward energy transfer term. A somewhat different meaning is given to the backscatter term in the context of *a priori* analyses of direct numerical simulations data. In isotropic turbulence simulations the rate of energy change of an individual wavenumber mode k may be calculated and is either negative or positive. The latter case corresponds to backscatter local in a wavenumber. When negative and positive contributions are averaged over wavenumber shells of radius k the total transfer is split into forward- and back-scatter, respectively, formally corresponding to the decomposition used in the analytical theories of turbulence. However, it has not been shown yet

that the backscatter calculated in DNS is indeed approximated by the backscatter term in the analytical theories. In fact the spectrum of backscatter computed from low Reynolds number turbulence simulations by Domaradzki *et al.* [11] does not have properties expected from theoretical analysis. Therefore caution must be used in identifying backscatter in DNS with the backscatter term in the analytical theories until detailed comparison for different flows is made. Another important distinction is that the theoretical net eddy viscosity is generally positive implying that it decreases the amplitudes of individual modes $\mathbf{k}$ while simulations show that individual modes may grow or decay because of the subgrid-scale interactions. Similarly, in a physical space representation the actual subgrid-scale dissipation is locally frequently negative while the classical eddy viscosity models always give positive values. It also must be noted that there is no simple relation between local backscatter in physical and spectral representation. Therefore, the backscatter term is used to qualitatively describe in all cases the same phenomenon, energy transfer from the subgrid to the resolved scales, but one has to be aware that in all of those case the quantitative definitions of backscatter are not identical.

Analyses of direct numerical simulations of various turbulent flows [11,12,13,14] established that the backscatter is comparable to and often larger than the net subgrid-scale dissipation. This clearly implies that accounting for backscatter is desirable in LES on purely physical grounds. However the motivation for modeling backscatter phenomena in typical applied turbulence LES is lacking. This is because important mean and rms turbulent quantities appear to be sensitive only to the net SGS dissipation. However, as argued by Schumann [15], it is likely that backscatter effects become more important in situations where subgrid scales contain a significant fraction of the total energy, or more generally, when the resolution is necessarily coarse as in all geophysical applications. Despite the lack of a strong practical motivation at the present time for modeling backscatter, its presence in turbulent flows constitutes a sufficient physical reason that motivates work in this area. Backscatter can be introduced into LES by using random forcing (Leith [16], Chasnov [17], Schumann [15]), or deterministically by extrapolating from the dynamics of the resolved scales in the framework of the dynamic models as discussed by Carati *et al.* [18], or in the framework

of the similarity models [19,20]. The stochastic models can be designed to provide proper amounts of net inverse energy transfer and the fact that the subgrid scales are not known makes random forcing a natural choice. However, as observed by Schumann [15], the subgrid scales being solutions of Navier-Stokes equations can not be completely random. The purely stochastic models are also unable to describe in a physically satisfactory manner the nonlinear interactions between highly correlated (smallest resolved and largest subgrid) scales which are responsible for the subgrid-scale energy transfer [11,21]. The effects of such strong correlations are observed by Härtel and Kleiser [22] in the wall region of channel flow where the subgrid-scales may constitute with the resolved scales part of the same physical coherent structure. Moreover, to be consistent, if the effect of the subgrid scales on the resolved scales is entirely random then not only backscatter but also forward transfer should be modeled in a non-deterministic fashion, and LES practice indicates that it is not necessary. Therefore, while some level of stochasticity in a SGS model is desirable, deterministic models offer a reasonable alternative in view of a lack of detailed information about statistical properties of SGS interactions.

The backscatter in the dynamic model has a good physical interpretation [18] but its origin in the eddy viscosity model appears to limit backscatter to values lower than observed in *a priori* tests. The similarity models provide the most natural way of introducing backscatter deterministically. However, in this approach one usually attempts to model the entire subgrid-scale stress, possibly a more difficult task than modeling backscatter separately and then combining it with a dissipative expression (giving a version of a mixed model). Moreover, such models often use formal similarities between subgrid stresses computed with different filter widths rather than known properties of the subgrid-scale interactions. As a result, for instance, the SGS stress tensor in the Bardina model [19] vanishes if the sharp spectral filter is employed. For other filters the stress tensor is nonzero but it significantly underestimates the real energy transfers as reported by Liu *et al.* [20].

These difficulties and uncertainties in accounting for backscatter in LES suggest that better models may be expected only if more information about physics of this process is employed in the

modeling. The goal of this paper is to propose procedures for modeling backscatter effects which are based on properties of nonlinear subgrid scale interactions observed in direct numerical simulations of turbulence.

2 Backscatter models

Using *a priori* analysis of isotropic turbulence data, Kerr *et al.* [14] have shown that most of the backscatter effects are described by the term obtained from the decomposition of the full nonlinear term in the vorticity form:

$$\mathbf{B} = (\mathbf{u}^{\mathcal{L}} \times \omega^{\mathcal{S}})^{\mathcal{L}}, \tag{1}$$

where $\mathbf{u}$ and ω are the velocity and the vorticity fields and the superscript $\mathcal{L}$ signifies filtering to large scales, resolved in LES, and $\mathcal{S}$ signifies filtering to subgrid scales, unknown in LES. If a tilde is used to denote filtering to the large scales the above formula becomes

$$\mathbf{B} = \tilde{\mathbf{u}} \times (\omega - \tilde{\omega}). \tag{2}$$

More specifically Kerr *et al.* [14] found that term (1) provides large but about equal amounts of forward and back-scatter such that it contributes very little to the net SGS energy transfer. The remaining terms in the decomposition are responsible for the majority of the net transfer. These results suggest that the effects of backscatter can be included in LES by adding to a purely dissipative SGS model which properly accounts for the net transfer, an additional term which is based on the above expression. This is the strategy that we explore in this paper.

Formulas (1) and (2) give the vector product of the resolved velocity with the unresolved vorticity, the result filtered subsequently to the resolved scales. To model this expression for the use in LES we need a model for the subgrid vorticity. Two such models based on the small-scale vorticity

production are discussed by Kerr *et al.* [14], but we consider another approach here. The simplest model is based on the similarity concept. The resolved scales are divided into large and small scales by an appropriate filtering operation and the above formulas are applied. If this filtering operation, often called "a test filtering" in the dynamic SGS models, is denoted by the overbar, the model is

$$\mathbf{B}^{(1)} = \overline{\tilde{\mathbf{u}} \times (\tilde{\omega} - \overline{\tilde{\omega}})}. \tag{3}$$

In what follows we will simplify the notation by dropping tilde, i.e. assuming implicitly that quantities without a tilde are the resolved LES quantities and the superscript $\mathcal{L}$ and the overbar signify the test filtering. The model (3) is then written simply as $\mathbf{B}^{(1)} = \overline{\mathbf{u} \times (\omega - \overline{\omega})}$.

Generally, a subgrid-scale model in a form of the divergence of a second-order tensor is preferred because this form assures that the mean momentum of the flow is affected by the subgrid-scale interactions only at the boundaries as required by the form of the SGS stress tensor in the LES equations. In particular, subgrid-scale interactions cannot generate a mean flow in isotropic turbulence. This condition is satisfied by (3) only if the sharp spectral filter is used as was the case in the *a priori* analysis of Kerr *et al.* [14]. If other filtering operations are to be used, the model (3) should be replaced by a model in the stress tensor form. The expression (1) can be written as

$$B_i = -\frac{\partial}{\partial x_j}(u_i^{\mathcal{S}} u_j^{\mathcal{L}})^{\mathcal{L}} + (u_j^{\mathcal{L}} \frac{\partial}{\partial x_i} u_j^{\mathcal{S}})^{\mathcal{L}}, \tag{4}$$

where the first term has a desired form suggesting using it as a model. This implies the backscatter stress tensor in a form $\tau_{ij} = (u_i^{\mathcal{S}} u_j^{\mathcal{L}})^{\mathcal{L}} = \overline{(u_i - \overline{u_i})\overline{u_j}}$.

The above models originated in the analyses of homogeneous, isotropic turbulence where the mean velocity vanishes and $\mathbf{u}(\mathbf{x}, t)$ is the fluctuating velocity. If the mean flow is non-zero and is included in the definition of $\mathbf{u}(\mathbf{x}, t)$ then both models will not be Galilean invariant because of proportionality to the large scale velocity $u_j^{\mathcal{L}}$. One way to recover the Galilean invariance of the models for cases with nonvanishing mean flow and to maintain their consistency with the original

analyses is to apply the modeling expressions to the fluctuating components of the velocity only. This approach is favored for the model (3) applied to homogeneous flows. For inhomogeneous flows the divergence form is preferred and in that case another standard method to make the model Galilean invariant is to redefine SGS stresses as proposed by Germano [23]:

$$\tau_{ij}^{(2)} = \overline{u_i^{\mathcal{S}} u_j^{\mathcal{L}}} - \overline{u_i^{\mathcal{S}}}\ \overline{u_j^{\mathcal{L}}} = \overline{(u_i - \overline{u_i})\overline{u_j}} - \overline{(u_i - \overline{u_i})}\ \overline{\overline{u_j}} \tag{5}$$

with the corresponding model

$$B_i^{(2)} = -\frac{\partial}{\partial x_j}\tau_{ij}^{(2)}. \tag{6}$$

Physically models (3) and (6) account for modifications of the large resolved scales $\mathcal{L}$ by the small resolved scales $\mathcal{S}$ while the small scales are being advected by the large ones.

In principle both formulas could also contain a multiplicative constant and another free parameter is the ratio of the filter width used in formulas (3) and (6) to the filter width of the LES. In the original backscatter expression (1), the multiplicative constant is equal to unity and we choose to keep this value as well in the modeling expressions (3) and (6). Therefore, the filter width ratio remains as the only free parameter. The models affect only the largest resolved scales determined by the filter $\mathcal{L}$ while it is known that the backscatter interactions affect all resolved scales in LES [11,13,24]. This suggests that the range of scales $\mathcal{S}$ should be made as small as possible while using these models. An analysis of DNS data for low Reynolds number flows and the results of LES reported in the next section indicate that the test filter cutoff wavenumber should be in the range between 50 and 90% of the LES cutoff value.

3 Large eddy simulations with backscatter models

Analyses of the direct numerical simulations data by themselves only suggest but do not guarantee that the desirable features of the models will be in fact observed in actual large eddy simulations. In this section we assess the backscatter models explicitly.

3.1 Forced isotropic turbulence

A simple case of isotropic turbulence with the inertial subrange was chosen to see if the models provide approximately equal amounts of forward and inverse transfers in LES without affecting significantly the net SGS transfer. First, we performed pseudo-spectral large eddy simulations of forced isotropic turbulence on a 32^3 grid. We employed the forcing scheme of Sullivan *et al.* [25] which keeps the total energy of several low wavenumber modes constant, but allows evolution of individual modes through nonlinear interactions, subject to the global energy constraint. The subgrid-scale model used was a constant spectral eddy viscosity discussed by Lesieur [26]

$$\nu_T = 0.402\sqrt{E(k_m)/k_m}, \tag{7}$$

where $E(k)$ is the energy spectrum and k_m is the maximum wavenumber in LES, i.e. the wavenumber marking the boundary between resolved and subgrid scales. The constant 0.402 in (7) is obtained assuming the inertial range with the Kolmogoroff constant $Ko = 1.4$. The program was run until statistically stationary state was reached. The molecular viscosity term was retained in the simulations and in the stationary state $\nu_T/\nu \approx 500$. After a stationary state was reached, the simulations were run for additional several hundred time steps keeping the eddy viscosity model (7) and adding backscatter models (3) and (6) to the LES equations.

In Fig. 1 we plot the spectral Kolmogoroff function defined as

$$Ko(k) = E(k)/(\epsilon^{2/3}k^{-5/3}) \tag{8}$$

for the base LES with the eddy viscosity model and for runs with the additional backscatter models. In (8), ϵ is the energy flux down the spectrum, equal to the energy input into the system necessary to maintain the steady state. For the perfect inertial range spectrum consistent with the eddy viscosity model used, (8) should be constant equal to 1.4. $Ko(k)$ in the simulations varies between 1 and 2.2 showing similar trends for all models used though adding the backscatter models results in slightly improved predictions. The level of variation in Ko is similar to that observed in typical

LES of isotropic turbulence and much better results should not be expected in view of the fairly simple eddy viscosity model used. The important feature observed in Fig. 1 is that all backscatter models used do not significantly affect the energy spectra providing results comparable to those obtained using the eddy viscosity model. However, the eddy viscosity has a purely dissipative effect on the energy of the flow resulting in the energy dissipation rate equal to the the energy input rate ϵ in the steady state. The role of the backscatter terms is to model a (positive) influx of energy from the subgrid to the resolved scales. In Fig. 2 we plot as a function of time (positive) backscatter and (negative) forward transfer components for the energy flux to/from the resolved scales associated with each model and normalized by the global transfer rate ϵ. These energy transfer rates were computed by summing respective positive and negative values of contributions that the models make to the kinetic energy equation in the physical space. In all cases the test filtering was done with the sharp spectral filter in each direction, x, y, and z, with the cutoff wavenumber $k_c = 3/4k_m$. Both models provide approximately equal amounts of forward- and back-scatter, between 60% and 80% of the global energy dissipation rate, depending on the model. These values compare favorably with values observed in *a priori* analyses of DNS data, but are significantly larger than found by Carati *et al.* [18] for the current state-of-the-art dynamic DLM(k) model.

3.2 Channel flow turbulence

We have performed large eddy simulations of turbulent channel flow using a pseudo-spectral Fourier-Chebyshev numerical method with the resolution of 32×32 modes in the streamwise x and the spanwise y directions and 65 modes in the vertical z direction. The physical parameters in the simulations were chosen to match parameters used in direct numerical simulations of the same problem performed by Kim *et al.* [29] at Reynolds number $Re = 3300$ based on the mean centerline velocity and the channel half width h. The corresponding Reynolds number based on friction velocity u_τ and h is approximately $Re_\tau = 180$. The LES results were compared with a DNS database of Gilbert [27] made availabe to us by Professor L. Kleiser (see also Gilbert and Kleiser [28] and Härtel *et al.* [22]). In these DNS channel flow was simulated with the resolution of 160^2(horizontal)$\times$129(vertical) modes

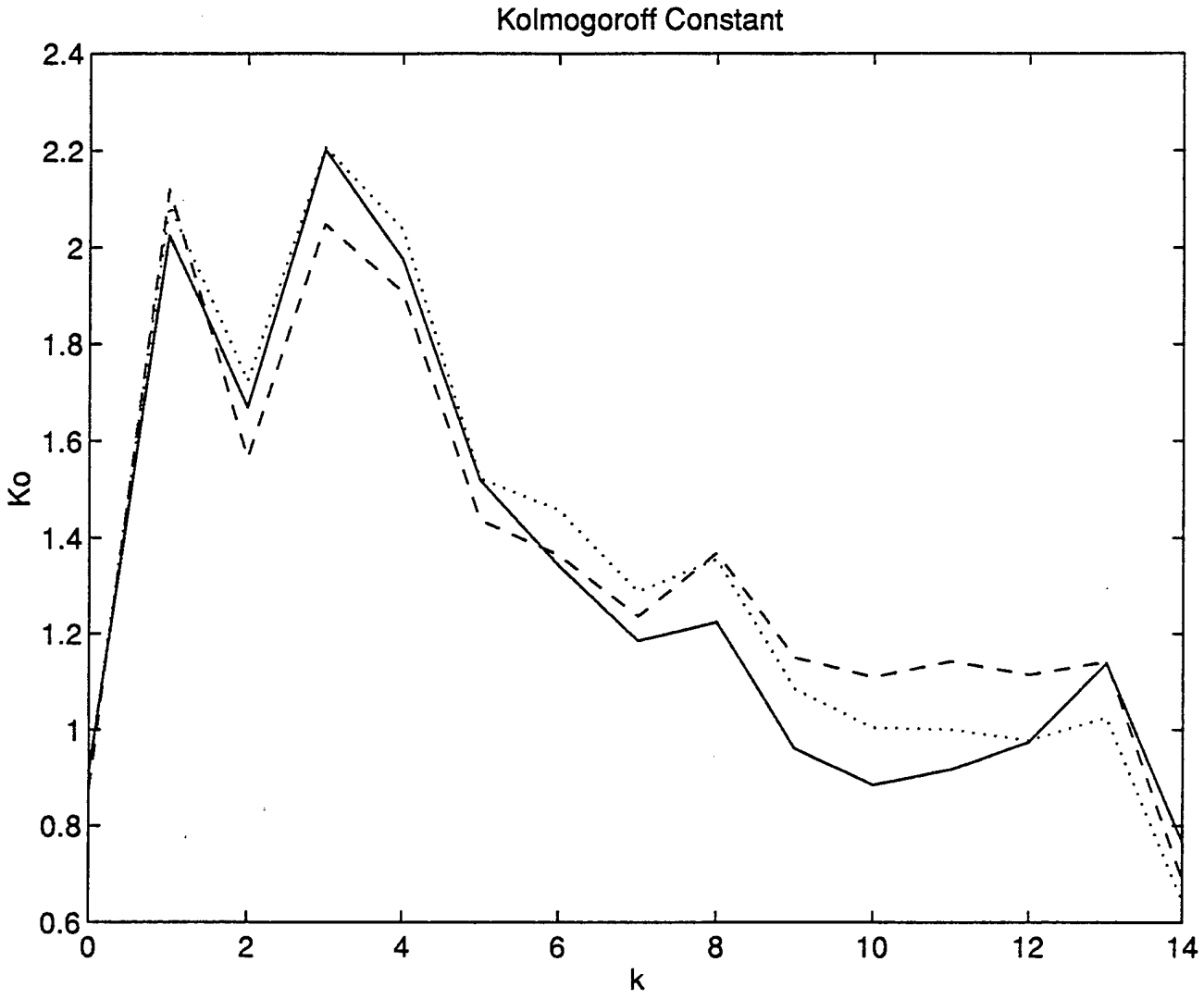

Figure 1: Predictions of the Kolmogoroff function. Solid line: eddy viscosity (7) without backscatter; broken line: backscatter model (3); dotted line: backscatter model (6).

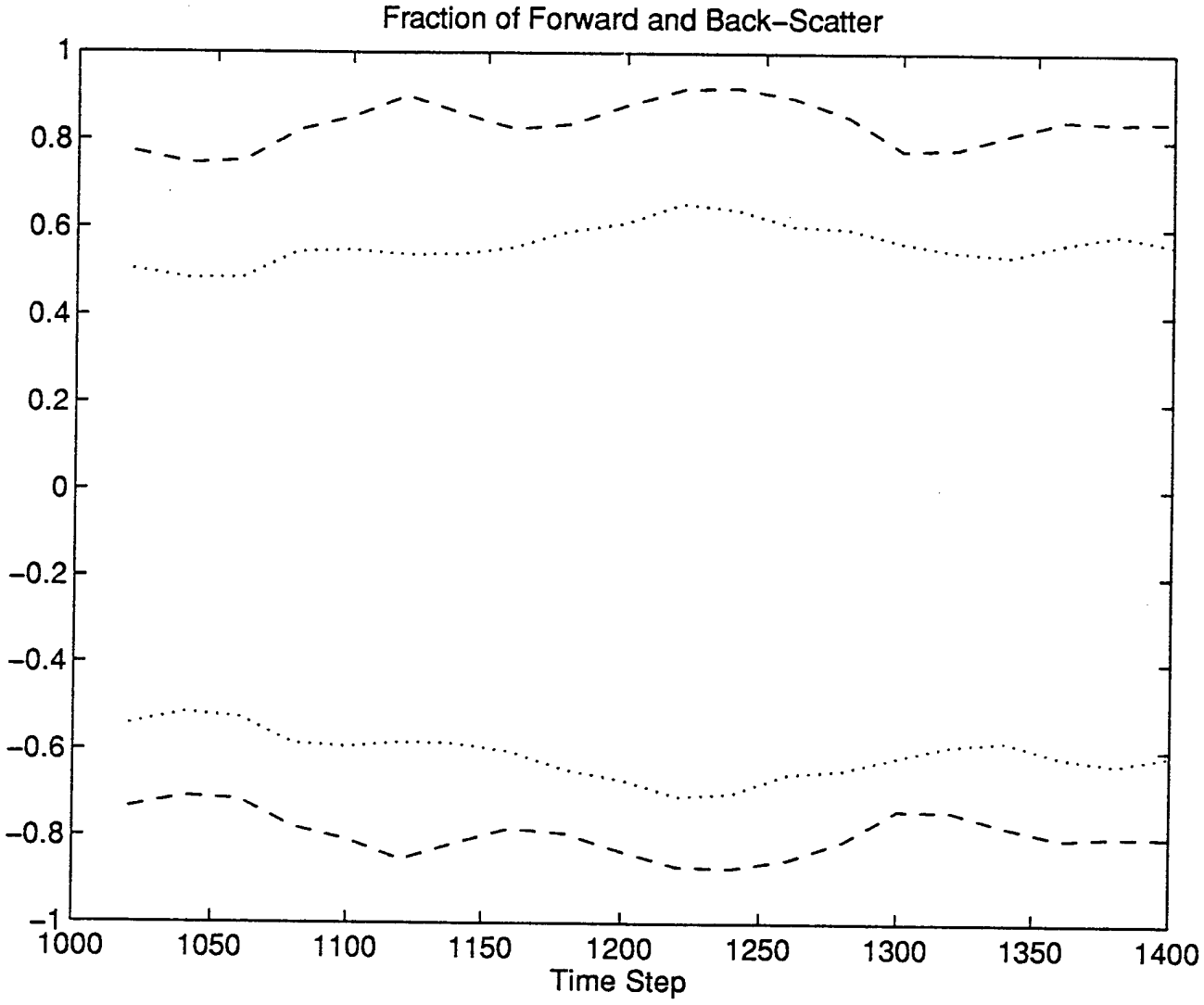

Figure 2: Forward-scatter (negative) and back-scatter (positive) of energy normalized by the energy transfer rate ϵ as a function of time. Broken line: backscatter model (3); dotted line: backscatter model (6).

at slightly higher Reynolds number $Re_\tau = 210$. Turbulence statistics in these simulations compare very well with DNS results of Kim *et al.* [29] and experimental results of Nishino and Kasagi [30]. For large eddy simulations the standard Smagorinsky model with constant $C_s = 0.1$ and van Driest wall damping was used as well as the backscatter model (6) with two test cutoff wavenumbers $k_c = 1/2k_m$ and $k_c = 3/4k_m$, where $k_c = ak_m$ signifies filtering in the two horizontal directions with cutoffs $k_{xc} = ak_{xm}$ and $k_{yc} = ak_{ym}$, respectively. No filtering in the vertical direction z was employed in the models. The simulations were run until a statistically stationary state was reached and continued for additional several thousand time steps to collect turbulence statistics.

Turbulent rms velocities computed for all models are plotted in Fig. 3 where they are compared with DNS results of Gilbert [27]. As expected from numerous tests of the Smagorinsky model reported in the literature it predicts rms velocities reasonably well. For a chosen value of $C_s = 0.1$ the streamwise velocity is predicted very well while the spanwise and normal velocity components are slightly under predicted. The net effect on the rms velocities of adding the modeling expression (6) to the Smagorinsky model is small since the models were designed not to affect significantly the energetics of the system. The backscatter model with $k_c = 3/4k_m$ shifts peaks of the horizontal velocity components too close to the wall but improves the normal velocity prediction in the wall region. For $k_c = 1/2k_m$ the streamwise and normal velocities are similar to the predictions of the Smagorinsky model, but the prediction of the spanwise component is significantly improved in the wall region. This case provides the best overall improvement in the rms values. The backscatter model (6) has also been implemented using a top hat filter with the filter width twice the mesh size in the streamwise and spanwise directions. In this case the effects of the backscatter model were found to be very small and the results for the rms velocities were virtually the same as for the pure Smagorinsky model. The differences between spectral and top hat filtering applied to the backscatter models can be better understood by calculating a nonconservative part of the SGS energy flux F_{SGS} (or SGS dissipation ϵ_{SGS}) associated with the models:

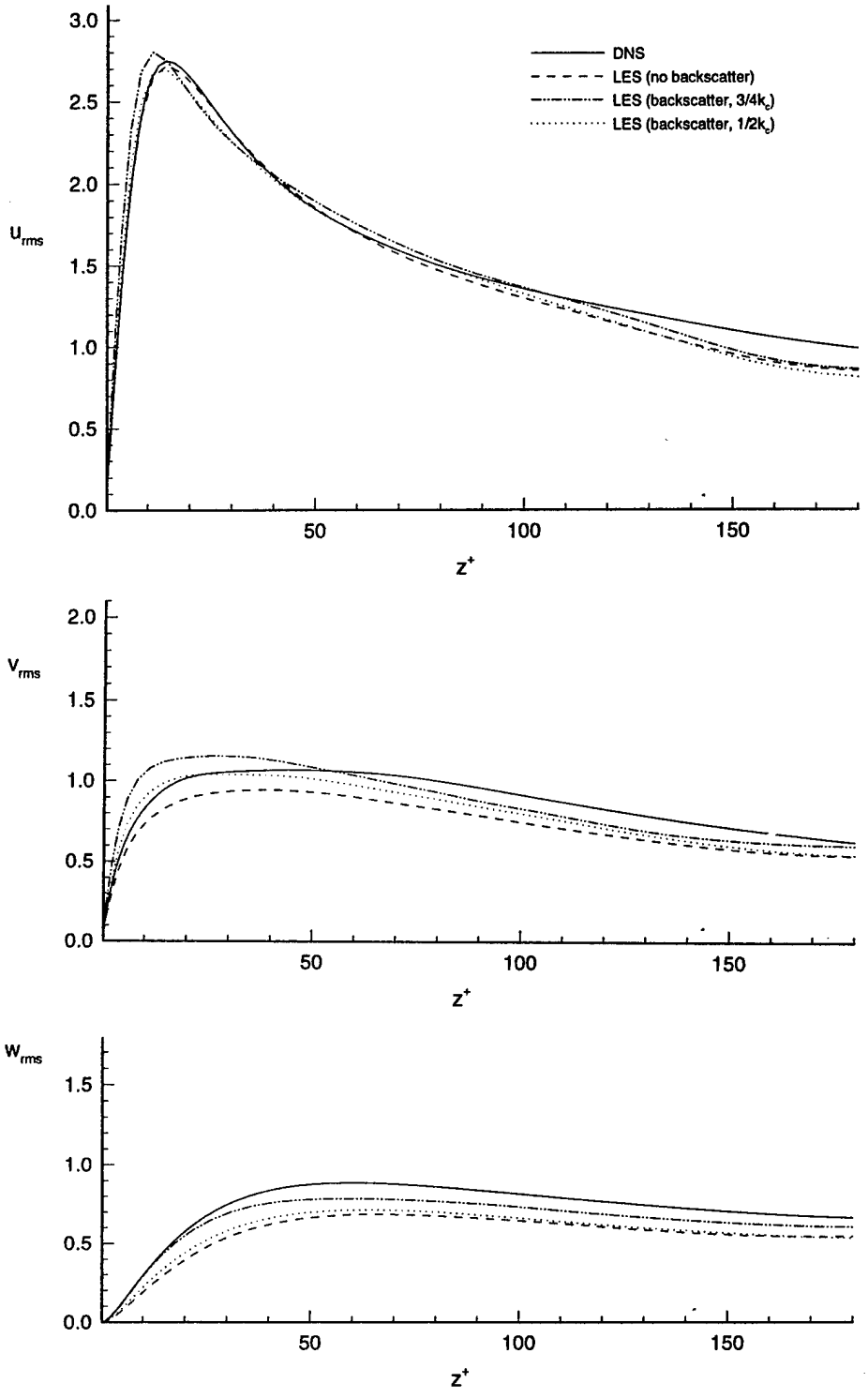

Figure 3: Fluctuating rms velocities normalized by u_τ as a function of the distance from the wall in wall units: solid line, DNS results; broken line, Smagorinsky model; dotted line, Smagorinsky model with backscatter model (6) for $k_c = 1/2k_m$; broken-dotted line, Smagorinsky model with backscatter model(6) for $k_c = 3/4k_m$. (a) streamwise component u_{rms}; (b) spanwise component v_{rms}; (c) normal component w_{rms}.

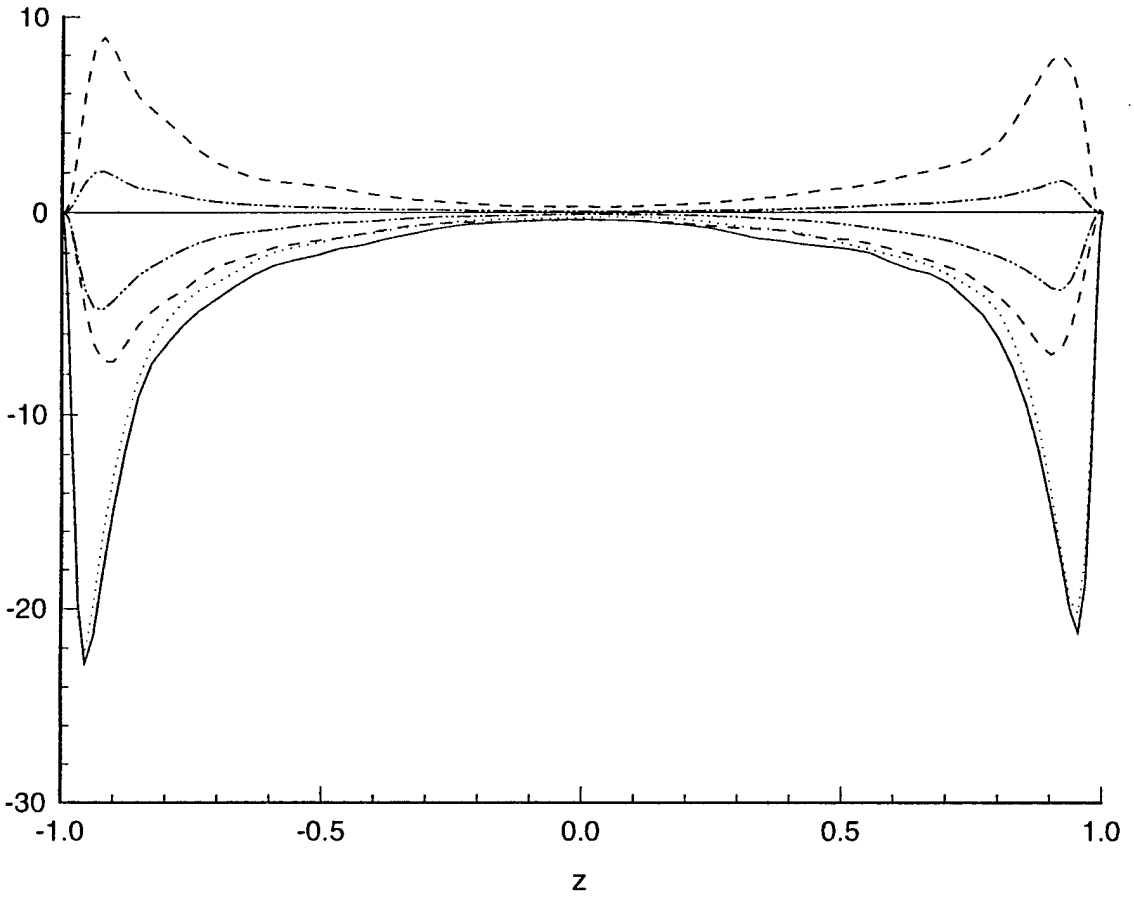

Figure 4: Contributions (negative: forward transfer, positive: backscatter) of different models to the subgrid-scale energy flux. Solid line, Smagorinsky model with a spectral cutoff filter; dotted line, Smagorinsky model with a tophat filter; broken lines, expression (6) with a spectral filter; broken-dotted lines, expression (6) with a tophat filter.

$$F_{SGS} = -\epsilon_{SGS} = \tau_{ij}\frac{\partial u_i}{\partial x_j}. \tag{9}$$

Contributions to this quantity from the Smagorinsky model and the backscatter model (6) for spectral and top hat filters are plotted in Fig. 4. In every horizontal plane the SGS flux is decomposed into its negative (forward transfer) and positive (backscatter) components. The Smagorinsky model is purely dissipative providing only forward transfer. There is formally no distinction between resolved velocity fields for both filters used and consequently the Smagorinsky SGS flux is the same in both cases. However, different test filters used in expression (6) will give different results. By design the backscatter model provides approximately equal amounts of forward transfer and backscatter, but effects of the model calculated with the top hat filter are significantly smaller than for the sharp spectral filter. This explains its small effect on the energetics observed in the rms results. The significant reduction of the backscatter for the top hat filter as compared with the sharp spectral filter is consistent with *a priori* analysis of Piomelli *et al.* [12]. However, since the resolved scales in LES reported in this paper are obtained by a spectral truncation the choice of the spectral filter for the backscatter model is preferred.

4 Conclusions

We have used the properties of subgrid-scale nonlinear interactions observed in DNS of turbulence to propose models accounting for the backscatter phenomenon. The modeling expressions can be added to any standard dissipative SGS model improving physical realism of a LES procedure. The models provide approximately equal amounts of forward- and back-scatter and affect only weakly the energetics of the system as predicted by the dissipative part of the full model. The models have a form similar to the nonlinear term in the Navier-Stokes equations and thus avoid numerical stability problems associated with modeling of backscatter by a negative eddy viscosity. The above properties of the models were suggested by the previous *a priori* analysis of DNS results and have been confirmed in actual large eddy simulations for turbulent isotropic and channel flows. The only

adjustable parameter in the models is a filter width which provides limited control over the amount of backscatter.

Acknowledgements

This work was supported by a contract No. N00014-96-1-0015 from the Office of Naval Research (contract monitor Dr. L.P. Purtell) and partially by the Rocketdyne Division of Rockwell International Corporation. Supercomputer time was provided by the San Diego Supercomputer Center. Additional computer resources were provided by a NSF Research Equipment Grant No. ECS-9424385.

[1]J. Smagorinsky, "General circulation experiments with the primitive equations", Mon. Weath. Rev. **93**, 99 (1963).

[2]R.H. Kraichnan, "Eddy viscosity in two and three dimensions", J. Atmos. Sci. **33**, 1521 (1976).

[3]J. Chollet and M. Lesieur, "Parametrization of small scales of three-dimensional isotropic turbulence utilizing spectral closures", J. Atmos. Sci. **38**, 2767 (1981).

[4]M. Germano, U. Piomelli, P. Moin, and W.H. Cabot, "A dynamic subgrid-scale eddy viscosity model", Phys. Fluids A**3**, 1760 (1991).

[5]D.K. Lilly, "A proposed modification of the Germano subgrid-scale closure method", Phys. Fluids A**4**, 633 (1992).

[6]S. Ghosal, T.S. Lund, P. Moin, K. Akselvoll "A dynamic localization model for large-eddy simulation of turbulent flows", J. Fluid Mech. **286**, 229 (1995).

[7]V.C. Wong and D.K. Lilly, "A comparison of two dynamic closure methods for turbulent thermal convection", Phys. Fluids A**6**, 1016 (1994).

[8]O. Metais and M. Lesieur, "Spectral large-eddy simulations of isotropic and stably-stratified turbulence", J. Fluid Mech. **239**, 157 (1992).

[9]M. Lesieur, "New trends in large-eddy simulations of turbulence", Annu. Rev. Fluid Mech. **28**.

[10]D.C. Leslie and G.L Quarini, "The application of turbulence theory to the formulation of subgrid modelling procedures", J. Fluid Mech. **91**, 65 (1979).

[11]J.A. Domaradzki, W. Liu, and M.E. Brachet, "An analysis of subgrid-scale interactions in numerically simulated isotropic turbulence", Phys. Fluids A**5**, 1747 (1993).

[12]U. Piomelli, W.H. Cabot, P. Moin, and S. Lee, "Subgrid-scale backscatter in turbulent and transitional flows", Phys. Fluids A**3**, 1766 (1991).

[13]J.A. Domaradzki, W. Liu, C. Härtel, and L. Kleiser, "Energy Transfer in Numerically Simulated Wall-Bounded Turbulent Flows", Phys. Fluids A **6**, 1583 (1994).

[14]R.M. Kerr, J.A. Domaradzki, G. Barbier "Small-scale properties of nonlinear interactions and subgrid-scale energy transfer in isotropic turbulence",Phys. Fluids **8**, 197 (1996).

[15]U. Schumann, "Stochastic backscatter of turbulence energy and scalar variance from random subgrid-scale fluxes", Proc. R. Soc. Lond. A**451**, 293 (1995).

[16]C.E. Leith, "Stochastic backscatter in a subgrid-scale model: plane shear mixing layer", Phys. Fluids A **2**, 297 (1990).

[17]J.R. Chasnov, "Simulation of the Kolmogoroff inertial subrange using an improved subgrid model", Phys. Fluids A**3**, 188 (1991).

[18]D. Carati, S. Ghosal, and P. Moin, "On the representation of backscatter in dynamic localization models", Phys. Fluids **7** 606 (1995).

[19]J. Bardina, J.H. Ferziger, and W.C. Reynolds, "Improved turbulence models based on large eddy simulation of homogeneous incompressible turbulence", Stanford University, Report TF-19, 1983.

[20]S. Liu, C. Meneveau, and J. Katz, "On the properties of similarity subgrid-scale models as deduced from measurements in a turbulent jet", J. Fluid Mech. **275**, 83 (1994).

[21]Y. Zhou, G. Vahala, "Reformulation of recursive-renormalization-group-based subgrid modeling of turbulence", Phys. Rev. E **47**, 2503 (1993).

[22]C. Härtel, L. Kleiser, F. Unger, and R. Friedrich, "Subgrid-scale energy transfer in the near-wall region of turbulent flows", Phys. Fluids **6**, 3130, (1994).

[23]M. Germano, "A proposal for a redefinition of the turbulent stresses in the filtered Navier-Stokes equations", Phys. Fluids **29**, 2323 (1986).

[24]J.A. Domaradzki and W. Liu, "Approximation of subgrid-scale energy transfer based on the dynamics of resolved scales of turbulence", Phys. Fluids A **7**, 2025 (1995).

[25]N.P. Sullivan, S. Mahalingham, and R.M. Kerr, "Deterministic forcing of homogeneous, isotropic turbulence", Phys. Fluids A**6**, 1612 (1994).

[26]M. Lesieur, *Turbulence in Fluids*, 2nd ed., (Martinus Nijhoff Publishers, Dordrecht, 1990).

[27]N. Gilbert, "Numerische Simulation der Transition von der laminaren in die turbulente Kanalströmung", DFVLR-Forschungsbericht 88-55, (DLR Göttingen, Germany, 1988).

[28]N. Gilbert and L. Kleiser, "Turbulence model testing with the aid of direct numerical simulation results", in *Proceedings of 8th Symposium on Turbulent Shear Flows*, (Munich, 1991).

[29]J. Kim, P. Moin, R.D. Moser, "Turbulence statistics in fully developed channel flow at low Reynolds number", J. Fluid Mech. **177**, 133 (1987).

[30]K. Nishino and N. Kasagi, "Turbulence statistics measurements in a two-dimensional channel flow using a three-dimensional particle tracing velocimeter", in *Proc. 7th Symposium on Turbulent Shear Flows*, (Stanford University, U.S.A., 1989).